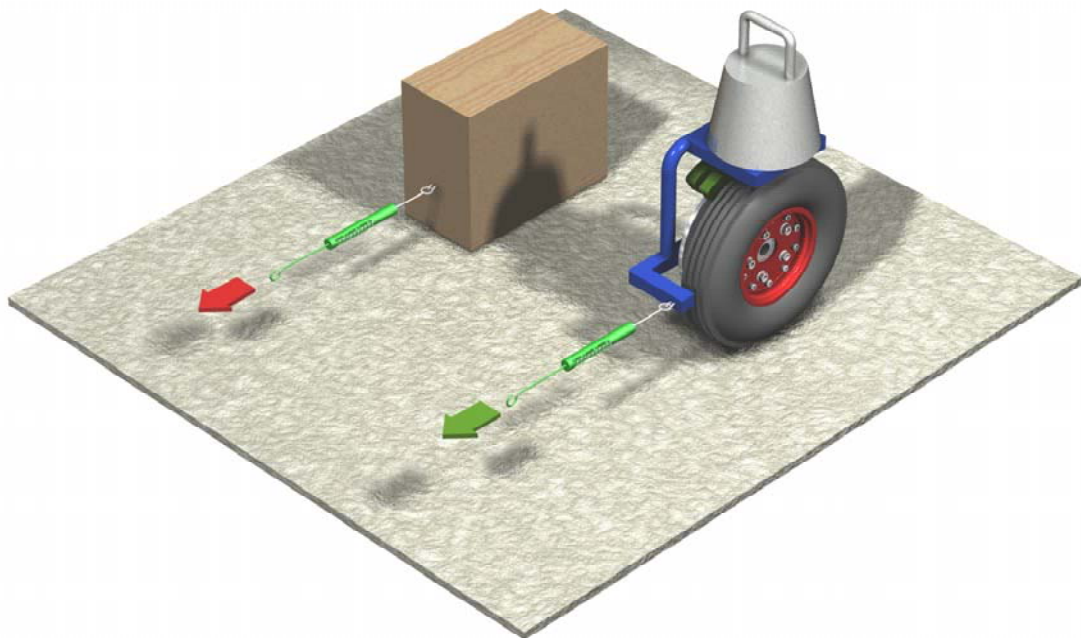


# Friction Fundamentals, Concepts and Methodology

Prepared for  
Transportation Development Centre  
Transport Canada  
October 1999





TP 13837E

# Friction Fundamentals, Concepts and Methodology

By

A. Andresen, B. Sc.  
MFT Mobility Friction Technology AS

J. C. Wambold, Ph. D.  
CDRM, Inc.

October 1999

## **NOTICES**

This report reflects the views of the authors and not necessarily those of the Transportation Development Centre or the sponsoring organizations.

The Transportation Development Centre does not endorse products or manufacturers. Trade or manufacturers' names appear in this report only because they are essential to its objectives.

Un sommaire français se trouve avant la table des matières.



1. Transport Canada Publication No. <b>TP 13837E</b>		2. Project No. <b>9555</b>		3. Recipient's Catalogue No.		
4. Title and Subtitle <b>Friction Fundamentals, Concepts and Methodology</b>				5. Publication Date <b>October 1999</b>		
				6. Performing Organization Document No.		
7. Author(s) <b>A. Andresen and J.C. Wambold</b>				8. Transport Canada File No. <b>ZCD2450-B-14</b>		
9. Performing Organization Name and Address <b>MFT Mobility Friction Technology Oberst Rodes vei 89b 1165 Oslo Norway</b>				10. PWGSC File No. <b>XSD-7-01054</b>		
				11. PWGSC or Transport Canada Contract No. <b>T8200-7-7540/001/XSD</b>		
12. Sponsoring Agency Name and Address <b>Transportation Development Centre (TDC) 800 René Lévesque Blvd. West Suite 600 Montreal, Quebec H3B 1X9</b>				13. Type of Publication and Period Covered <b>Final</b>		
				14. Project Officer <b>A. Boccanfuso</b>		
15. Supplementary Notes (Funding programs, titles of related publications, etc.) <b>Co-sponsored by NASA, the FAA, and the Aerodrome Safety Branch of Transport Canada</b>						
16. Abstract <p>This report is intended to provide background material for designers and users of braking slip measurement devices, with emphasis on topics related to comparison and harmonization of friction measurement devices.</p> <p>It describes different aspects of measuring braking slip friction on travelled surfaces, especially those found during weather changes on aerodrome movement areas in the winter. In practice, all types of surfaces and conditions are encompassed, ranging from bare and dry to pavements covered with precipitation deposits, and thus a year-round context is provided.</p> <p>The mechanics of various combinations of tire-surface interaction mechanisms are discussed. A step-by-step, parallel case presentation of a force-measuring friction device and a torque-measuring friction device highlights the difficulties of obtaining mechanical error-free measurements of braking slip friction.</p> <p>Models for the interaction between a braked tire and a surface are presented and discussed, as are several approaches to harmonization of friction measuring devices and ways in which harmonized results could be used to predict aircraft wheel-braking performance. Both the International Friction Index, as proposed by the World Road Association, and the International Runway Friction Index, as proposed by the Joint Winter Runway Friction Measurement Program, are briefly presented and discussed.</p> <p>The report suggests normalized friction measurements for the comparison of friction measurement devices and segmented runway condition maps to monitor friction at airports.</p>						
17. Key Words <b>Friction measurement device, tribometer, International Runway Friction Index, IRFI, International Friction Index, IFI, harmonization, braking slip friction, tire-surface friction</b>				18. Distribution Statement <b>Limited number of copies available from the Transportation Development Centre</b>		
19. Security Classification (of this publication) <b>Unclassified</b>		20. Security Classification (of this page) <b>Unclassified</b>		21. Declassification (date) <b>—</b>	22. No. of Pages <b>xxi, 90</b>	23. Price <b>Shipping/ Handling</b>



1. N° de la publication de Transports Canada TP 13837E		2. N° de l'étude 9555		3. N° de catalogue du destinataire	
4. Titre et sous-titre Friction Fundamentals, Concepts and Methodology				5. Date de la publication Octobre 1999	
				6. N° de document de l'organisme exécutant	
7. Auteur(s) A. Andresen et J.C. Wambold				8. N° de dossier - Transports Canada ZCD2450-B-14	
9. Nom et adresse de l'organisme exécutant MFT Mobility Friction Technology Oberst Rodes vei 89b 1165 Oslo Norway				10. N° de dossier - TPSGC XSD-7-01054	
				11. N° de contrat - TPSGC ou Transports Canada T8200-7-7540/001/XSD	
12. Nom et adresse de l'organisme parrain Centre de développement des transports (CDT) 800, boul. René-Lévesque Ouest Bureau 600 Montréal (Québec) H3B 1X9				13. Genre de publication et période visée Final	
				14. Agent de projet A. Boccanfuso	
15. Remarques additionnelles (programmes de financement, titres de publications connexes, etc.) Coparrainé par la NASA, la FAA et la Direction de la sécurité des aéroports de Transports Canada					
16. Résumé <p>Ce rapport, préparé à l'intention des concepteurs et utilisateurs d'appareils de mesure du frottement, résume l'état des connaissances sur le sujet, en insistant particulièrement sur la comparaison et l'harmonisation des divers appareils.</p> <p>Il aborde différents aspects de la mesure de la résistance au glissement de pneus lors du freinage sur une surface de roulement, notamment sur une chaussée aéronautique soumise à des conditions météorologiques fluctuantes en hiver. De fait, tous les types et états de surface sont étudiés, allant des chaussées dégagées et sèches aux chaussées contaminées par des précipitations : sont ainsi couvertes les conditions correspondant aux quatre saisons de l'année.</p> <p>Les chercheurs exposent les concepts mécaniques qui régissent les interactions au sein de diverses combinaisons pneu-chaussée. Ils présentent méthodiquement et en parallèle deux appareils de mesure du frottement, l'un fondé sur la mesure de la force, l'autre, sur la mesure du couple, et mettent ainsi en lumière la difficulté d'obtenir, à l'aide d'un appareil mécanique, des mesures justes de la résistance au glissement en freinage.</p> <p>Le rapport présente des modèles de l'interaction pneu-chaussée lors du freinage, de même que plusieurs façons d'envisager l'harmonisation des appareils de mesure du frottement. Il montre également comment les résultats obtenus à l'aide de ces appareils peuvent servir à prédire la performance en freinage d'un aéronef. Il présente enfin succinctement l'<i>International Friction Index</i> proposé par l'Association mondiale de la route et l'Indice international de la glissance des pistes proposé par le Programme conjoint de recherche sur la glissance des chaussées aéronautiques l'hiver.</p> <p>Le rapport suggère des mesures normalisées du frottement aux fins de la comparaison des appareils de mesure du frottement, de même que des plans de découpage des pistes en tronçons aux fins de la mesure de leur glissance.</p>					
17. Mots clés Appareil de mesure du frottement, tribomètre, Indice international de la glissance des pistes, IRFI, <i>International Friction Index</i> , IFI, harmonisation, résistance au glissement en freinage, adhérence pneu-chaussée			18. Diffusion Le Centre de développement des transports dispose d'un nombre limité d'exemplaires.		
19. Classification de sécurité (de cette publication) Non classifiée		20. Classification de sécurité (de cette page) Non classifiée		21. Déclassification (date) —	22. Nombre de pages xxi, 90
					23. Prix Port et manutention

## ACKNOWLEDGEMENTS

The team of people working together in the Joint Winter Runway Friction Measurement Program (JWRFMP) and on the Vehicle-Pavement Systems committee of The American Society for Testing and Materials (ASTM) have shared their ideas and research findings openly and frequently as work progressed on the common task to harmonize friction measures.

The authors of this report, Arild Andresen and James C. Wambold, consider themselves members of that team and extend an appreciation to the many other team workers that brought up ideas, supplied references, and provided engineering and research data that helped shape this report.

Professors John J. Henry and Charles E. Antle, both retired from Pennsylvania State University shared their lifelong experiences with friction measurement and statistical analysis. Walter Horn and Thomas J. Yager, from NASA Langley Research Center, related friction topics to past experiments and findings, and designed field tests to gain new knowledge. Jean-Claude Deffieux, of the French Civil Aviation Authority, and Armann Norheim, of the Norwegian Civil Aviation Authority, inspired the authors to include aspects of friction measurement important to providers and users of runway friction information.

During the course of the JWRFMP, several reports and papers were produced, many of which are referenced in this report.

The authors are indebted to Paul Carson, Transport Canada, for reviewing the report material and providing many valuable comments on the form and subject of the report, especially the mathematical presentation of physical modelling..

Most of all, the authors wish to extend their thanks to Al Mazur, Transport Canada, for sharing the visions of the authors and acknowledging the need to produce this report and, most importantly, to Angelo Boccanfuso for securing the funding for this project.

ASTM has acknowledged the work done by the JWRFMP by initiating standard development processes to run in parallel with the research program. The authors and several members of the research program are also key resources in the standards development processes.





## EXECUTIVE SUMMARY

Transport Canada commissioned MFT Mobility Friction Technology AS to author a report summarizing tire-surface friction knowledge as it applies to runway friction measurement. The report is in the form of a thesis and includes topics of tire-surface friction engineering with emphasis on comparison and harmonization of friction measurement devices. An overview of recent developments in tire-surface friction modelling and standard measures\* of friction is presented, including the International Friction Index and the International Runway Friction Index. Suggestions for new friction measurement techniques are outlined.

Friction measurement devices are also called tribometers. The friction that arises from the partial sliding or skidding of a tire on a surface is called braking slip friction.

Theoretical analysis of the mechanics of interaction between a braked tribometer wheel and a contaminated surface shows that the measured braking slip friction values are adversely influenced by any presence of loose or fluid winter-contaminants. Fluid or loose particle displacement drag, tire-rolling resistance and planing (water-, slush-, and snowplaning) introduce errors in the reported friction value. The best measuring performance is achieved on bare, base surfaces (i.e., pavement, ice and compacted snow with no additional cover of loose particles or fluid). When a cover of loose particles or fluid is present on a base surface, the combined adverse effect on the reported friction value increases with increasing travel speed of the tribometer.

Tribometers of different types exhibit different dynamic friction characteristics. When using a normal load on the wheel axis to calculate the friction coefficient, the reported friction value of a horizontal force-measuring tribometer will include errors from tire-rolling resistance, any displacement drag and planing. The reported friction value of a torque-measuring device includes no errors from displacement drag or tire-rolling resistance. In situations of planing or compaction of snow, the normal force has a ground reaction force from the braking slip area and a reaction force from the area where the tire is detached from the useful braking surface and rests on the fluid or snow. Since the ground reaction force in the braking slip area is smaller than the force on the wheel axis in such cases, the reported friction value can be conservatively low for either a force-measuring or torque-measuring tribometer.

Tribometers processes measuring signals with much noise, a well-known characteristic of braking slip friction. Non-uniformity of the surface is believed to be a major source for the variability of reported friction values. On rigid pavement the tribometer tire will yield and be the sacrificed part of the tire-surface interaction. On less rigid compacted snow or ice, the surface material often yields and becomes the sacrificed part of the tire-surface interaction.

Because of the variability in reported friction values, descriptive statistics should accompany a friction measurement to describe the quality of the measurement. These statistics are the average friction value, the number of samples used for calculating the average and the standard deviation of the sample values. With these three statistics, the standard error, coefficient of variation and confidence can be calculated.

The descriptive statistics vary with number of samples, and tribometers report average friction values based on different sample sizes. To compare the qualities of measurements, the descriptive statistics must refer to the same sample size for the same measured length of surface. To accommodate this, a scheme of normalized friction measures is suggested as follows: an average friction value is processed for every 10-m measured distance; an average friction value is reported for each 100-m distance together with the associated descriptive statistics for a fixed sample size of 10.

\* Unit of friction measurement

In recent years comparative field tests of several types of tribometers have revealed that repeatability of single tribometers and reproducibility of several tribometers of the same type, as a rule of thumb, is in the 0.05 friction coefficient range expressed as a standard error statistic. A single reported friction measurement for a 100-m distance, therefore, has an uncertainty of  $\pm 0.05$  friction coefficient. This poses a problem relative to current qualitative gradations of runway friction, such as the estimated braking action tables for winter contaminated runways published in guidelines by several aviation organizations. Each grade, such as Good, Medium-to-Good, Medium, etc., is defined for a 0.05 friction coefficient range. With the uncertainty of tribometers demonstrated, they are not capable of reliably distinguishing grades less than 0.10 friction coefficient.

The poor repeatability and reproducibility also poses a quality problem for the harmonization of tribometers of different types. As an approximation, a harmonization translation of a reported friction value of one device type to another has an uncertainty of  $\pm 0.05$  friction coefficient in 19 of 20 cases.

The World Road Association (PIARC) proposed in 1995 an International Friction Index (IFI) for use in surveys of pavement friction. The IFI acknowledges the speed dependency of braking slip friction on wet pavements and includes measurements of macrotexture. The IFI is in essence a method of harmonizing friction and texture measurement devices. The reference of harmonization is a virtual average performance of the participating devices in an extensive field-test program conducted in 1992. The IFI is a universal, two-parametric index with a friction number related to a chosen measurement slip speed of harmonization and a speed number related to macrotexture measurements. Both the American Society for Testing and Materials (ASTM) and the International Organization for Standardization (ISO) have developed standards for the IFI.

The Joint Winter Runway Friction Measurement Program and the ASTM have developed an International Runway Friction Index (IRFI) to become a common harmonized measure of friction for tribometers. Unlike the IFI, the IRFI does not acknowledge speed dependency of friction or influence by macrotexture. The IRFI uses a physical reference device to determine harmonization constants. The initial ASTM standard for IRFI was issued in 2000.

The report suggests including friction models in harmonization methods for tribometers. Different sets of friction model parameters define different surface classifications. Harmonization constants shall be determined and applied for each surface classification in an attempt to reduce the uncertainty of harmonized friction values.

## SOMMAIRE

MFT Mobility Friction Technology AS a été chargée par Transports Canada de produire un rapport résumant l'état des connaissances sur l'adhérence pneu-chaussée applicables à la mesure de la glissance des chaussées aéronautiques. Le rapport, qui se présente sous la forme d'une thèse, porte sur la technologie de la mesure de l'adhérence pneu-surface, en insistant particulièrement sur la comparaison et l'harmonisation des résultats obtenus avec divers appareils de mesure. Il fait le survol des derniers modèles d'adhérence pneu-chaussée mis au point et des mesures standard\* du frottement, présentant au passage l'*International Friction Index* et l'Indice international de la glissance des pistes. Il formule également des suggestions en vue de nouvelles techniques de mesure du frottement.

Les appareils de mesure du frottement sont aussi appelés tribomètres. La résistance offerte par le pneu lorsqu'il glisse ou dérape partiellement sur une chaussée est appelée résistance au glissement (ou frottement ou adhérence).

L'analyse théorique des principes mécaniques à la base de l'interaction entre la roue d'un tribomètre et une surface contaminée lors du freinage révèle que la présence de contaminants sous forme de particules libres ou de liquides nuit à l'adhérence de la roue. La traînée due au déplacement des liquides ou des particules libres, la résistance au roulement du pneu et le «planage» (sur l'eau, la bouillie neigeuse ou la neige) influent sur le coefficient d'adhérence enregistré. Les mesures les plus précises sont prises sur chaussée dégagée (c.-à-d. une chaussée sèche ou couverte de glace ou de neige tassée, mais exempte de particules libres ou de liquide). Lorsque la chaussée est mouillée ou recouverte de particules libres, le coefficient d'adhérence diminue d'autant plus que le tribomètre roule vite.

Différents types de tribomètres affichent différentes caractéristiques d'adhérence dynamique. Ainsi, lorsqu'on applique une charge normale à l'axe de la roue d'un tribomètre horizontal mesurant la force, le coefficient d'adhérence enregistré est entaché des erreurs attribuables à la résistance du pneu au roulement, à la traînée due au déplacement et au planage. Quant au coefficient d'adhérence enregistré par un tribomètre mesurant le couple, il ne comprend aucune erreur attribuable à la traînée due au déplacement ou à la résistance au roulement. Lorsque l'essai a lieu sur une chaussée mouillée ou couverte de neige tassée, la charge normale s'oppose à une force de réaction du sol dans la zone de glissement de freinage et à une autre force de réaction dans la zone où le pneu est en contact non pas avec la surface de freinage utile, mais avec la précipitation liquide ou la neige. Comme la force de réaction du sol dans la zone de glissement est plus faible que la charge exercée sur l'axe de la roue, il se peut que le coefficient d'adhérence enregistré par les deux types de tribomètres soit exagérément faible.

Les signaux traités par les tribomètres s'accompagnent d'un bruit important, une caractéristique bien connue de l'étude du frottement. La non-uniformité de la chaussée pourrait jouer un rôle important dans la variabilité des coefficients d'adhérence mesurés. Ainsi, sur une chaussée rigide, le pneu cède et devient l'élément sacrifié dans l'interaction pneu-chaussée. À l'inverse, sur une chaussée moins rigide recouverte de neige tassée ou de glace, c'est souvent le matériau présent sur la chaussée qui cède et devient ainsi l'élément sacrifié de l'interaction pneu-chaussée.

En raison de la variabilité des coefficients d'adhérence enregistrés, il importe, pour mieux juger de la qualité des résultats, de leur adjoindre des statistiques descriptives, soit le coefficient d'adhérence moyen, le nombre de valeurs (taille de l'échantillon) utilisées pour le calcul de la moyenne et l'écart type de la moyenne. Ces trois statistiques permettent de calculer l'erreur-type, le coefficient de variation et la confiance.

\* Unité de mesure du frottement

Les statistiques descriptives, notamment les coefficients d'adhérence moyens, varient selon la taille de l'échantillon. Or, pour pouvoir juger de la qualité des données, les statistiques descriptives doivent se rapporter à des échantillons de même taille découlant de l'étude d'une même longueur de chaussée. Il est proposé, à cet égard, un ensemble normalisé de mesures, soit un coefficient d'adhérence moyen par tronçon de 10 m, un coefficient d'adhérence moyen par tronçon de 100 m, et les statistiques descriptives connexes pour une taille d'échantillon fixe de 10.

Ces dernières années, des essais comparatifs sur le terrain de plusieurs types de tribomètres ont révélé que les résultats obtenus avec un même tribomètre (indicateurs de répétabilité) et avec plusieurs tribomètres du même type (indicateurs de reproductibilité) comportent une erreur-type de 0,05. Ainsi, une seule mesure de l'adhérence obtenue pour une distance de 100 m comporte un degré d'incertitude de  $\pm 0,05$ . Cela pose un problème pour ce qui est des gradations qualitatives actuellement utilisées pour décrire la glissance des pistes, comme les tableaux d'efficacité estimative des freins sur des chaussées hivernales contaminées, publiés par plusieurs organismes du monde de l'aviation. En effet, chaque gradation (Bonne, Moyenne à bonne, Moyenne, etc.) est définie en fonction d'une incertitude de 0,05 du coefficient d'adhérence. Ainsi, avec leur incertitude avérée, les tribomètres ne peuvent différencier de façon fiable des écarts inférieurs à 0,10 du coefficient d'adhérence.

Les piètres répétabilité et reproductibilité des résultats posent également un problème de qualité pour l'harmonisation des tribomètres de différents types. À titre d'approximation, l'application, à des fins d'harmonisation, d'un coefficient d'adhérence enregistré par un type d'appareil à un autre type d'appareil comporte une marge d'erreur de  $\pm 0,05$ , 19 fois sur 20.

L'Association mondiale de la route (AIPCR) proposait en 1995 un *International Friction Index* (IFI) devant servir aux études sur la glissance des chaussées. L'IFI reconnaît que sur une chaussée mouillée, la résistance au glissement en freinage dépend de la vitesse, et il comprend des mesures de la macrotecture. Essentiellement, l'IFI est une méthode qui permet d'harmoniser les appareils de mesure du frottement et de la texture. La donnée de référence, aux fins de l'harmonisation, est une performance moyenne, dite virtuelle, des appareils mis en oeuvre, mesurée au cours d'un programme d'essais de grande envergure mené en 1992. L'IFI est un indice universel, à deux paramètres, qui donne une valeur de frottement rapportée à une vitesse de glissement choisie, ainsi qu'une valeur de vitesse reliée aux mesures de la macrotecture. L'American Society for Testing and Materials (ASTM) et l'Organisation internationale de normalisation (ISO) ont toutes deux élaboré des normes relatives à l'IFI.

Le Programme conjoint de recherche sur la glissance des chaussées aéronautiques l'hiver et l'ASTM ont mis au point l'Indice international de la glissance des pistes (IRFI) dans le but d'en faire une échelle commune de valeurs d'adhérence pour les tribomètres. Contrairement à l'IFI, l'IRFI ne tient compte ni du lien entre l'adhérence et la vitesse, ni de l'effet de la macrotecture de la chaussée. L'IRFI utilise un appareil de référence pour déterminer les constantes d'harmonisation. La première norme ASTM visant l'IRFI a été publiée en 2000.

Le rapport suggère de fonder l'harmonisation des tribomètres sur des modèles du frottement. Différents ensembles de paramètres rattachés aux modèles définissent différentes catégories de chaussées. Des constantes d'harmonisation doivent être établies et appliquées pour chaque catégorie de chaussée, afin de réduire l'incertitude associée aux valeurs de frottement harmonisées.

# CONTENTS

- 1 Introduction 1**
- 1.1 Who is This Report For? .....1
- 1.2 Focus on Operational Friction Measurements at Airports .....1
- 1.3 The Research of Contaminated Travelled Surfaces.....2
- 1.4 The Friction Measurement Devices .....2
- 1.5 Focus on Braking Slip Friction .....3
- 2 Tribology System Elements 4**
- 3 The Nature of Braking Slip Forces 6**
- 3.1 Main Mechanisms of Braking Slip Friction.....6
- 3.2 Surface Shear Strength Limitation.....7
- 3.3 Simple Friction Models.....8
  - 3.3.1 Amontons Friction Model.....8
  - 3.3.2 Slip Speed and Slip Ratio.....9
  - 3.3.3 Friction as Function of Travel Speed and Slip Speed .....10
  - 3.3.4 Vehicle Braking Friction.....11
- 4 Mechanics of Tribometer Tire-Surface Interactions 12**
- 4.1 Mechanics of a Wheel in a Constant and Continuous Measuring Mode.....12
  - 4.1.1 Rolling Resistance.....12
  - 4.1.2 Applied Braking Force .....14
- 4.2 Contaminant Displacement Drag Force on a Free-Rolling Tire .....15
- 4.3 Combined Tire-Rolling Resistance, Displacement Drag and Braking Slip Forces .....17
  - 4.3.1 Friction Forces from Contaminant Dynamic Planing .....19
  - 4.3.2 The Nature of the Fluid Lift Force.....21
  - 4.3.3 The Moving Position of the Fluid Lift Force .....21
  - 4.3.4 Fluid Lift Effects on the Tire-Surface Friction When Free Rolling .....22
- 4.4 Tire-Rolling Resistance, Fluid Displacement Drag, Fluid Planing and Applied Braking...23

4.4.1	The Moving Position of the Fluid Lift Force for a Braked Tire .....	25
4.5	Forces in Loose Snow .....	25
4.5.1	Resistance from Separate Compacting and Displacement Drag Forces.....	26
4.5.2	Resistance from One Resultant External Dynamic Force.....	27
4.5.3	Variability of Friction Coefficients under Influence of a Resultant Dynamic Resistive Force .....	30
<b>5</b>	<b>Characteristics of Dynamic Contaminant Resistive Forces</b>	<b>38</b>
5.1	Resistance Force from the Compacting of Snow .....	38
5.2	The Compacting of Loose Snow with a Non-Braked Wheel.....	38
5.3	Dynamic Contaminant Planing Propagation.....	40
5.3.1	Fluid Planing with Different Tire Designs .....	40
5.3.2	Critical Planing Speed .....	42
5.4	Resistive Forces from Fluid Displacement Drag on Rigid Base Surfaces.....	42
5.5	Differences of Braking Slip Friction Between Rigid and Non-Rigid Surfaces.....	44
5.6	Contact Pressure .....	44
<b>6</b>	<b>Summary of Mechanics of Tire-Surface Friction</b>	<b>47</b>
<b>7</b>	<b>Variability of Friction Measures</b>	<b>48</b>
7.1	Descriptive Statistics.....	48
7.1.1	Average (Mean).....	48
7.1.2	Standard Deviation .....	48
7.1.3	Coefficient of Variation .....	49
7.1.4	Standard Error .....	49
7.1.5	Confidence Limits .....	50
7.2	Normalized Friction Measurements .....	51
7.3	Device Variability .....	51
7.4	Surface Variability.....	52
7.5	Variance in Friction Device Comparisons.....	53
7.5.1	Assumptions when Evaluating Friction Values.....	56
<b>8</b>	<b>Surface Classifications</b>	<b>57</b>

8.1	ICAO Deposit Codes.....	57
8.2	Frictional Characteristics of Surfaces .....	57
8.2.1	Base Surface and Surface Conditions .....	59
8.2.2	Grouping Friction Processes from Friction-Slip Speed Curves.....	59
8.2.3	Measuring Speed as a Variable .....	60
8.2.4	Measuring Speed and Slip Speed as Variables .....	61
<b>9</b>	<b>Runway Friction Mapping</b>	<b>62</b>
9.1.1	Average Friction Values .....	62
9.1.2	The Runway Grid as an Extended Measurement Tool .....	62
9.1.3	Runway Grid Geometry .....	63
9.1.4	Data Content of a Runway Grid Repository .....	63
9.1.5	Friction-Speed Relationships for Different Surfaces .....	64
<b>10</b>	<b>Modern Tire-Pavement Friction Models</b>	<b>66</b>
10.1	Penn State, PIARC and Rado Models.....	66
10.2	Three-Dimensional Modelling of Tire-Surface Friction .....	69
10.3	Comparison of Exponentially Modelled Friction Measurement Devices .....	74
<b>11</b>	<b>Standard Tire-Surface Friction Measurements</b>	<b>76</b>
11.1	The International Friction Index (IFI).....	76
11.2	The Harmonization Procedure.....	77
11.3	The International Runway Friction Index (IRFI).....	78
11.3.1	Some Design Requirements for the IRFI .....	79
11.3.2	Inhibiting Progress.....	79
11.4	An Architecture for the IRFI and the AFI.....	81
11.5	The ASTM E-2100-00 Ground Device Harmonizer .....	82
11.5.1	The Quality of the ASTM E-2100-00 Harmonizer.....	83
11.6	Other Ground Device Harmonizers .....	84
11.6.1	A Simple Modelling Harmonizer .....	84
11.6.2	A Hybrid Statistical and Modelling Harmonizer .....	85

11.7 Harmonization Reference .....	86
11.8 Information Flow of Harmonized Friction Values to Principal Users .....	87
References.....	89
Bibliography .....	90



# LIST OF FIGURES

- Figure 1 - Sample tribosystems for braking slip friction ..... 4
- Figure 2 - An exploded view of a tire-surface interface..... 6
- Figure 3 - Three theoretical sample compositions of major influences on braking slip ..... 7
- Figure 4 - Pairs of objects of same material of different size and weight having the same and constant coefficient of friction..... 8
- Figure 5 - Two wheels of different size and type on the same surface..... 9
- Figure 6 - A case of braking slip friction with automotive tires on a dry surface ..... 10
- Figure 7 - Rolling resistance force with a free-rolling tire at constant speed ..... 13
- Figure 8 - Forces and moments of a constant braked wheel on a clean and dry rigid surface ..... 14
- Figure 9 - Horizontal drag forces acting on a free-rolling friction tester tire due to fluid contaminant displacement ..... 16
- Figure 10 - Combined rolling resistance, drag and brake forces on a friction tester wheel in steady state ..... 18
- Figure 11 - Free-rolling tribometer wheel with fluid lift and drag ..... 20
- Figure 12 - A case of diminishing tire-rolling resistance force  $F_R$  as the planing propagates with increased speed..... 23
- Figure 13 - Braked tribometer wheel with fluid dynamic lift and displacement drag ..... 24
- Figure 14 - Reaction force system for a tribometer wheel in loose snow ..... 26
- Figure 15 - Reaction force system for a tribometer wheel in loose snow with surface material shear ..... 28
- Figure 16 - Variability of different definitions of reported friction coefficients with angle of dynamic resistive force..... 31
- Figure 17 - Variability with of different definitions of reported friction coefficients with magnitude of dynamic resistive force ..... 32
- Figure 18 - Braking slip friction coefficient as a function of magnitude and direction of resistive force from a contaminant deposit in a calculation example..... 33
- Figure 19 - Difference between a force and torque measuring tribometer braking slip friction coefficient as a function of magnitude and direction of resistive force from a contaminant deposit in a calculation example ..... 33
- Figure 20 - Difference between a force and torque measuring tribometer braking slip friction coefficient as a function of magnitude and direction of resistive force from a contaminant deposit in a calculation example ..... 34
- Figure 21 - An example of the significance of tire radius and position of ground reaction force in loose snow for a braking slip friction coefficient calculated with the ground reaction force as the vertical force..... 35
- Figure 22 - An example of the significance of tire radius and position of ground reaction force in loose snow for a braking slip friction coefficient calculated with static weight as the vertical force..... 35
- Figure 23 - An actual case of reported friction values by a combined force- and torque-measuring tribometer for natural fresh snow ..... 36
- Figure 24 - Resistive force due to compression of loose snow as influenced by initial snow depth and initial snow density [5]..... 39
- Figure 25 - Vertical displacement factor,  $k_{VD}$ , for a type VII aircraft tire as a function of initial snow depth and initial snow density according to [5] ..... 39
- Figure 26 - Two different fluid planing progress models used in study. Dark areas have base surface contact. Planing factors  $k_p$  indicated,  $k_p = 0$ , meaning no fluid planing ..... 41
- Figure 27 - Fluid film distribution in automotive tire footprint ..... 43
- Figure 28 - Theoretical fluid displacement drag force for a tire geometry equivalent to the ASTM E-1551 tire for a case with 3 mm water film and a case with 3 mm snow. The snow density is 30 percent of water. .... 43
- Figure 29 - Shear stress distribution in the contact patch during braking on a rigid surface ..... 45

Figure 30 - Friction due to adhesion by a rubber slider on a dry, rigid surface as a function of vertical contact pressure.....	45
Figure 31 - The slope correlation coefficient versus net contact pressure of friction measurement devices by [9] .....	46
Figure 32 - Sample data from wet pavement friction measurements showing <i>StdErr</i> as a function of number of samples. The average friction value was 0.66 and 0.68 for the surfaces with a high and low <i>StdDev</i> respectively. ....	49
Figure 33 - Sample data from wet pavement friction showing how the confidence range for a 95 percent confidence level may vary in two cases of <i>StdDev</i> as a function of number of samples. The average friction value was 0.66 and 0.68 for the surfaces with a high and low <i>StdDev</i> respectively. ....	50
Figure 34 - Proposed system of normalized friction measurements.....	51
Figure 35 - Average of 6 reported friction values for 12 tribometers of the same type at 65 km/h in self-wetting mode on a continuous track of 8 asphalt pavements each 100 m in length and of different asphalt recipe.....	52
Figure 36 - Surface variability expressed as average standard deviation versus macrotexture based on the test data of Figure 35.....	53
Figure 37 - A scatter chart of two friction devices that have measured on the same variety of ice and snow surfaces at speeds ranging from 40 to 90 km/h.....	54
Figure 38 - A scatter chart of two friction devices that have measured on the same variety of ice and snow surfaces at speeds ranging from 40 to 90 km/h.....	55
Figure 39 - A scatter chart of two friction devices that have measured on the same wet asphalt surfaces at 65 km/h.....	55
Figure 40 - Friction values for runway surface conditions.....	58
Figure 41 - Cross sections of travelled surfaces illustrating a suggested visual surface classification.....	59
Figure 42 - Characteristic friction values for variable- and fixed-slip measuring modes on different surfaces.....	60
Figure 43 - Simplified general relationships of friction with speed as variable for different conditions of a runway surface segment.....	61
Figure 44 - Empirical translation between variable-slip speed and fixed-slip friction relationships.....	64
Figure 45 - Sample distribution of friction-speed relationships for different surface types and conditions on a runway.....	65
Figure 46 - A sample actual runway friction profile of mixed conditions during a weather change with light precipitation, 2 hours after application of de-icer liquid.....	65
Figure 47 - A sample plot of friction model for the International Friction Index (IFI).....	67
Figure 48 - A sample Rado model plot.....	68
Figure 49 - A sample comparison between PIARC and Rado friction models.....	69
Figure 50 - Series of variable-slip measurements with an automotive tire at different measuring speeds on dry concrete pavement [13].....	70
Figure 51 - Friction as a function of slip ratio for different surfaces and conditions as measured by a variable-slip device at the same measuring speed 65 km/h.....	71
Figure 52 - Three-dimensional plot of friction versus travel speed and slip ratio for a sacrificial tire scenario.....	71
Figure 53 - Three-dimensional plot of friction versus travel speed and slip ratio for a sacrificial surface scenario.....	72
Figure 54 - Three-dimensional plot of friction versus travel speed and slip ratio for a smooth ice surface.....	73
Figure 55 - Fitted exponential friction-speed curves for two devices.....	75
Figure 56 - The power transform equation for the pair of exponential equations plotted in Figure 55.....	75
Figure 57 - Calibration constants for IFI are taken at a harmonizing slip speed of 60 km/h. The reference curve is named the Golden Curve. It is an average of all participating devices in the 1992 experiment. ....	78
Figure 58 - Many-to-many correlation of friction devices to aircraft. A small number of arbitrarily chosen aircraft types and friction devices are shown. ....	80

Figure 59 - Harmonizing to a common set of friction parameters for friction testers ..... 81

Figure 60 - Schematic of IRFI and AFI architecture and association with ASTM standards  
development ..... 82

Figure 61 - A schematic of the ASTM E-2100-00 Harmonizer..... 83

Figure 62 - A surface classification scheme based on exponential friction model parameters ..... 85

Figure 63 - Information flow of harmonized friction values ..... 88

**LIST OF TABLES**

Table 1 – ICAO Deposit Codes ..... 57



## LIST OF SYMBOLS AND ABBREVIATIONS

$A$	1) Calibration constant for the International Friction Index 2) Master-to-reference device calibration constant for the International Runway Friction Index
$A_D$	Area in the vertical plane associated with contaminant deposit displacement drag
$A_L$	Contact area between a tire and a fluid
$A_R$	Real contact area between a tire and a surface
$A_S$	Area of shearing contact between a tire and a surface
$B$	1) Calibration constant for the International Friction Index 2) Master-to-reference device calibration constant for the International Runway Friction Index
$C_D$	Coefficient of displacement drag
$CV$	Coefficient of variation
$\hat{C}$	Shape factor in the Rado friction model (log normal)
$E$	A force, or a sum of forces, that constitute an error term in a measured braking slip force
$F$	Force
$F_B$	Force due to braking slip friction
$F_C$	Horizontal force due to compacting of snow or slush
$F_{CG}$	Reaction force in the tire-surface contact area due to horizontal compacting force
$F_{CL}$	Lift force due to compacting of snow or slush
$F_{CV}$	A resultant force being the sum of compaction and vertical displacement forces
$F_D$	Force resulting from positive displacement of fluid or plastic material in the frontal area of a tire
$F_{DG}$	Reaction force in the tire-surface area due to contaminant displacement drag
$F_E$	Resultant dynamic contaminant deposit force
$F_G$	Reaction force from the ground
$F_L$	Lift force due to dynamic fluid viscous resistance (Petroff's equation)
$F_{LG}$	Reaction force in tire-surface contact area due to dynamic fluid lift or compacting lift
$F_M$	The horizontal force measured by a friction measuring device at the wheel axis
$F_{MD}$	Reaction force at a wheel axis due to contaminant displacement drag
$F_R$	Force due to pneumatic tire rolling resistance
$F_S$	Resultant resistive reaction force in the tire-surface contact area
$F_W$	Applied vertical force on a wheel axis, equal to a device mass multiplied by the gravity constant, or a controlled, vertically applied force
$F_X$	Force applied at the wheel axis in direction of the x-axis (direction of travel)
$I$	Angular moment of inertia
$L$	Length

$M$	Moment
$M_B$	Applied brake moment about a wheel axis
$MTD$	Mean texture depth
$S$	Slip speed
$S_C$	Critical slip speed value in a Rado friction model (log normal friction model)
$S_P$	Speed number of the PIARC friction model or the International Friction Index
$StdErr$	Standard Error
$StdDev$	Standard deviation
$T_M$	The moment measured by a friction measuring device about the wheel axis
$T_X$	Texture measurement, generic
$V$	Travel speed
$V_B$	Tangential speed of a braked wheel in the tire-surface contact area
$V_C$	Critical planing speed
$V_0$	Speed constant
$a$	<ol style="list-style-type: none"> <li>1) Horizontal distance between a point of application of the vertical ground reaction force and vertical line through the wheel axis</li> <li>2) Calibration constant for texture measurement with the International Friction Index</li> <li>3) Local device-to-master device calibration constant for the International Runway Friction Index</li> <li>4) Zero intercept parameter for exponential friction model</li> <li>5) Longitudinal acceleration</li> </ol>
$b$	<ol style="list-style-type: none"> <li>1) Horizontal distance between vertical through the wheel axis and point of application for a dynamic lift force</li> <li>2) Calibration constant for texture measurement with the International Friction Index</li> <li>3) Local device-to-master device calibration constant for the International Runway Friction Index</li> <li>4) Speed parameter for an exponential friction model</li> </ol>
$c$	Vertical distance between a tire-surface contact plane and a point of application for a resultant dynamic contaminant deposit force
$g$	Gravitational acceleration constant
$k_C$	Compacting resistance factor
$k_L$	Dynamic fluid lift coefficient
$k_P$	Fluid planing factor
$k_{PB}$	Braked wheel planing ratio
$k_{PL}$	Dynamic fluid lift coefficient including deflected tire radius and tire-surface contact area

$k_{VD}$	Vertical displacement factor
$l$	Length of a tire-surface contact area
$n$	Number of data points or measurements, sample size
$r$	Deflected tire radius
$t$	Contaminant deposit thickness
$w$	Width of the tire-surface contact area
$\alpha$	Angle
$\lambda$	Slip ratio, $S/V$
$\gamma$	Specific gravity
$\mu$	1) Friction coefficient as the ratio of a horizontal force to a vertical force in the tire-surface contact area. 2) A reported friction value of a tribometer.
$\mu_{10}, \mu_{100}$	Average coefficient of friction over a 10 m or 100 m measured distance
$\mu_B$	Braking slip friction coefficient, $F_B/F_W$
$\mu_L$	A reported friction value of a large tribometer
$\mu_{peak}$	A maximum or peak friction coefficient value in a variable-slip measurement
$\mu_R$	Tire-rolling friction coefficient, $F_R/F_W$
$\mu_S$	A reported friction value of a small tribometer
$\rho$	Contaminant fluid or particle mass density
$\sigma$	Normal stress or contact pressure
$\sigma_S$	Normal stress in the shear area of a tire-surface contact patch
$\tau_{ult}$	Ultimate shear stress of a surface material
$\nu$	Dynamic viscosity
$\omega$	Angular velocity
$\omega_B$	Angular velocity of a braked wheel
<i>ABS</i>	Antilock Braking System
<i>AFI</i>	Aircraft Friction Index
<i>ASTM</i>	American Society for Testing and Materials
<i>CRFI</i>	Canadian Runway Friction Index
<i>ICAO</i>	International Civil Aviation Organization
<i>IFI</i>	International Friction Index
<i>IRFI</i>	International Runway Friction Index
<i>ISO</i>	International Organization for Standardization

<i>JB</i>	James Brake Index
<i>JWRFMP</i>	Joint Winter Runway Friction Measurement Program
<i>NASA</i>	National Aeronautics and Space Administration
<i>PIARC</i>	Permanent International Association of Road Congresses (The organization has changed its name to World Road Association (PIARC))
<i>SAE</i>	Society of Automotive Engineers
<i>SNOWTAM</i>	Snow and Ice Notices to Airmen (ICAO form)



# 1 INTRODUCTION

## 1.1 Who is This Report For?

This report was undertaken as a theoretical background study to provide the people working together in the Joint Winter Runway Friction Measurement Program (JWRFMP) with a friction engineering reference text. Although the generated friction phenomenon between a braked wheel and a travelled surface may be covered in many different textbooks of science and engineering, no single source has been found that is dedicated to the measurement of braking slip friction as practised by aviation and highway administrations.

There are hundreds of research papers that report on various aspects of braking slip friction. This report does not purport to reflect an overview or summary of findings from a literature study. Rather, it is a collection of topics that were visited by the authors during planning of field tests, analysis of collected data and design work for a harmonized unit of friction measure, mainly as part of the JWRFMP and the standards development process within American Society for Testing and Materials (ASTM) Committee E17 on Vehicle-Pavement Systems.

The report covers elementary mechanics, dynamic influences on friction by winter contaminants, physical modelling of friction, elements of applied statistics, variability of friction measures and standard friction measures. Since the treatment of these topics seeks to establish sound ways of comparing and harmonizing friction measurements, some aspects may require further investigation or careful evaluation before they are fully accepted in the field of tire-surface friction measurement.

This report is intended to serve as a guide or discussion text for researchers, tire-surface measurement method designers, equipment manufacturers and operators in the field of measuring braking friction by public service regulators, aircraft operators and other users of runway friction information.

## 1.2 Focus on Operational Friction Measurements at Airports

The JWRFMP has, in recent years, conducted research to bring about a better understanding of braking friction and the ways of measuring it for the needs of the international aviation community. The focus of the JWRFMP was on winter conditions of runways where safety of the travelling public is at the highest risk. This is why friction measurement services are offered at many airports during the winter.

The capability of the runway to interact with the aircraft landing wheels to provide sufficient directional control below minimum air speed and sufficient wheel braking effect for landing and accelerate-stop manoeuvres is critical for safe operations.

However, the quality of the friction measurements has been questioned for uniformity in reported friction values for the same runway conditions and relevance to predicting aircraft braking performance. On the one hand, all sectors of the air transport community recognize the need for consistent and reliable information about the runway operational characteristics, including frictional properties. On the other hand, aviation regulators, aircraft manufacturers and others have raised a question as to whether current friction measurement practices truly contribute to the overall safety for aircraft ground operations.

Aircraft pilots using airports during winter continue to demand friction measurements as indispensable information for their work. The pilots experience a variance in reported friction numbers from different airports for the same runway conditions. A major reason for this variance

is the use of different types of friction measurement devices and different measurement practices at different airports. Although in theory a friction coefficient by definition is a dimensionless ratio of a horizontal resistance force to motion to a vertical load force, in practice the reported friction coefficients have different proprietary units of measure of friction.

Bringing different types of standard friction measurement devices to report to a common standard unit of measure is called harmonization. Harmonization of the friction measurements across all devices and practices will greatly benefit the pilot as an end user of friction measurements.

This report addresses aspects of friction measurement of travelled surfaces that can affect the design and practice of harmonization methods.

### **1.3 The Research of Contaminated Travelled Surfaces**

Wheel braking on bare pavement, dry or wet, has been heavily researched with regard to slip friction. From this point on, "slip friction" will be used in this report to clearly distinguish braking friction with tires from classical static friction. Travel speed, degree of braking, tire type and surface texture are established parameters influencing the braking slip friction.

Hydroplaning is an example of a well researched phenomenon on wet pavement under summer conditions. The phenomenon of hydroplaning, whereby a tire loses contact with the rigid ground and results in loss of ground control forces for a vehicle, has caused many accidents, some of which have resulted in the loss of human lives. NASA Langley Research Center was instrumental in work that identified the phenomenon, researched the interaction between water on pavement and tires, and engineered solutions to the problem. Grooved pavements of runways, monitoring of pavement macrotexture and rubber deposits, and reporting of rutting and standing water are airport practices directed at preventing hydroplaning from occurring. The critical hydroplaning speed, a characteristic speed below which vehicle operation is considered safe, can be predicted with engineering equations that were developed by NASA [1].

Wheel braking on runway surfaces under winter conditions has been researched to a lesser degree. The many different types of surfaces and conditions in the winter add complexity to the research.

### **1.4 The Friction Measurement Devices**

A number of different types of devices have been invented and deployed at airports to provide information about the runway surface frictional characteristics. Few devices have been designed specifically for predicting aircraft wheel braking performance. These devices have to meet demands for ease of use, low cost of purchase and maintenance, consistency of measured results and reliability of operation. Devices that measure acceleration during a change of velocity or that measure force for a continuous braked wheel have become very popular.

In this report the focus is on the common characteristics of devices rather than on the individual device types used for friction measurement. The goal is to establish a basis for harmonization of their outputs.

The friction measurement devices in use at airports can be grouped into three families.

1. Fixed slip testers that have a fixed and continuous level of applied braking on the measuring wheel.
2. Variable-slip testers that have a variable controlled level of braking, usually with a governing time function that is repeated in continuous cycles.

3. Decelerometer testers, where the brakes of the host vehicle are applied sufficiently hard to lock the wheels and retard the vehicle for a short distance and time. The vehicle is accelerated to the same initial speed before another deceleration is initiated.

The braking slip testers (both fixed and variable) are typically outfitted with strain gauges to measure the following:

- one force parallel with the surface, using the static weight as the normal load;
- two forces, one parallel with the surface and one normal to the surface;
- one torque measurement of the wheel braking moment using the static weight as the normal load; or
- combination of force and torque measurements.

## **1.5 Focus on Braking Slip Friction**

Measurements of friction as reported by friction testers are really aggregated measurement of different forces induced by motion that are present in variable quantities for different pairs of braked wheels and surfaces. The purpose of braking a wheel is to make controlled use of what may be called the braking slip friction.

Other forces induced by the motion are not controllable and constitute unwanted influences on the braking slip friction. The rolling resistance stems from the mechanics of the rolling tire. Contaminant displacement drag by water, snow and slush resists the movement of the vehicle and are sensed by a tire. Contaminant fluid or loose particles can detach the tire from the rigid surface interacting with it to provide braking slip forces. This fluid film can create viscous lubrication.

On winter-contaminated runways, all of these phenomena can be present in different mixes.

Several other resistive forces can be important to the stopping of a vehicle. Aerodynamic drag, impingement drag, and engine reverse thrust are examples of non-frictional stopping forces. Discussion regarding the the stopping of a vehicle is outside the scope of this report; the reader is referred to textbooks on vehicle dynamics that cover stopping a vehicle.

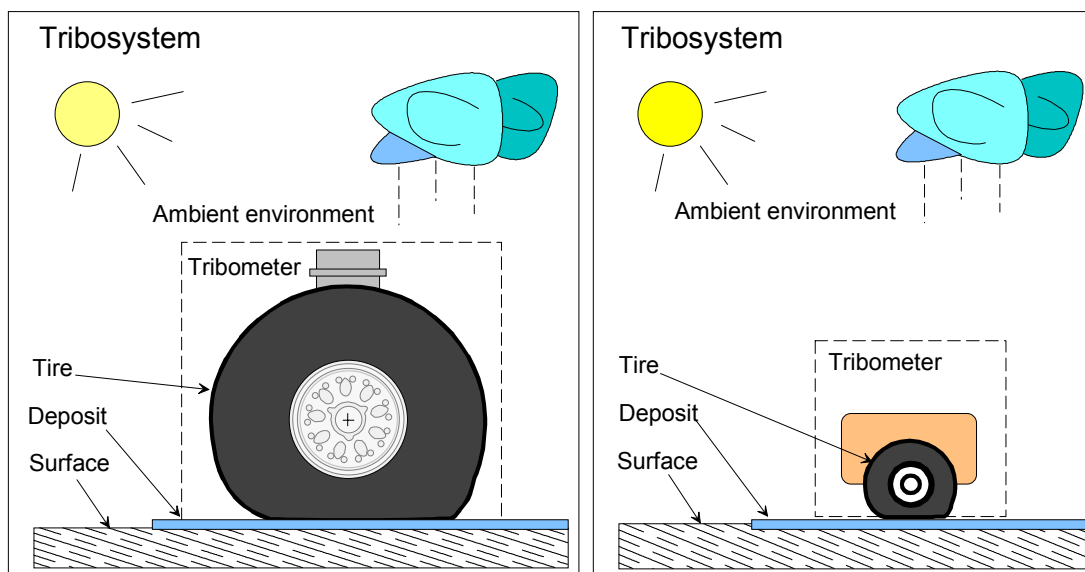
## 2 TRIBOLOGY<sup>1</sup> SYSTEM ELEMENTS

The complexity of tire-surface interaction can be overwhelming. Analysing the interaction in the context of a tribology system offers the benefit of a common, structured approach.

Tribology, as defined by Bhushan [2], is the science and technology of interacting surfaces in relative motion and of related subjects and practices. Friction, wear and lubrication are the disciplines associated with tribology. Braking slip friction in tire-surface interactions qualifies as a discipline within tribology.

Two tribological system models are illustrated in Figure 1. Tire, surface, deposit and ambient environment are tribo-elements. The machines to detect and report the braking slip friction with the mounted tires are tribometers.

For travelled winter surfaces, a note should be made about the changing role of a deposit. In the case of snow precipitation, the fresh snow may start out as a deposit on a pavement surface. The rolling wheel will displace and compress it, if it is compressible. As the layer thickness of the deposit increases, and assuming its density and plasticity are such that it compacts under a rolling wheel, the deposit eventually becomes a surface when rolled over by the wheel. It is a new surface when no more of the underlying pavement surface is in contact with the tire. As the precipitation continues, a snow deposit builds on the compacted snow surface.



Aircraft landing gear braking on a runway surface

Surface friction measurement device

**Figure 1 - Sample tribosystems for braking slip friction**

Since a feedback-controlled braked vehicle wheel also indirectly monitors and applies information about the braking slip friction, the term tribometer can be applied for vehicle wheel systems as well as friction measurement devices.

In this report, the term tribometer is used for a friction measurement device, a friction tester or a vehicle surface-tire system.

<sup>1</sup> From Greek *tribos*, literally the science of rubbing, as revived by Jost in 1966.

From a tribological system point of view, the braking slip friction is a system output. For each unique tribosystem, the braking slip friction will have a theoretical unique performance characteristic determined by the characteristics of the tribo-elements and the operating mode of the tribometer, such as load, travel speed and degree of braking.

Studies of performance of several similar tribosystems may conclude that there are some common performance characteristics, but studies of one tribosystem should not be used to generalize about other or dissimilar systems.

The tribosystem approach suggests a classification of each of the tribo-elements to achieve a manageable number of unique systems to work with in research as well as real-life applications.

### 3 THE NATURE OF BRAKING SLIP FORCES

#### 3.1 Main Mechanisms of Braking Slip Friction

Although the mechanisms of braking slip friction is not fully understood, the process is by many experts regarded as a composition of three main elements:

1. Adhesion,
2. Hysteresis,
3. Shear (wear, tear).

Figure 2 depicts these mechanisms in the tire-surface interface. The shear is indicated for a non-rigid surface material only.

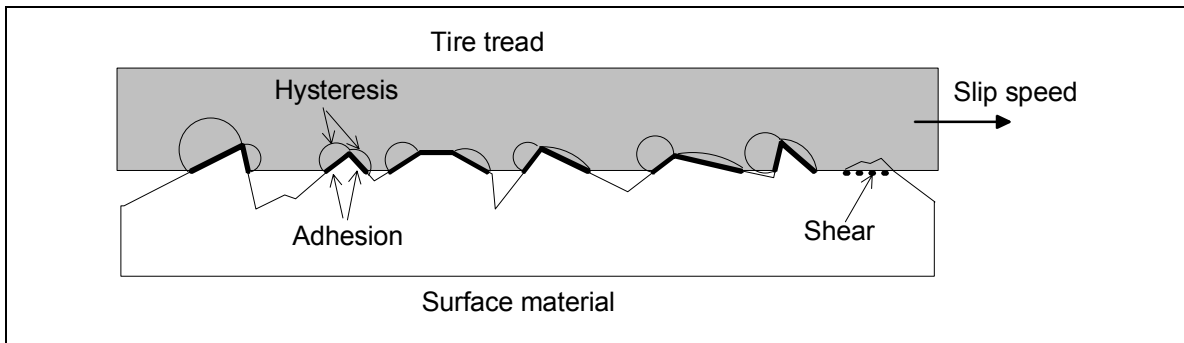


Figure 2 - An exploded view of a tire-surface interface

The braking slip force,  $F_B$ , can be viewed as a sum of three terms:

$$F_B = F_{adhesion} + F_{hysteresis} + F_{shear} \quad (1)$$

Surface texture influences all three mechanisms. The adhesion force is proportional to the real area of adhesion between tire and surface asperities. The hysteresis force is generated within the deflecting and visco-elastic tire tread material and is a function of speed. The shear force is proportional to the area of shear developed. Generally, adhesion is related to micro texture whereas hysteresis is mainly related to macrotexture. For wet pavements, adhesion drops off with increased speed while hysteresis increases with speed, so that above 90 km/h, the macrotexture has been found to account for over 90 percent of the friction. In the case of winter friction on snow and ice, the shear strength of the contaminant is the limiting factor.

Figure 3 depicts typical compositions of the braking slip friction mechanisms for two different surfaces interacting with the same tire. The pie chart on the left depicts a rigid surface such as a dry, bare pavement. The pie chart in the middle depicts a wet pavement. The pie chart on the right depicts a non-rigid surface material.

For a tire tread in contact with a rigid surface, the shear force is usually regarded as small. Adhesion and hysteresis make up 80 to 90 percent of the braking slip force. Pieces of tire tread are torn off when interfacing with a rigid surface. The tire is therefore called the sacrificial part of the braking slip friction process.

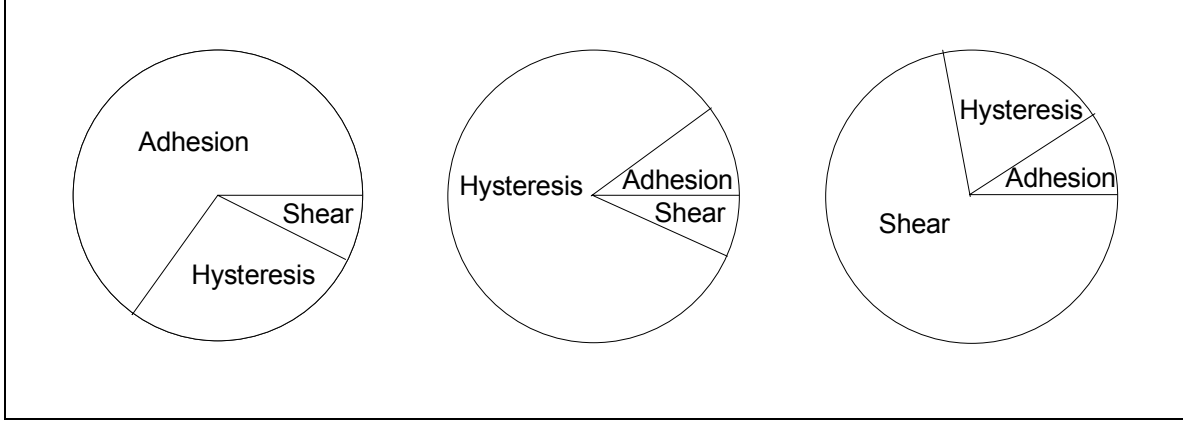


**Figure 3 - Three theoretical sample compositions of major influences on braking slip**

A significant shear force contribution implies that the sacrificial component is being sheared. In other words, the shear force is proportional to the product of the ultimate shear stress of the surface material and the real area of shearing contact.

Because of the markedly different compositions of braking slip mechanisms for rigid versus non-rigid surfaces, a question is raised whether the braking slip process can be considered sufficiently uniform for different compositions to be included in the same comparison of friction testers. Intuitively, the nearly same compositions of braking slip mechanisms would produce the best correlations. Thus, comparison of devices on compacted or rolled snow would differ from comparisons on pavement.

### 3.2 Surface Shear Strength Limitation

Rewriting (1) in the form of a braking slip friction coefficient, (i.e., dividing all terms by the vertical force,  $F_W$ ), we have

$$\mu_B = \frac{F_B}{F_W} = \frac{F_{adhesion}}{F_W} + \frac{F_{hysteresis}}{F_W} + \frac{F_{shear}}{F_W} \quad (2)$$

Multiplying the nominator and denominator by the area of shearing contact,  $A_S$ , the shear term in (2) can be expanded and transformed to

$$\frac{F_{shear} \cdot A_S}{F_W \cdot A_S} = \frac{\tau_{ult}}{\sigma_S} \quad (3)$$

where  $F_{shear}/A_S$  is the ultimate shear stress,  $\tau_{ult}$ , and  $F_W/A_S$  is the normal stress,  $\sigma_S$ . A fine point here is that the shear area is only a part of the total real contact area, as the full vertical load is distributed on both the shearing area and any adhesion area. But as the adhesion area becomes smaller, the vertical load is fully absorbed by the normal stress of the shear area, as written.

If the adhesion and hysteresis parts diminish relative to the shear in a given friction process, the braking slip friction approaches a measure of shear strength of the surface material as a function of the normal stress, also called the contact pressure.

$$\mu_B \approx \frac{\tau_{ult}}{\sigma_S} \quad (4)$$

Since friction measurement devices operate with a fixed vertical force, the absence of adhesion and hysteresis components would mean that the friction device would measure the ultimate shear strength of the non-rigid surface material as indicated in the following equation:

$$\mu_B \approx \text{constant} \cdot \tau_{ult} \quad (5)$$

If it can be assumed that the shear strength of a certain winter contaminant material is nearly constant, it may be possible to predict the ultimate braking slip friction for a tire to a certain extent on basis of recognition of the winter surface materials and the ambient conditions. The problem with this idea is the lack of classification and methods for classifying winter contaminants as travelled surfaces, not to mention that tire contact pressure improves the shear strength and would not be accounted for with this method.

### 3.3 Simple Friction Models

#### 3.3.1 Amontons Friction Model

The simplest friction model for two objects in contact and undergoing opposing movement is the familiar Amontons<sup>2</sup> friction model. It states that the pulling force required to sustain an opposing motion of a pair of interfacing objects is directly proportional to the perpendicular contact force. This pulling force is called the friction force and is independent of the apparent contact area. The factor of proportion has been named the coefficient of friction,  $\mu$ . In Figure 4, the perpendicular contact force is the weight of the block,  $F_W$ . The Amontons equation is

$$F = \mu \cdot F_W \quad (6)$$

The friction is a measure of the resistive interaction of the interfacing objects. The friction is a characteristic of the two objects. The Amontons equation works best for solid objects.

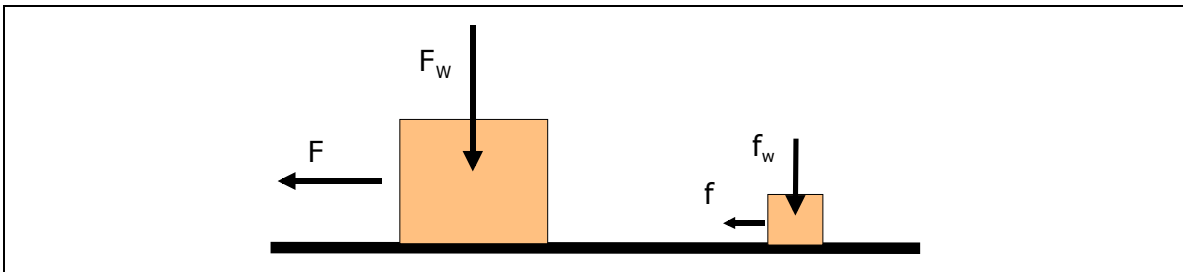


**Figure 4 - Pairs of objects of same material of different size and weight having the same and constant coefficient of friction**

This friction model is commonly used to estimate the force required to sustain the opposing motion when the perpendicular contact force and the friction coefficient for the interfacing materials are known.

If the Amontons model holds true equally well both for the friction measurement device and the aircraft tire interaction with the runway, a friction coefficient acquired with the ground friction measurement device could be applied to the aircraft wheel (see Figure 5).

<sup>2</sup> Guillaume Amontons, French physicist, 1699.



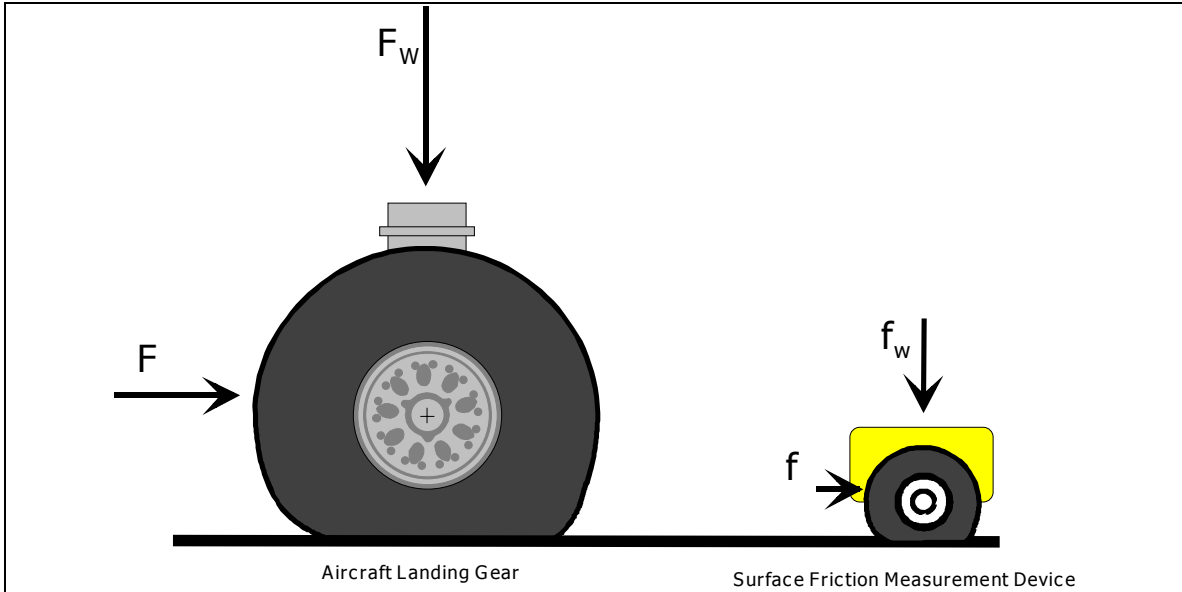


**Figure 5 - Two wheels of different size and type on the same surface**

In the interaction between a pneumatic tire and a surface, dependencies on many parameters are encountered for the friction coefficient. This makes the Amontons friction model invalid for application with pneumatic tires. It is evidenced by the fact that different types of friction measurement devices report different values of the friction coefficient when measuring the same surface. In essence, this is the reason why it is necessary to transform friction values to a common unit of measure. It must be acknowledged that each type of device equipped with a tire has its own proprietary set of reported numbers expressing friction.

There are several reasons for this diversity. The flexible tire object manufactured from visco-elastic materials is a cause of non-linearity. The irregularity of the surface, called texture, is another major factor. Different tire-surface pairs exhibit different non-linearity characteristics of friction. Wet pavement with low texture content against a bald tire tread, for example, will have a pronounced reduction in the coefficient of friction as travel speed increases.

Friction is a phenomenon of surfaces in contact under opposing motion. The relative motion is called slip speed.

### 3.3.2 Slip Speed and Slip Ratio

The difference in tangential speed for a point on the tire circumference in the contact area when it is free-rolling versus braked at a constant travel speed of the wheel axis is called slip speed. The tangential speed for a free-rolling tire is equal to the travel speed. When the tire is braked, its tangential speed is less than the travel speed, as the travel speed is kept constant.

When  $V$  is the travel speed and  $V_B$  is the tangential speed of the tire when braked, the slip speed,  $S$ , is  $V - V_B$ . The tangential speed is the rotational speed,  $\omega$ , multiplied by the deflected tire radius,  $r$ .

$$S = V - V_B = \omega \cdot r - \omega_B \cdot r = 1 - \frac{\omega_B}{\omega} \quad (7)$$

By measuring the rotational speeds of the tire in free-rolling mode,  $\omega$ , and braked mode,  $\omega_B$ , the slip speed can be calculated with (7).

The ratio of the slip speed to the travel speed is called a slip ratio,  $\lambda$ . It can be expressed as

$$\lambda = \frac{S}{V} = \frac{V - V_B}{V} = 1 - \frac{V_B}{V} \quad (8)$$

### 3.3.3 Friction as Function of Travel Speed and Slip Speed

Figure 6, which is based on a plot in [3], illustrates how braking slip friction can vary with travel speed and degree of braking, in terms of slip ratio.

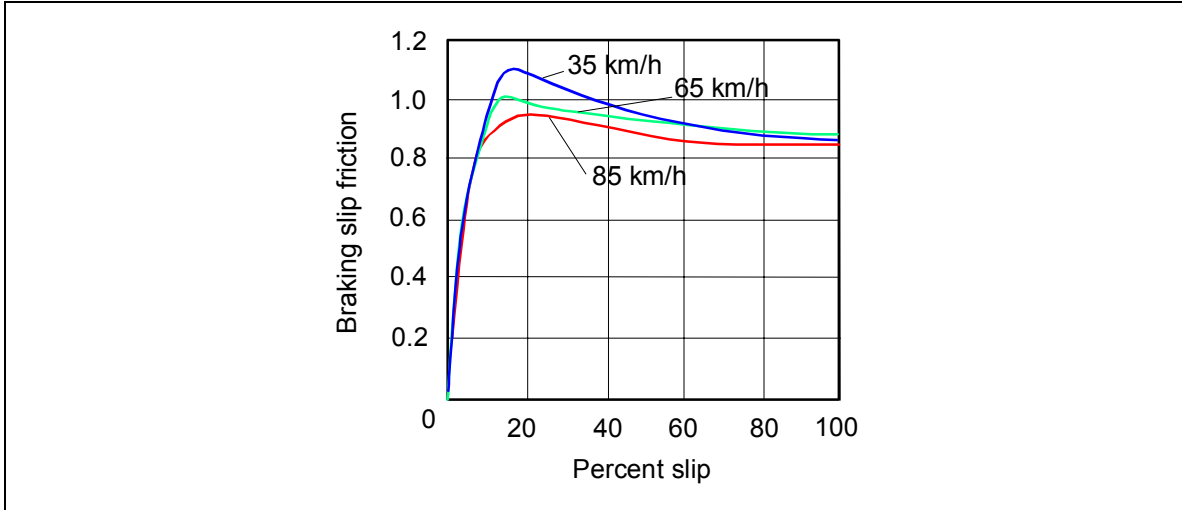


Figure 6 - A case of braking slip friction with automotive tires on a dry surface

Figure 6 suggests that a simplified, universal friction model for tire-surface object pairs can be expressed with a speed variable and a degree of braking called slip speed. With reference to Figure 5, where  $F_w$  and  $f_w$  are the weights of the vehicles on the wheels, the resistive forces for each tire-device configuration are

$$F(S, V) \approx \mu_L(S, V) \cdot F_w \quad (9)$$

and

$$f(S, V) \approx \mu_S(S, V) \cdot f_w \quad (10)$$

Since different friction measuring tires measure different friction values because of differences in contact area, rubber compound and other parameters, then

$$\mu_L(S, V) \neq \mu_S(S, V) \quad (11)$$

Therefore,

$$F(S, V) \neq \mu_S(S, V) \cdot F_w \quad (12)$$

There are circumstances in which the friction has negligible influences of travelling speed and degree of braking, but for a universal friction model those circumstances are special cases.

To circumvent (12), a frequent tactic is to fix the measuring speed and slip speed and compare the device-tire configurations at those speeds.

### 3.3.4 Vehicle Braking Friction

When braking a vehicle to stop from low speeds on a level surface, the braking slip friction force generated in the tire-surface interaction equals a decelerating force acting on the vehicle mass:

$$F_{braking} = F_{deceleration} \quad (13)$$

The applied braking force is equal to the deceleration force of the vehicle body mass according to Newton's law:

$$\mu \cdot F_W = \frac{F_W}{g} \cdot a \quad (14)$$

where  $g$  is the gravitational constant and  $a$  is the deceleration. Simplifying the expression, the friction coefficient is

$$\mu = \frac{a}{g} \quad (15)$$

This is a popular relationship used in determining the average friction coefficient (over the speed range) by measuring the deceleration of the vehicle. It is also frequently used in rough estimates of the average braking performance of vehicles in terms of deceleration on a surface, assuming the friction coefficient is valid for the vehicle-surface pair.

At higher speeds, or when better accuracy is required, the braking equation can include other resistive terms such as aerodynamic resistance, longitudinal slope of the surface, displacement drag from liquid, fluid or plastic materials, impingement drag on the vehicle body from loose surface material, hydroplaning effects, brake efficiencies, weigh-in-motion and other parameters. Since these effects are not braking slip friction by nature, they must be assessed and used to correct a measured deceleration value to determine a braking slip friction coefficient. Or, when modelling the stopping of a vehicle, the effects of non-friction influences must be properly included.

## 4 MECHANICS OF TRIBOMETER TIRE-SURFACE INTERACTIONS

To understand the braking slip friction processes on a macroscale, it is helpful to look at the mechanics of the interaction between a braked wheel with a pneumatic tire and different surface types and conditions.

The material covered here is general. An actual tribometer design will have a unique geometry and a unique suspension that will require its own unique elaboration of mechanics. A distinction is made between force-measuring devices and torque-measuring devices. The different features of these two groups of devices are highlighted. Intermittent or spot measuring tribometers are not fully addressed in this report.

In this report, torque refers to measured moments transmitted by an axle. Applied torque on an axle to produce braking is referred to as an applied moment.

The reader is referred to the list of suggested reading in the bibliography for more detail.

### 4.1 Mechanics of a Wheel in a Constant and Continuous Measuring Mode

Continuously measuring friction measurement devices operate at a constant travel speed. Furthermore, fixed slip devices have no angular acceleration of the measuring wheel. Therefore, fixed slip continuous friction measurement devices may be studied in steady-state equilibrium.

Sections 4.1.1 through 4.4.1 treat individual aspects in a cumulative manner, starting with a free-rolling tire, then adding drag, planing from a fluid contaminant and, finally, brake actuation.

#### 4.1.1 Rolling Resistance

Even when free-rolling on a hard, non-contaminated surface, there is a resistive force to the tire movement. This is due to the natural and characteristic deflection of a pneumatic tire when rolling. Figure 7 shows the forces acting on a wheel and tire. The host vehicle pulls the tribometer at a constant speed with force  $F_X$ . The normal load on the measuring wheel is  $F_W$ .

A small longitudinal tire slip force in the footprint supports the deflection work. As a result, the normal pressure distribution becomes uneven, such that the resultant normal force (centre of pressure) from the ground,  $F_G$ , is leading the vertical through the wheel centre, and thereby creates a balancing resistive moment. The distance  $a$  by which the resultant force is leading the wheel axle is increasing with accelerating travel speed.

The rolling resistance moment,  $F_G \cdot a$ , must be opposed with a moment,  $F_R \cdot r$ , applied about the wheel axis, if the wheel is to maintain a constant rotation and travel speed typical of continuous friction measurement devices. The wheel in Figure 7 can only produce this opposing moment by tire slip in the contact area when wheel-bearing resistance is disregarded. The surface is reacting to the slip with the force  $F_R$ . If the surface is incapable of sustaining this slip, the wheel will not rotate. It will instead slide in its load-deflated state. This rarely happens, since the attainable friction force in all practical cases is greater than  $F_R$ .

Summation of the moments about the wheel axis yields

$$F_G \cdot a - F_R \cdot r = 0 \tag{16}$$

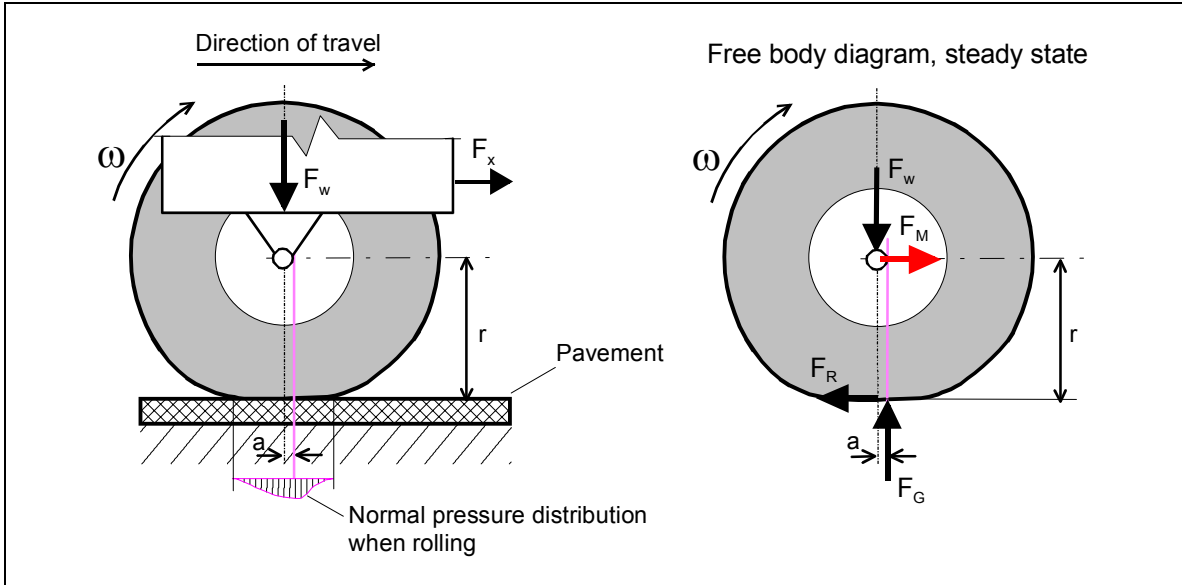


**Figure 7 - Rolling resistance force with a free-rolling tire at constant speed**

There is no torque transmitted over the wheel axle to other shafts or axles. A torque-measuring tribometer is designed to measure the axle torque and therefore would measure zero.

Solving for  $F_R$ ,

$$F_R = \frac{a}{r} \cdot F_G \quad (17)$$

Equation (15) is a definition of tire rolling resistance. The resistive slip force,  $F_R$ , is equal to the ground reaction force,  $F_G$ , multiplied by a ratio of geometric parameters,  $a/r$ .

In this scenario  $F_G = F_W$ , and therefore by substitution in (15), the tire rolling resistance for a free-rolling case can be written

$$F_R = \frac{a}{r} \cdot F_W \quad (18)$$

From summation of horizontal forces in a steady-state equilibrium,

$$F_R - F_M = 0 \quad (19)$$

Or rewritten,

$$F_M = F_R \quad (20)$$

A force-measuring tribometer can measure the rolling resistance force if the design allows the applied brake moment to be uncoupled.

Since the nature of the tire rolling resistance involves slip in the tire-surface contact area, a friction coefficient can be defined as

$$\mu_R = \frac{F_R}{F_W} = \frac{\frac{a}{r} \cdot F_W}{F_W} = \frac{a}{r} \quad (21)$$

The tire rolling resistance is geometrically defined. Both  $a$  and  $r$  may vary with tire design, tire load, speed, degree of braking, influence of contamination, etc.

For dry, rigid horizontal surfaces, the rolling resistance is typically observed to be in the range of 0.5 to 3 percent of the carried weight.

The tire rolling resistance is a tire property and is called tire rolling resistance for clarity to differentiate it from other forms of resistance to rolling, stemming from influences of contaminants as described in later sections. The tire rolling resistance is associated with the presence and location of the ground reaction force,  $F_G$ , in the rigid surface contact region with a tire.

#### 4.1.2 Applied Braking Force

To measure braking slip friction, a tribometer must apply a braking moment. A scenario with braking is depicted in Figure 8. A constant applied braking slip force,  $F_B$ , works opposite to the rotation of the wheel. The applied brake moment,  $M_B$ , is the product of the applied force and the radius of the sprocket wheel. The tire rolling resistance force couple ( $F_R$  and  $F_M$ ) is always present when the wheel is rotating.

A brake moment causes the wheel rotation to slow down and creates a slip resistive force,  $F_B$ , in the tire-surface contact area. An increased pulling force,  $F_x$ , is required to uphold the tribometer at a constant speed of travel.

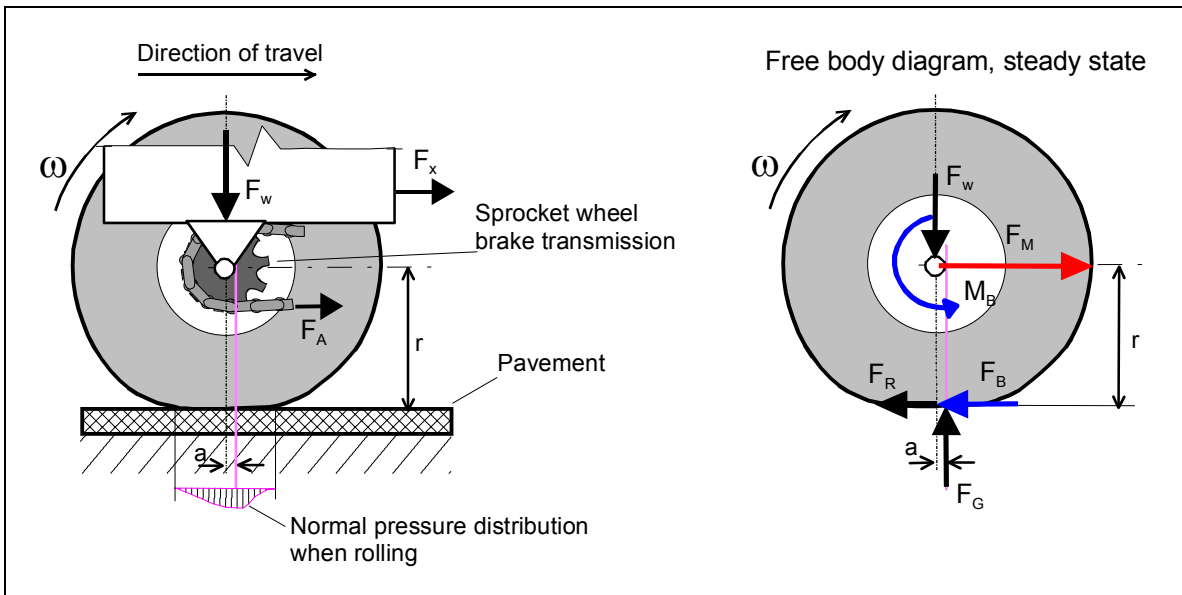


**Figure 8 - Forces and moments of a constant braked wheel on a clean and dry rigid surface**

Summing the moments about the wheel axis in equilibrium at steady state,

$$M_B - F_B \cdot r - F_R \cdot r + F_G \cdot a = 0 \quad (22)$$

A torque-measuring tribometer will, by design, measure the reaction of the applied brake moment, called the measured torque,  $T_M$ , that is equal to the applied brake moment,  $M_B$ . Solving (22) for  $T_M$ ,

$$T_M = M_B = F_B \cdot r + F_R \cdot r - F_G \cdot a \quad (23)$$

If it can be assumed that the tire deformation during braking has the same basic relationship for tire rolling resistance as for the free-rolling case, and  $F_G$  acts in the vertical plane only, then  $F_R \cdot r$  equals  $F_G \cdot a$  and the measured torque is

$$T_M = F_B \cdot r \quad (24)$$

A torque-measuring tribometer does not measure tire-rolling resistance. The braking slip force is equal to the measured torque divided by the deflected radius.

By summation of horizontal forces at steady state

$$F_M - F_B - F_R = 0 \quad (25)$$

Solving for  $F_M$ ,

$$F_M = F_R + F_B \quad (26)$$

A force-measuring tribometer measures braking slip and tire-rolling resistance. When the objective is to measure braking slip, the tire-rolling resistance is an error term.

At this point it is instructive to note a simple way to determine tire-rolling resistance by designing and building a friction tester to measure both torque and horizontal force. Solving for  $F_R$  in (26) and substituting for  $F_B$  using (24)

$$F_R = F_M - \frac{T_M}{r} \quad (27)$$

So far, the forces and moments due to the rolling resistance force and applied braking moment have been discussed. This scenario is valid for friction measurements of clean, dry and rigid surfaces.

Next, drag forces due to fluid contaminant displacement will be studied when a measuring wheel is kept free rolling at a constant speed. This is useful for investigations of displacement drag parameters.

## 4.2 Contaminant Displacement Drag Force on a Free-Rolling Tire

When there is a fluid layer of water, slush or powder snow on the surface, the tire has to displace the fluid contaminant material to maintain contact with the ground or base surface. This scenario is depicted in Figure 9. The displacement causes a resistance to the wheel movement that acts in opposition to the direction of travel and in a plane parallel with the ground surface. It is presumed that the drag force acts in the centre of the normal frontal area of tire-fluid contact plane,  $A_D$ .

The drag force is proportional to this frontal area,  $A_D$  (tire width multiplied by layer thickness), travel velocity squared and the mass density of the fluid contaminant material,  $\rho$ . A coefficient of drag,  $C_D$ , must be experimentally determined for the object and fluid pair.

$$F_D = \frac{1}{2} \cdot C_D \cdot \rho \cdot A_D \cdot V^2 \quad (28)$$

The wheel is supported by the ground and by the suspension at the wheel spin axis. The forces of these support points,  $F_{DG}$  and  $F_{MD}$ , must balance the exerted drag force,  $F_D$ . See the drawing in the lower right corner of Figure 9. The resultant measured force,  $F_M$ , includes a reaction force

due to the applied drag force,  $F_D$ , called  $F_{MD}$ . In addition, the resultant measured force includes a tire-rolling resistance reaction force.

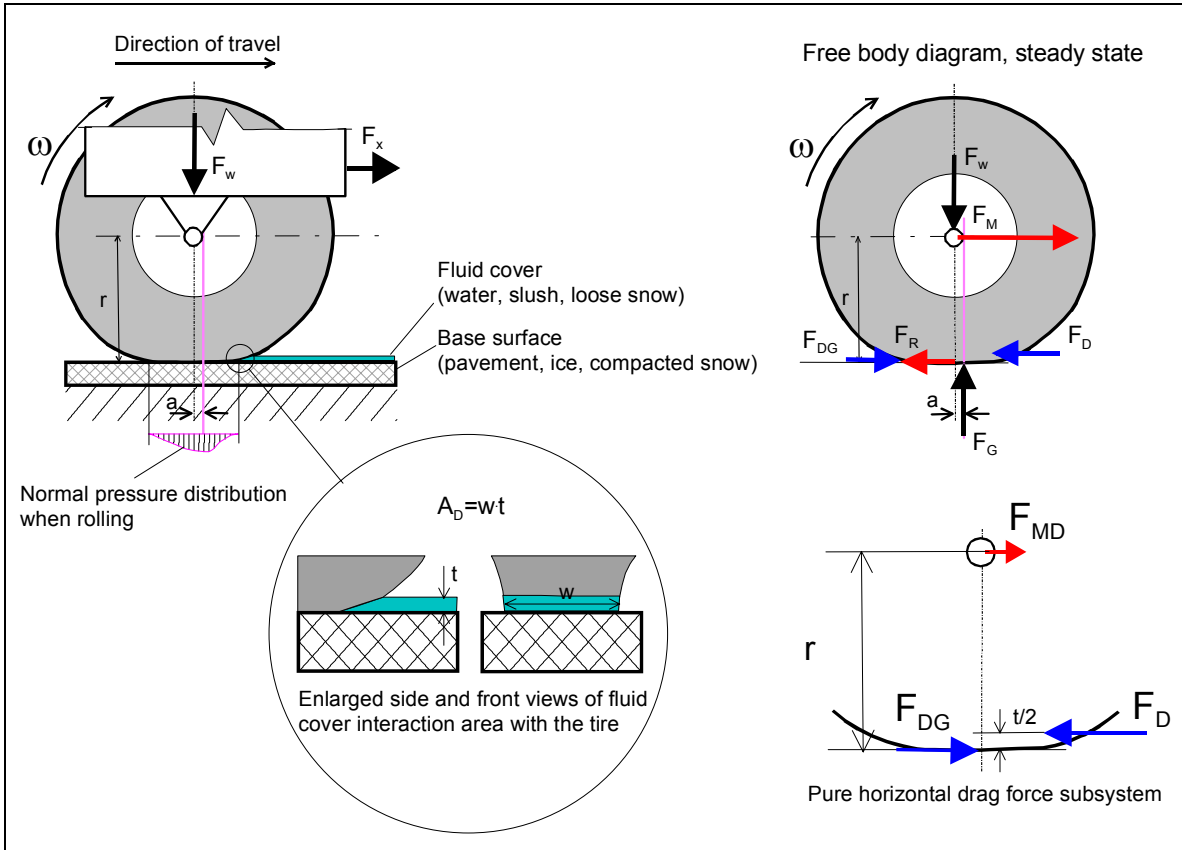


**Figure 9 - Horizontal drag forces acting on a free-rolling friction tester tire due to fluid contaminant displacement**

In the horizontal drag force subsystem, a summation of moments about the wheel axis yields

$$F_{DG} \cdot r - F_D \cdot \left( r - \frac{t}{2} \right) = 0 \quad (29)$$

Solving for  $F_{DG}$ ,

$$F_{DG} = F_D \cdot \left( 1 - \frac{t}{2 \cdot r} \right) \quad (30)$$

From summation of horizontal forces in the same subsystem,

$$F_{MD} + F_{DG} - F_D = 0 \quad (31)$$

Substituting for  $F_{DG}$  in (25) using (23), the measured drag force component is

$$F_{MD} = F_D - F_D \cdot \left( 1 - \frac{t}{2 \cdot r} \right) = \frac{t}{2 \cdot r} \cdot F_D \quad (32)$$



The influence of the displacement drag on the measured horizontal force is a small fraction equal to  $t/2 \cdot r$  of the actual displacement drag force.

By summation of horizontal forces in the complete free body diagram,

$$F_M + F_{DG} - F_R - F_D = 0 \quad (33)$$

By substituting for  $F_{DG}$  using (30), solving for  $F_M$  and simplifying,

$$F_M = F_R + F_D \cdot \frac{t}{2 \cdot r} \quad (34)$$

The measured horizontal force at the wheel axis is the sum rolling resistance and a fraction of the displacement drag.

To determine a drag force from a measurement, by solving (33) for  $F_D$ ,

$$F_D = \frac{2 \cdot r}{t} \cdot (F_M - F_R) \quad (35)$$

It is necessary to know the tire-rolling resistance force,  $F_R$ , the fluid cover thickness,  $t$ , and the deflected tire radius,  $r$ , in order to compute the exerted fluid displacement drag force,  $F_D$ , from a force measurement at the wheel spin axis.

A torque-measuring tribometer does not measure drag in this scenario. Horizontal reaction forces in the ground support and wheel axis support balance both the exerted displacement drag and tire-rolling resistance forces. A summation of moments about the wheel axis yields zero.

A force-measuring tribometer will measure a displacement drag force component as long as  $t$  is larger than zero and the ground surface can provide the reaction friction shear force,  $F_{DG}$ . Since rolling resistance also is supported by the ground shear strength, the sum of the forces acting opposite to each other must be less than the ultimate shear strength of the contact area. This can be written as

$$F_R - F_{DG} \leq \tau_{ult} \cdot A_R \quad (36)$$

where  $\tau_{ult}$  is the ultimate shear strength of the surface material and  $A_R$  is the real area of contact between tire and surface.

### 4.3 Combined Tire-Rolling Resistance, Displacement Drag and Braking Slip Forces

In this section, constant braking is added to the previous scenario (see Figure 10).

For a force-measuring tribometer, summation of horizontal forces and solving for the resultant measured force at the wheel axis yields

$$F_M = F_B + F_R + F_D - F_{DG} \quad (37)$$

Substituting for  $F_{DG}$  using (28), the resultant measured force is

$$F_M = F_B + F_R + F_D \cdot \frac{t}{2 \cdot r} \quad (38)$$

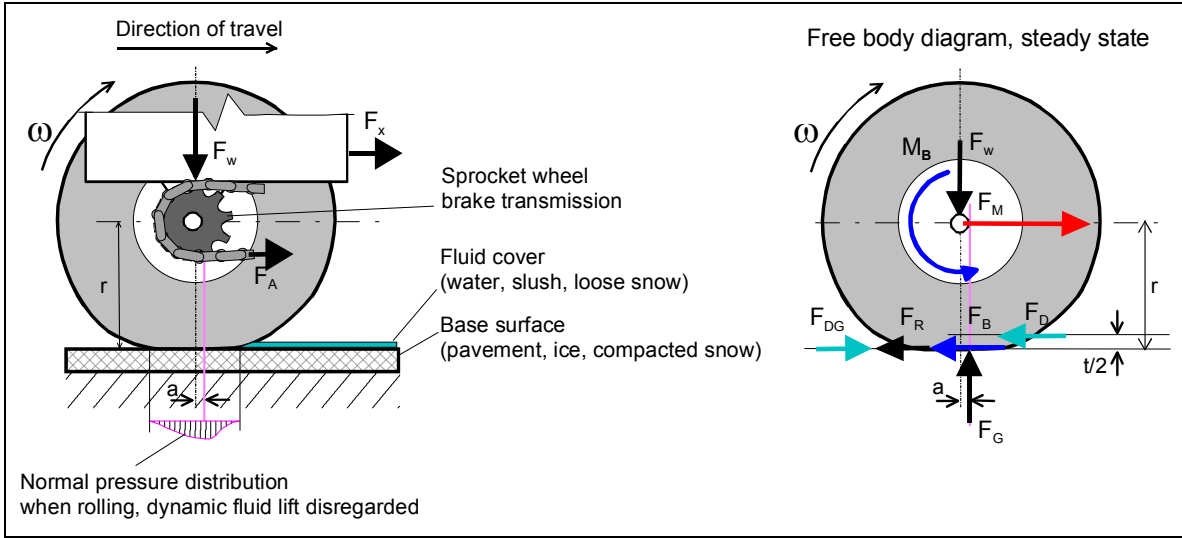


**Figure 10 - Combined rolling resistance, drag and brake forces on a friction tester wheel in steady state**

The force-measuring device thus includes rolling resistance and drag effects in its reported friction value for this scenario. If the objective is to measure the braking slip friction of the brake force,  $F_B$ , the horizontal force of the reported friction coefficient has an error term,  $E$ ,

$$\mu_M = \frac{F_M}{F_W} = \frac{F_B + E}{F_W} \quad (39)$$

where

$$E = F_R + F_D \cdot \frac{t}{2 \cdot r} \quad (40)$$

This error term makes the tribometer report a higher braking slip than the true value.

The summation of moments about the wheel roll axis yields

$$M_B + F_{DG} \cdot r - F_D \cdot \left( r - \frac{t}{2} \right) + F_G \cdot a - F_R \cdot r - F_B \cdot r = 0 \quad (41)$$

But  $F_{DG} \cdot r$  equals  $F_D \cdot (r - t/2)$  and  $F_R \cdot r$  equals  $F_G \cdot a$ ; therefore,

$$M_B - F_B \cdot r = 0 \quad (42)$$

or, since the applied brake moment is equal to the measured torque,

$$T_M = M_B = F_B \cdot r \quad (43)$$

Torque-measuring tribometers typically use the measured torque divided by a value for deflected radius to represent the braking slip force,  $F_B$ . The coefficient of friction reported is

$$\mu = \frac{F_B}{F_W} = \frac{T_M}{r \cdot F_W} \quad (44)$$

Thus, the reported friction value is not a function of tire-rolling resistance or fluid displacement drag effects. The reported friction value reflects the actual braking slip friction.

It is important to be aware of the differences in error terms of the reported coefficient of friction by a force-measuring tribometer versus a torque-measuring tribometer when comparing their results on contaminated surfaces.

#### 4.3.1 Friction Forces from Contaminant Dynamic Planing<sup>3</sup>

Planing occurs when the fluid<sup>4</sup> contaminant material is trapped under the rolling tire in sufficient quantities at a high enough travelling speed to detach some or the entire tire tread from the base surface. Some, or all, of the tire rides on the trapped fluid contaminant, which acts like a lubricant.

The fluid contaminant gets trapped because there is insufficient time for the fluid to flow out of the footprint area. Also, the surface and tire tread may not have sufficient grooves or voids to allow the fluid to fill into these spaces, and thus escape readily from the tire footprint area.

As the trapped fluid enters the leading edge of the contact area between tire and surface, it gives rise to a fluid lift force acting to separate the tire from the base surface. When the fluid penetration covers all of the contact area with the ground, the tire-surface friction becomes approximately zero. The travel speed in this instance is called the critical hydroplaning speed when the fluid is water.

A scenario dealing with the mechanics of friction tester tires with fluid planing is depicted in Figure 11. This is a free-rolling tire with no brake applied. A major difference from earlier scenarios is the divided reaction force from the ground. There are two forces,  $F_G$  and  $F_L$ , that carry the normal load,  $F_W$ .  $F_G$  is the ground reaction force from the base surface still in contact with the tire.  $F_L$  is a resultant dynamic fluid lift force from the area of interspersed fluid.

The line of attack for the ground reaction force,  $F_G$ , is shifted back in the contact length, distance  $a$  from the vertical line through the wheel axis. As a result of this shift in location of  $F_G$ , the tire-rolling resistance force,  $F_R$ , acts counterclockwise in Figure 11. The fluid lift force has a line of attack that is a distance,  $b$ , from the vertical line through the wheel axis. The fluid lift force has horizontal ground reaction force,  $F_{LG}$ , acting in the tire-surface contact area. The sum of  $F_R$  and  $F_{LG}$  constitutes a resultant rolling resistance force. The fluid lift force,  $F_L$ , sustains no shear forces in its contact area with the tire and, therefore, no slip to support tire-rolling resistance in this area.

Assuming that it acts in the centre of the interspersed fluid contact area,  $F_L$  always acts ahead of the vertical through the wheel axis until full planing has occurred. At full planing it acts vertically through the wheel axis.

As the planing progresses,  $F_G$  reduces to zero at full planing. The line of attack for the resultant normal reaction force is therefore always ahead of the wheel axis position. In that position it resists the rotation of the wheel in the same manner as tire-rolling resistance when there is no fluid present.

The reaction force arising from the remaining ground contact,  $F_G$ , has a line of attack before and after the roll axis position, depending on the degree of planing.

<sup>3</sup>Called hydroplaning when the fluid is water.

<sup>4</sup> It is debatable whether to consider and call the different loose winter contaminant material fluids. Here it is used to associate with the established engineering for fluids.

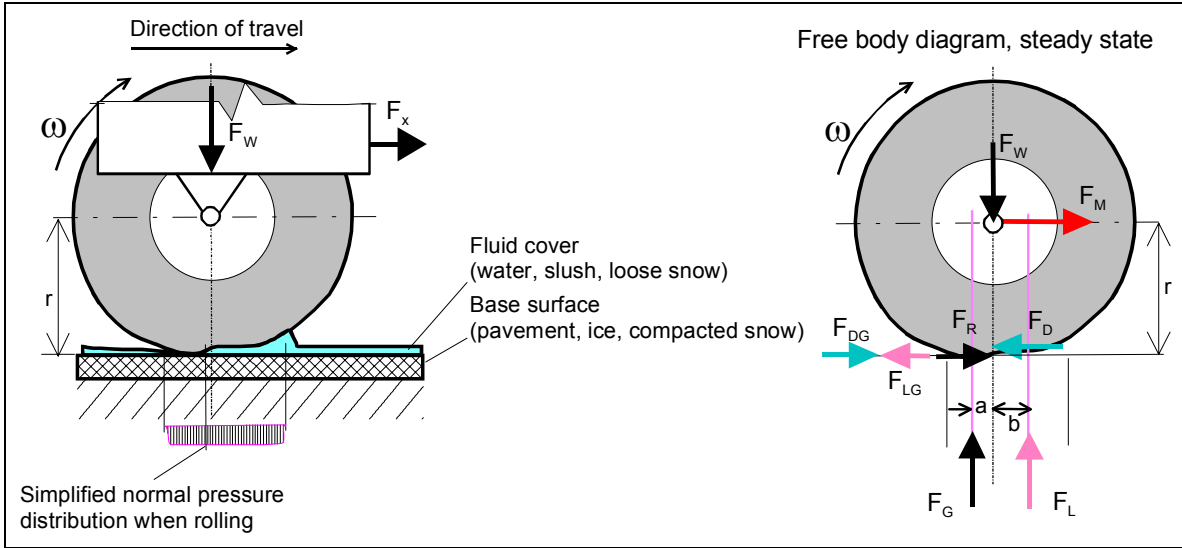


**Figure 11 - Free-rolling tribometer wheel with fluid lift and drag**

The sum of surface reaction forces is equal to the static weight carried by the wheel:

$$F_W = F_G + F_L \quad (45)$$

A torque-measuring tribometer measures zero, as all terms in a summation of moments about the wheel axis reduce to zero.

The fluid lift force,  $F_L$ , has a reaction force,  $F_{LG}$ , in the contact surface between tire and ground. By taking the moment about the wheel axis,

$$F_L \cdot b = F_{LG} \cdot r \quad (46)$$

From (45) the horizontal fluid lift reaction force is

$$F_{LG} = \frac{b}{r} \cdot F_L \quad (47)$$

Summation of horizontal forces in equilibrium at steady-state yields

$$F_M + F_R + F_{DG} - F_D - F_{LG} = 0 \quad (48)$$

With a fluid lift and drag acting on the tire, the horizontally measured force is

$$F_M = F_D - F_{DG} + F_{LG} - F_R \quad (49)$$

Substituting for  $F_{DG}$  using (30) and for  $F_{LG}$  using (47), and simplifying,

$$F_M = \frac{t}{2 \cdot r} \cdot F_D + \frac{b}{r} \cdot F_L - F_R \quad (50)$$

Since  $F_R = \frac{a}{r} \cdot F_G$  and  $F_G = F_W - F_L$ , then

$$F_R = \frac{a}{r} \cdot (F_W - F_L) \quad (51)$$

Substituting for  $F_R$  using (51) in (50), and simplifying,

$$F_M = \frac{t}{2 \cdot r} \cdot F_D + \frac{a+b}{r} \cdot F_L - \frac{a}{r} \cdot F_W \quad (52)$$

A force-measuring tribometer with a decoupled brake measures effects of displacement drag, fluid lift and planing.

#### 4.3.2 The Nature of the Fluid Lift Force

Using Petroff's equation [4] for bearing lubrication, the fluid dynamic lift force can be expressed as

$$F_L = k_L \cdot r \cdot \rho \cdot A_L \cdot V \quad (53)$$

where  $k_L$  is the fluid dynamic lift coefficient,  $\rho$  is the fluid mass density,  $A_L$  is gross tire-fluid contact area and  $V$  is the travel speed. The fluid dynamic lift coefficient depends on fluid viscosity and has a unit 1/time.

The propagation of planing is different for different tire designs; therefore, there is no fixed general relationship between the offset distances  $a$  and  $b$  from the vertical through the wheel axis. See section 5.3.1 for a discussion of planing contact area for different tires.

Horn and Dreher [1] discuss two effects of water on tire-pavement interaction. One effect is hydroplaning, where inertia of the wheel and density properties of the fluid predominate. The other is thin film lubrication, where viscous properties of the fluid predominate.

#### 4.3.3 The Moving Position of the Fluid Lift Force

A linear relationship between speed and the propagation of the planing front under high-pressure aircraft tires can be assumed as demonstrated by Horne and Dreher [1]. At full planing the lift propagation length  $l = L$ . The speed at full planing is called the critical planing speed,  $V_C$ . The ratio of the propagation length to the full length is set equal to the ratio of measuring speed to critical planing speed. This can be expressed as

$$\frac{l}{L} = \frac{V}{V_C} \quad (54)$$

or, solving for  $l$ ,

$$l = \frac{V}{V_C} \cdot L \quad (55)$$

To build a mathematical model of the fluid lift force, it can be assumed that the lift force is proportional to the separation area (length  $l$ , width  $w$ ), the speed and the density of the fluid. It is also proportional to the curvature of the lift area (i.e.,  $F_X$  or  $F_M$  the radius of the tire). Thus,

$$F_L = k_L \cdot w \cdot l \cdot r \cdot \rho \cdot V \quad (56)$$

Using (55),  $l$  may be substituted and  $\rho \cdot V=1$  may be set, since density and speed effects are already included in  $V_C$ .

$$F_L = k_L \cdot w \cdot r \cdot L \cdot \frac{V}{V_C} \quad (57)$$

The group  $w \cdot r \cdot L$  represents geometric tire properties and can therefore be included in a new tire coefficient,  $k_{PL}$ , such that

$$F_L = k_{PL} \cdot \frac{V}{V_C} \quad (58)$$

Equation (58) is a model equation to study the fluid lift as a dependent variable of travel speed and a set of constant parameters for a given tire configuration.

#### 4.3.4 Fluid Lift Effects on the Tire-Surface Friction When Free Rolling

The fluid lift phenomenon reduces the contact area for supporting the tire-surface slip resistive forces. In a free-rolling mode the only resistive force is due to rolling resistance when disregarding fluid displacement drag. The tire-rolling resistance coefficient of friction is

$$\mu_R = \frac{F_R}{F_G} \quad (59)$$

With no fluid lift, drag or brake (59) represents the tire-rolling resistance slip friction coefficient on a clean surface. It is then a maximum attainable value,  $\mu_{Rlim}$ . The tire-rolling resistance slip friction force is

$$F_R = \mu_{Rlim} \cdot F_G \quad (60)$$

But in this scenario  $F_G$  is equal to  $F_W - F_L$  and therefore,

$$F_R = \mu_{Rlim} \cdot (F_W - F_L) \quad (61)$$

Therefore, substituting  $F_L$  with equation (58),

$$F_R = \mu_{Rlim} \cdot \left( F_W - k_{PL} \cdot \frac{V}{V_C} \right) \quad (62)$$

When considering a tire configuration with a constant normal load, the braking slip friction force equation can be rearranged and a factor,  $k_X$ , introduced, defined as

$$k_X = \frac{k_{PL}}{F_W} \quad (63)$$

Then, the friction force equation becomes

$$F_R = \mu_{Rlim} \cdot F_W \cdot \left( 1 - k_X \cdot \frac{V}{V_C} \right) \quad (64)$$

At the boundary condition of full planing where  $V = V_C$ ,  $k_X$  must be equal to one for  $F_R$  to be zero. Thus, the general braking slip friction force equation is

$$F_R = \mu_{Rlim} \cdot F_W \cdot \left(1 - \frac{V}{V_C}\right) \quad (65)$$

or, expressed in terms of a fluid planing ratio,  $k_P$ , for a free-rolling wheel,

$$k_P = \frac{V}{V_C} \quad (66)$$

Therefore, by substitution,

$$F_R = \mu_{Rlim} \cdot F_W \cdot (1 - k_P) \quad (67)$$

Thus, the fluid lift or planing effects on the friction characteristics amount to a reduction of the slip friction force equal to a fraction of the maximum attainable friction force value for the surface that is proportional to the planing ratio.

For a force-measuring friction device, the measured friction,  $F_M$ , is equal to  $F_R$  when disregarding fluid displacement drag effects. Figure 12 shows that the braking slip friction diminishes as the partial planing progresses, and that it is proportional to the speed and inversely proportional to the critical planing speed for the tire-surface combination. The  $V_C$  parameter is a constant parameter for the tire-surface combination.

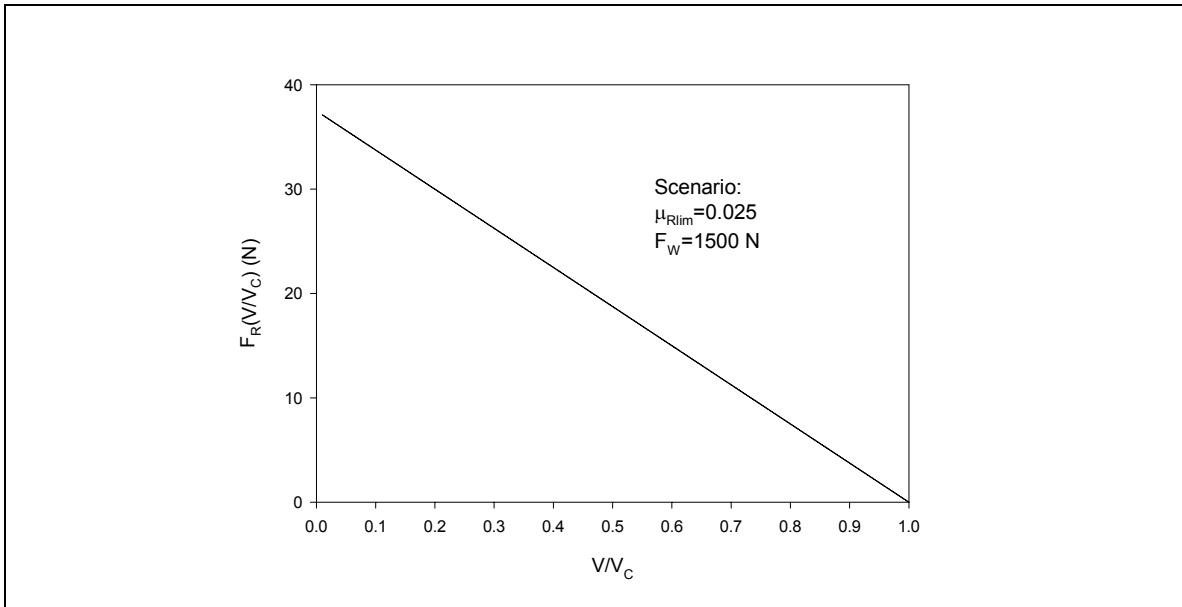
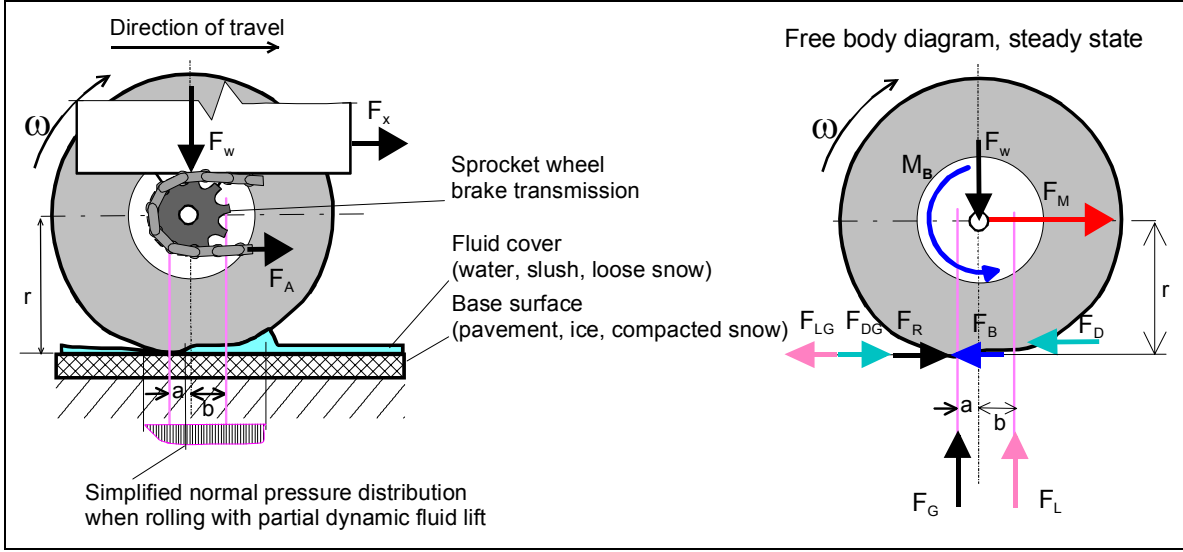


Figure 12 - A case of diminishing tire-rolling resistance force  $F_R$  as the planing propagates with increased speed

#### 4.4 Tire-Rolling Resistance, Fluid Displacement Drag, Fluid Planing and Applied Braking

A scenario with tire rolling-resistance, fluid displacement drag, fluid planing and braking is depicted in Figure 13.



**Figure 13 - Braked tribometer wheel with fluid dynamic lift and displacement drag**

The equilibrium sum of horizontal forces is

$$F_M + F_{DG} - F_D - F_{LG} + F_R - F_B = 0 \quad (68)$$

which is the same as (48) except for the addition of the brake force,  $F_B$ . Adding the braking slip force to (52), the measured horizontal force at the wheel axis is

$$F_M = F_B + F_D \cdot \frac{t}{2 \cdot r} + F_L \cdot \frac{a+b}{r} - F_W \cdot \frac{a}{r} \quad (69)$$

A force-measuring tribometer reports displacement drag, fluid lift and tire-rolling resistance in addition to the braking slip friction.

When the objective is to measure the braking slip force,  $F_B$ , the measured force has an error term,  $E$ , where

$$E = F_D \cdot \frac{t}{2 \cdot r} + F_L \cdot \frac{a+b}{r} - F_W \cdot \frac{a}{r} \quad (70)$$

The displacement drag force can be calculated or evaluated with (28). The fluid lift force can be calculated or evaluated with (53).

The equilibrium sum of moments about the wheel spin axis is

$$M_B + F_L \cdot b - F_{LG} \cdot r - F_G \cdot a + F_R \cdot r + F_{DG} \cdot r - F_D \cdot \left( r - \frac{t}{2} \right) - F_B \cdot r = 0 \quad (71)$$

But  $F_{DG} \cdot r$  equals  $F_D \cdot (r - t/2)$ ;  $F_L \cdot b$  equals  $F_{LG} \cdot r$ ; and  $F_G \cdot a$  equals  $F_R \cdot r$ ; therefore, solving for  $M_B$ ,

$$M_B = F_B \cdot r \quad (72)$$

Since a torque-measuring tribometer measures  $T_M = M_B$ , only braking slip is measured in this scenario.



#### 4.4.1 The Moving Position of the Fluid Lift Force for a Braked Tire

In contrast to the free-rolling planing behaviour, the progression of the planing with increasing travel speed is more moderate when braking is applied. When braked, the wheel rotates more slowly than for free rolling, but the travel speed is kept constant. The slower rotation traps less fluid to support the same fluid lift as for a free-rolling wheel.

A braked rotation speed can be expressed as the travel speed multiplied by a slip ratio. The speed that acts to trap the fluid is then  $V - V\lambda$ , where  $\lambda$  is the slip ratio.

Thus, equation (55) can be modified to

$$l = \frac{V \cdot (1 - \lambda)}{V_C} \cdot L \quad (73)$$

Distances  $a$  and  $b$  can therefore, by substitution for  $l$ , be expressed as functions of the measuring speed,  $V$ , the slip ratio,  $\lambda$ , the critical planing speed,  $V_C$ , and the footprint length,  $L$ .

For fixed-slip tribometers,  $\lambda$  is a constant. The free-rolling planing factor equation (66) can therefore be transformed to a braked wheel planing factor,  $k_{PB}$ , where

$$k_{PB} = \frac{V \cdot (1 - \lambda)}{V_C} \quad (74)$$

For low-viscosity and non-compacting fluid contaminants, an increasing braking action will reduce the planing to almost nothing as the rotation speed reaches zero. For high-viscosity and compacting fluid contaminants, it may be observed that a compacting element of the planing remains in effect with an increasing braking action. The tire is skiing on the compressed contaminant. This mechanism is little understood.

The deflected rolling radius  $r$  will be reduced under the influence of braking. The positions of lines of action  $a$  and  $b$  will vary with the braking and speed. For low-viscosity fluid contaminants,  $b$  will be reduced to zero at locked wheel braking.

## 4.5 Forces in Loose Snow

This section discusses a scenario with the friction tester wheel in a sufficient depth of loose snow that does not allow the wheel to touch the original rigid base surface. As the tire rolls, a new snow base surface is formed in its path.

The mechanisms at work are displacement drag, rolling resistance, planing, compaction and braking slip friction. The braking slip friction is generated on the instantaneously formed new base.

Sections 4.5.1 to 4.5.3 are theoretical discussions, as published research results confirming mathematical models of a braked tire in loose snow are scarce or unavailable. A simplified theoretical analysis is, nevertheless, useful to provide an idea of which forces may act in a mechanical model, and how these may vary to influence the friction coefficient.

The magnitude and line of direction of the external dynamic forces acting on the tire from loose snow vary significantly with the physical properties of snow. Snow crystal shapes, density, free water content and age are some frequently cited properties of snow. Fluid displacement drag (28) and fluid lift (53) equations have reached acceptance by researchers and engineers when applied to non-compressible fluids like water.

Equations (28) and (53) are natural departure points in determining to what extent loose snow could be modelled in the same way. A common practice in aviation engineering is to convert the snow density for a known deposit depth to a corresponding deposit depth of water and then apply the equation for fluid displacement drag (28).

#### 4.5.1 Resistance from Separate Compacting and Displacement Drag Forces

A rolling wheel in loose snow will compact a major part of the snow volume in its path. A minor part is displaced laterally with the wheel acting like a plow. A free-rolling wheel will compact a larger amount than a braked, but rotating wheel. A locked wheel will practically only displace the loose snow like a plow and perform very little compacting.

A friction tester wheel in deep snow is depicted in Figure 14. A fraction of the snow layer,  $c$ , is compacted. There is no sure way of measuring  $c$ , but an indication may be found by comparing the density of a fixed volume before and after compacting, allowing for some escape of snow laterally.

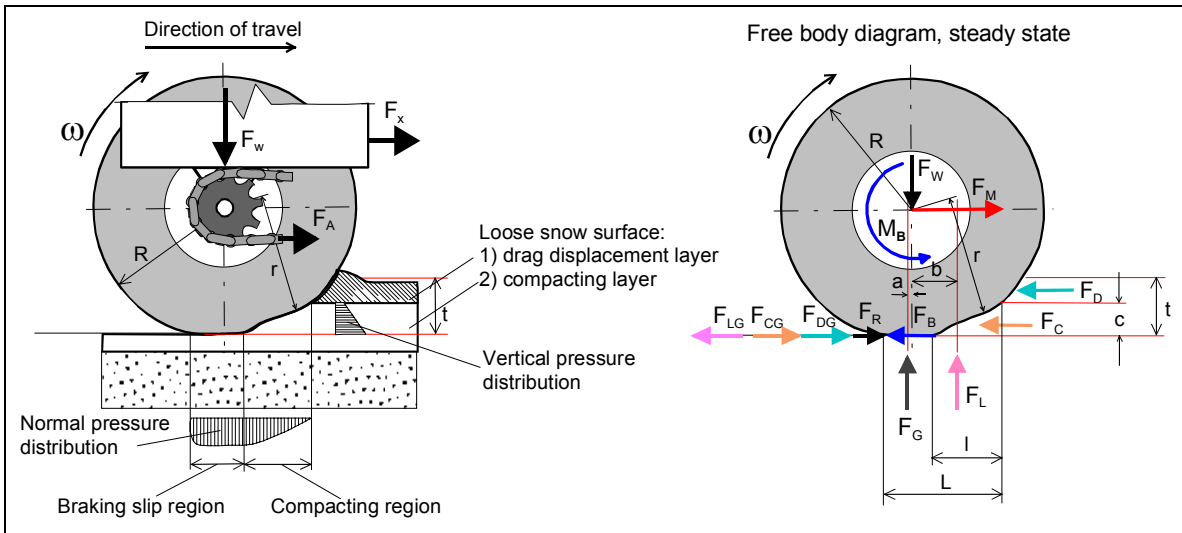


**Figure 14 - Reaction force system for a tribometer wheel in loose snow**

The normal pressure distribution under the tire can be assumed even in a braking slip region and tapered in the compacting region. It can be assumed that the vertical pressure distribution will be tapered, as shown in Figure 14.

The loose snow scenario, including compacting resistance, has commonalities with the dynamic fluid lift scenario. The vertical reaction forces include a ground reaction force,  $F_G$ , in the tire-surface contact area, and a compacting reaction force,  $F_{CL}$ , in the compacting area.

The displacement drag (plowing) and compacting resistance forces act on the tire in two separate regions. The displacement drag force,  $F_D$ , acts at a distance from the wheel axis equal to  $r-1/2(t+c)$ . The compacting resistance force,  $F_C$ , acts at a distance from the wheel axis depending on tire design and inflation pressure, snow density and plasticity, but is here assumed to act at a distance equal to  $r-c/3$ .

The equilibrium sum of moments about the wheel axis is

$$\begin{aligned}
& M_B - F_B \cdot r + F_L \cdot b - F_{LG} \cdot r + F_{CG} \cdot r - F_C \cdot \left( r - \frac{c}{3} \right) \\
& + F_{DG} \cdot r - F_D \cdot \left( r - \frac{t+c}{2} \right) + F_R \cdot r - F_G \cdot a = 0
\end{aligned} \tag{75}$$

For a rigid surface, however,  $F_{DG} \cdot r$  equals  $F_D \cdot (r - 1/2(t+c))$ ,  $F_{CG} \cdot r$  equals  $F_C \cdot (r - c/3)$ ,  $F_{LG} \cdot r$  equals  $F_L \cdot b$ , and  $F_G \cdot a$  equals  $F_R \cdot r$ . Eliminating equalities and solving for  $M_B$ ,

$$M_B = F_B \cdot r \tag{76}$$

Since a torque-measuring tribometer measures  $T_M = M_B$ , only braking slip is measured in this scenario.

$$T_M = M_B = F_B \cdot r \tag{77}$$

The equilibrium sum of horizontal forces is

$$F_M + F_{CG} + F_{DG} + F_R - F_B - F_C - F_D - F_{LG} = 0 \tag{78}$$

Substituting for  $F_{CG}$ ,  $F_{DG}$  and  $F_{LG}$ , and solving for  $F_M$ , the measured force by a force-measuring tribometer is

$$F_M = F_B + \frac{c}{3 \cdot r} \cdot F_C + \frac{(t+c)}{2 \cdot r} \cdot F_D + \frac{b}{r} \cdot F_L - \frac{a}{r} \cdot F_G \tag{79}$$

Since  $F_G = F_W - F_L$ , by substitution,

$$F_M = F_B + \frac{1}{r} \cdot \left( \frac{c}{3} \cdot F_C + \frac{(t+c)}{2} \cdot F_D + (a+b) \cdot F_L - a \cdot F_W \right) \tag{80}$$

Thus, a force-measuring tribometer reports forces from braking slip, compacting, displacement drag, fluid lift and tire-rolling resistance. When the objective is to measure braking slip,  $F_B$ , the measured force has an error term,  $E$ , where

$$E = \frac{1}{r} \cdot \left( \frac{c}{3} \cdot F_C + \frac{(t+c)}{2} \cdot F_D + (a+b) \cdot F_L - a \cdot F_W \right) \tag{81}$$

If compacting does not take place (i.e.,  $c$  reduces to zero), the error term becomes the same as for a braked wheel with displacement drag and fluid lift (70).

The horizontal compacting resistance force,  $F_C$ , is proportional to speed and frontal area of the loose snow layer approaching the tire, and inversely proportional to the tire radius.

#### 4.5.2 Resistance from One Resultant External Dynamic Force

To evaluate (81), reasonable values must be assumed for  $t$ ,  $b$  and  $c$ , and estimate values must be assumed for the forces. Such an approach may be cumbersome.

To discuss the influences of the fluid contaminant on the measured torque or horizontal force, it may serve better to evaluate the resultant external force impacting the tire from displacement drag, compacting and lift. In Figure 15 such a resultant force is shown to act at a point on the tire circumference. The point of application is positioned by a distance  $b$  from the vertical through the wheel axis and a distance  $c$  above the ground. At this point ( $b,c$ ) the line of direction of the

resultant force may vary depending on the speed of travel, density, tire radius, etc. The variation in direction is represented by the angle  $\alpha$ . The angle can vary between zero and 90 degrees. The positions of the point of attack in terms of the  $b$  and  $c$  co-ordinates and the angle  $\alpha$  are assumed to be independent of each other in the calculations. A limited discussion of the propagation of planing, and therefore the varying point of application of a dynamic external force, is given in section 5.3.1. A case of tire deformation due to dynamic external forces is depicted in Figure 27.

From Figure 15 it can be shown that the resultant resistive reaction force,  $F_S$ , acting in the tire-surface contact area,  $A_R$ , is the sum of reaction forces from the loose deposit, tire-rolling resistance and applied brake force.

$$F_S = F_E \cdot \sin\alpha \cdot \frac{b}{r} - F_E \cdot \cos\alpha \cdot \left(1 - \frac{c}{r}\right) - F_R + F_B \quad (82)$$

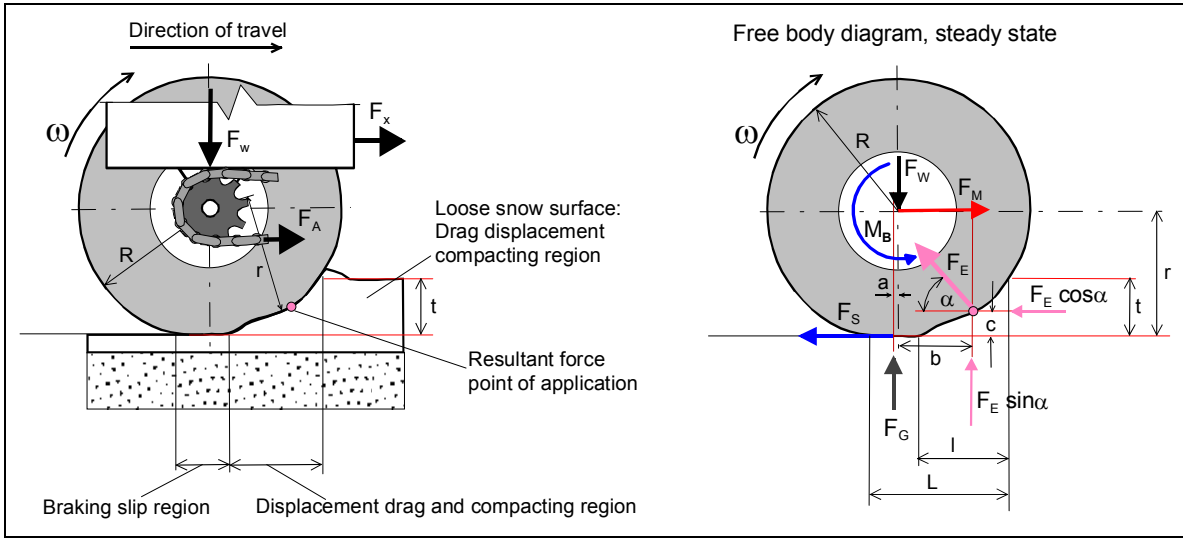


**Figure 15 - Reaction force system for a tribometer wheel in loose snow with surface material shear**

To find an expression for the measured force with a torque-measuring tribometer, summation of moments about the wheel axis yields

$$M_B + F_E \cdot \sin\alpha \cdot b - F_E \cdot \cos\alpha \cdot (r - c) - F_S \cdot r - F_G \cdot a = 0 \quad (83)$$

The horizontal force measured by a torque-measuring tribometer is equal to the measured torque divided by the deflected radius,  $r$ . Solving for  $F_M = M_B / r$ ,

$$F_M = F_S + F_E \cdot \cos\alpha \cdot \left(1 - \frac{c}{r}\right) - F_E \cdot \sin\alpha \cdot \frac{b}{r} + F_G \cdot \frac{a}{r} \quad (84)$$

Substituting for  $F_S$  using (82), and since  $F_R = F_G \cdot a/r$  by definition, (84) reduces to

$$F_M = F_B \quad (85)$$

When the contact area for braking slip friction is reduced under the influence of external dynamic forces on the tire, the braking slip friction coefficient is

$$\mu_B = \frac{F_B}{F_G} = \frac{F_M}{F_G} \quad (86)$$

From summation of vertical forces,

$$F_W = F_G + F_E \cdot \sin\alpha \quad (87)$$

Solving (87) for  $F_G$  and substituting in (85), the braking slip friction coefficient value reported by a torque-measuring tribometer can be written as

$$\mu_B = \frac{F_B}{F_G} = \frac{F_M}{F_W - F_E \cdot \sin\alpha} \quad (88)$$

A torque-measuring tribometer may therefore have an error term,  $E$ , in the denominator of the friction coefficient:

$$\mu_M = \frac{F_M}{F_W + E} \quad (89)$$

where the error term in the denominator is

$$E = -F_E \cdot \sin\alpha \quad (90)$$

For a force-measuring tribometer the summation of horizontal forces in Figure 15 yields

$$F_M - F_S - F_E \cdot \cos\alpha = 0 \quad (91)$$

Or, solving for  $F_M$ , substituting  $F_S$  using (82) and rearranging,

$$F_M = F_B + F_E \cdot \sin\alpha \cdot \left(\frac{a+b}{r}\right) + F_E \cdot \cos\alpha \cdot \frac{c}{r} - F_W \cdot \frac{a}{r} \quad (92)$$

Solving (92) for  $F_B$  the braking slip friction coefficient is

$$\mu_B = \frac{F_B}{F_G} = \frac{F_M - F_E \cdot \sin\alpha \cdot \left(\frac{a+b}{r}\right) - F_E \cdot \cos\alpha \cdot \frac{c}{r} + F_W \cdot \frac{a}{r}}{F_W - F_E \cdot \sin\alpha} \quad (93)$$

When the objective is to measure braking slip friction, there are error terms in the nominator and denominator:

$$\mu_B = \frac{F_M + E_1}{F_W + E_2} \quad (94)$$

where

$$E_1 = F_W \cdot \frac{a}{r} - F_E \cdot \sin\alpha \cdot \left(\frac{a+b}{r}\right) - F_E \cdot \cos\alpha \cdot \frac{c}{r} \quad (95)$$

and

$$E_2 = -F_E \cdot \sin\alpha \quad (96)$$

The error term,  $E_1$ , represents a sum of tire-rolling resistance and non-friction dynamic resistive forces from loose contaminant displacement drag and compacting.

### 4.5.3 Variability of Friction Coefficients under Influence of a Resultant Dynamic Resistive Force

Different tribometer designs may define and calculate the friction coefficient differently. The error introduced by the dynamic forces of a loose or fluid contaminant deposit will therefore also have different effects on the reported friction value.

For a torque-measuring tribometer, the horizontal force in the nominator of the friction coefficient fraction is calculated as the measured torque divided by a deflected radius for the tire type used. The radius is often taken as a constant in the calculation to get the measured horizontal force,  $F_M$ . The torque-measuring device therefore measures the horizontal force without any error effects by the dynamic resistive force from the loose contaminant.

The vertical force, on the other hand, is affected by the loose contaminant through a lift force,  $F_E \cdot \sin \alpha$ . The stronger the dynamic resistive force is and the steeper the angle is for the line of its direction, the larger the lift force becomes. The area of the tire where the lift force is acting is assumed to have negligible skin friction and no slip friction. The braking slip friction process takes place in the area of the tire where the ground surface reaction force,  $F_G$ , is acting.  $F_G$  becomes less than the static weight value as the value of the lift force increases.

For a torque-measuring tribometer, the true or theoretical braking slip friction coefficient defined as the ratio  $F_M/F_G$  will therefore increase with increasing dynamic resistive contaminant force because the denominator of the coefficient decreases.

If the instrumentation measures the lift force  $F_E \cdot \sin \alpha$ , then  $F_G$  can be computed as  $F_W - F_E \cdot \sin \alpha$ .

If there is no instrumentation to measure the vertical force, the static weight,  $F_W$ , is used as the denominator in the calculation of the reported friction coefficient.

A force-measuring tribometer may have the same options as the torque-measuring tribometer with respect to which vertical force to use in the denominator. However, the options are different with the horizontal force. A horizontal force measurement by a force-measuring tribometer includes effects of the dynamic resistive force as an error term. Finding the true braking slip force,  $F_B$ , either requires data for the position of the point of application of the dynamic resistive force and its magnitude or a parallel torque-measuring instrumentation. The latter is implemented in many tribometer designs.

#### 4.5.3.1 Calculation Examples for Different Definitions of a Friction Coefficient

A chosen set of parameters representing a theoretical device and a theoretical case of measurement geometry is valuable for discussing variability caused by the dynamic resistive force. By examples of calculations, the sensitivity of the parameters can be visualized.

A tribometer with a normal load of 1400 N and a tire with radius of 40 cm measures friction in 2 cm deep loose natural snow on a pavement. The steady-state equilibrium of forces at any instant of measurement is described in Figure 15. The position of the point of application of the dynamic resistive force is not measurable, but reasonable values of  $a$ ,  $b$  and  $c$  are chosen to study the magnitude and angle of direction of the resistive force.

In Figures 16 and 17 the four methods for calculating a braking slip friction coefficient are shown as plots versus the angle of the line of direction of the dynamic resistive force, and its magnitude for a theoretical case of a typical tribometer measuring on loose snow.

In Figure 16 four different definitions of friction coefficient are plotted versus the angle  $\alpha$ . The parameters of geometry are given on the right side of the graph. For a force-measuring tribometer, the measured force is 300 N and the magnitude of the dynamic resistive force has been determined to be 100 N.

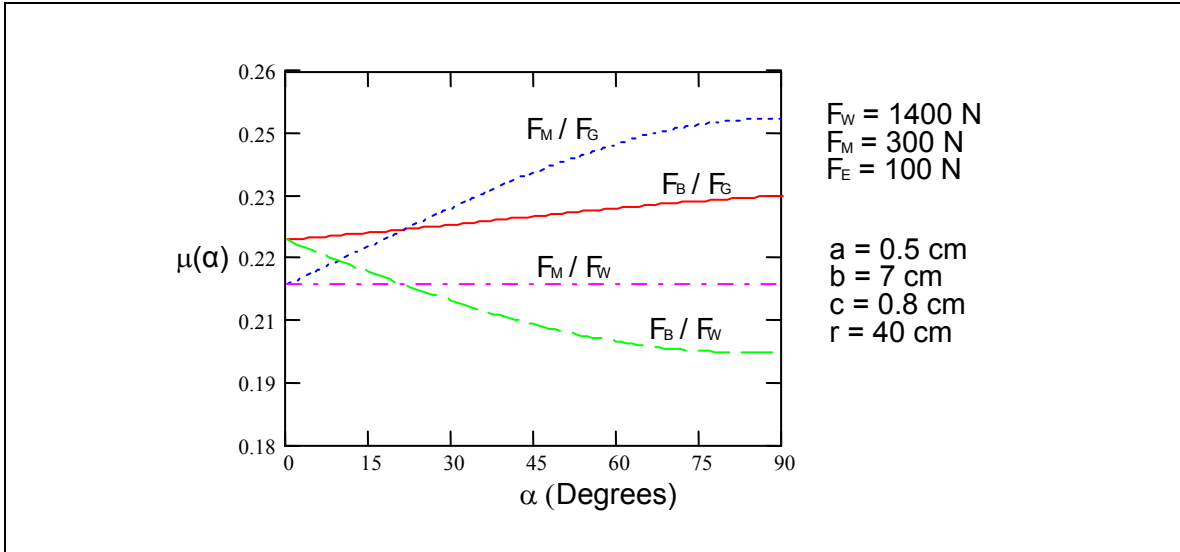


**Figure 16 - Variability of different definitions of reported friction coefficients with angle of dynamic resistive force**

If a simple definition of friction coefficient  $F_M / F_W$  is used (i.e., the measured horizontal force divided by the static weight), the friction coefficient is a constant horizontal line.

Defining the friction coefficient as the measured horizontal force divided by the ground reaction force,  $F_M / F_G$ , the sine term of the ground reaction force introduces variability with the angle  $\alpha$ . The friction coefficient increases with increasing angle.

With the assumed parameter values for the location of the point of application of the dynamic resistive force and an assumed value,  $a$ , for the point of application of the ground reaction force, the true theoretical braking slip force,  $F_B$ , can be calculated. For a force-measuring tribometer, the reported horizontal force is larger than the braking slip force.

A definition of friction coefficient as  $F_B / F_W$  yields a decaying friction coefficient with increasing values of the angle.

A definition of friction coefficient as  $F_B / F_G$ , on the other hand, yields a slightly increasing friction coefficient with increasing values of the angle.

The calculation examples for the different definitions of the coefficient of friction are repeated for a fixed angle and varying dynamic resistive force, and the results are shown in Figure 17. When the angle is 20 degrees, the trends are the same as for a varying angle for the definitions  $F_M / F_G$ ,  $F_M / F_W$  and  $F_B / F_W$ .

The largest difference among the different definitions of friction coefficient is about 0.05 coefficient units.

#### 4.5.3.2 Calculation Example of True Braking Slip Friction

For the theoretical braking slip friction coefficient  $F_B / F_G$ , a three-dimensional surface plot is shown in Figure 18 for the same set of measurement parameters assumed in section 4.5.3.1.

It can be observed that, as the magnitude of the dynamic resistive force and the angle both increase, the theoretically true braking slip friction coefficient generally increases. Only for small values of  $\alpha$  does the friction coefficient decrease moderately. The maximum friction coefficient value is approximately 0.05 coefficient units higher than the smallest. When the magnitude of the

dynamic resistive force varies between zero and 400 N while the measured horizontal force is 300 N, the largest difference through variation of angles 0 to 90 degrees is approximately 0.05 coefficient units.

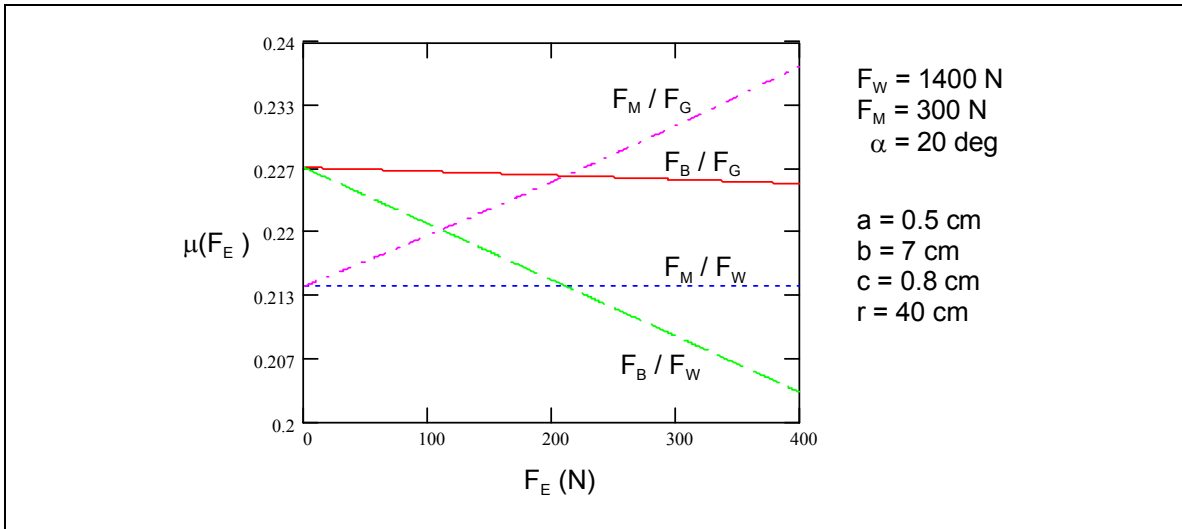


**Figure 17 - Variability with of different definitions of reported friction coefficients with magnitude of dynamic resistive force**

As shown in section 4.3, a torque-measuring tribometer calculates the horizontal force by dividing the measured torque by the deflected radius. This calculated force equals  $F_B$  according to (85).

When torque- or force-measuring tribometers with equal loads and test tires measure the same surface, any measured difference equals the effect of tire-rolling resistance and other dynamic resistive contaminant forces. For a tribometer outfitted to measure both torque and force, the difference can be measured directly by the same device.

The difference can be expressed with (92) solved for  $F_M - F_B$ :

$$F_M - F_B = F_E \cdot \sin \alpha \cdot \left( \frac{a+b}{r} \right) + F_E \cdot \cos \alpha \cdot \frac{c}{r} - F_W \cdot \frac{a}{r} \quad (97)$$

Note that the equation is valid for the scenario of Figure 15 where  $a$  is a distance trailing the vertical line through the wheel axis. When the dynamic resistive force  $F_E$  reaches zero,  $a$  changes to a leading position relative to the vertical line through the wheel axis and becomes a negative value.

#### 4.5.3.3 Calculation Example of the Difference Between a Force- and a Torque-Measuring Tribometer

For the theoretical calculation case, the difference in friction coefficient  $(F_M - F_B)/F_G$  is plotted for all possible angles up to 90 degrees and a range of dynamic resistive force values up to 400 N in Figure 19.

It is seen, from the intercept of the surface plot with the  $F_E - \alpha$  plane, that a minimum combination of dynamic resistive force and angle is required for the tribometer-type difference  $(F_M - F_B)/F_G$  to be greater than zero. When that requirement is met, the difference in reported friction coefficient increases with increasing magnitude and angle of the dynamic resistive force. For the plotted example, the maximum difference is approximately 0.05 friction coefficient units.



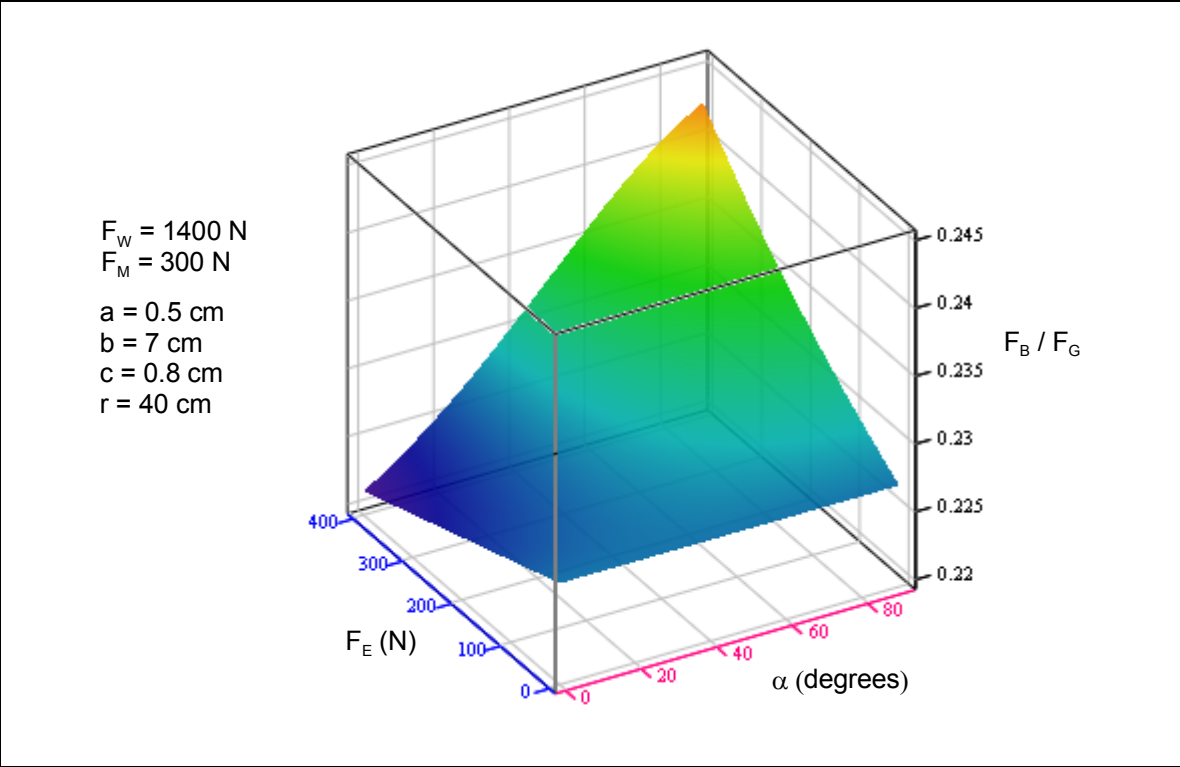


Figure 18 - Braking slip friction coefficient as a function of magnitude and direction of resistive force from a contaminant deposit in a calculation example

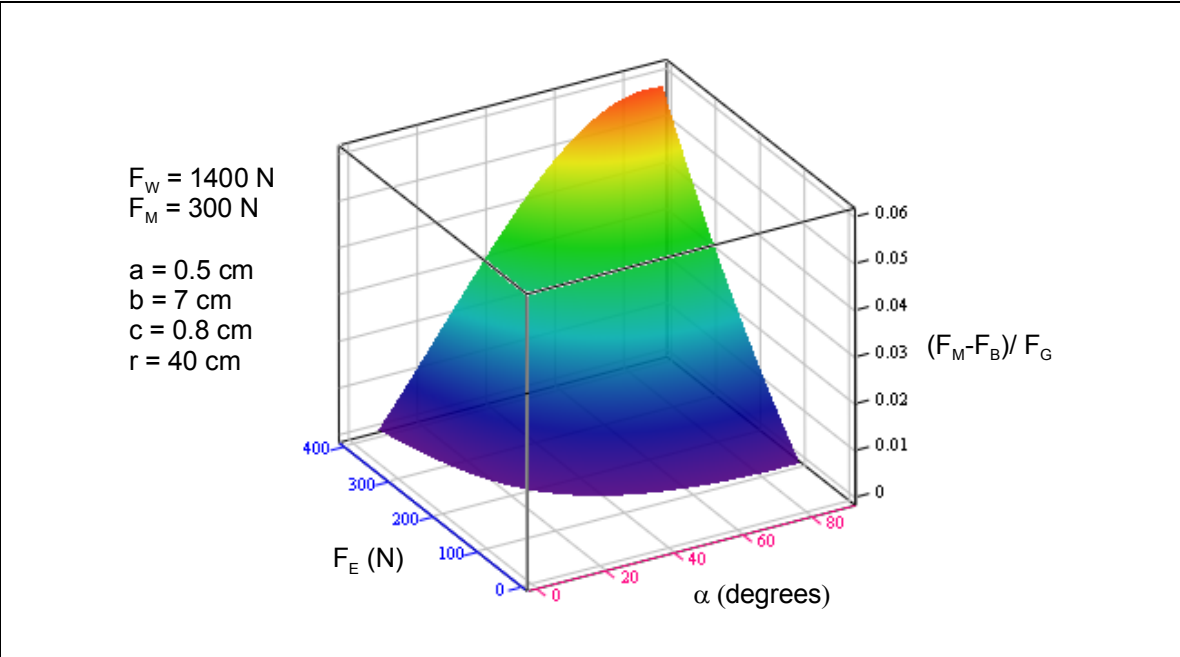
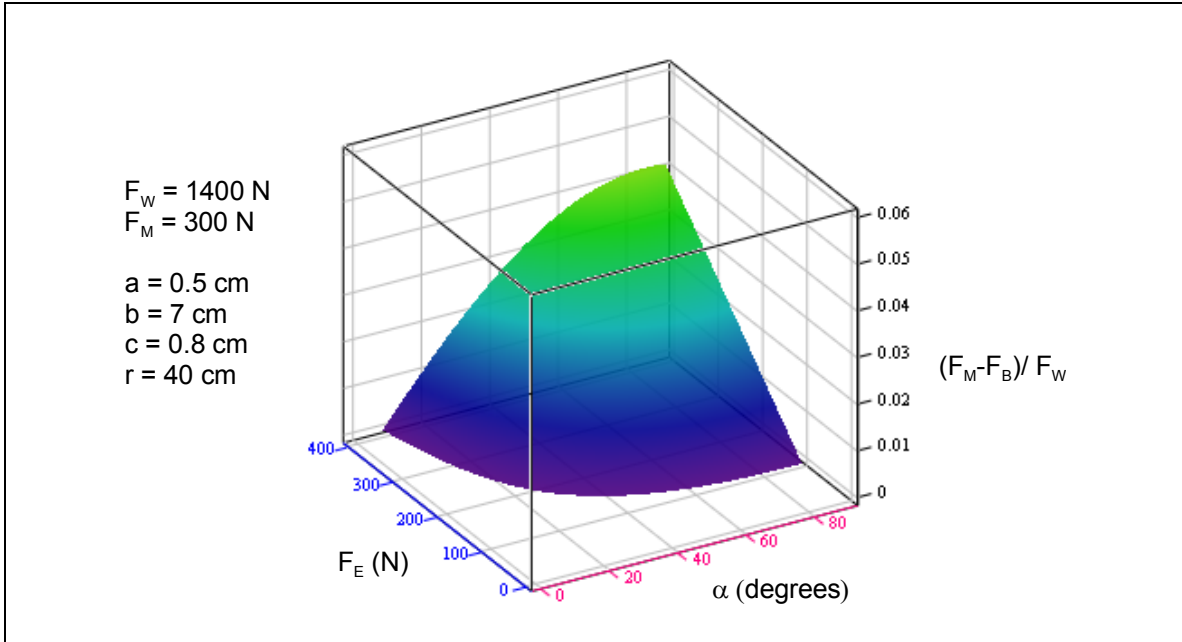


Figure 19 - Difference between a force- and torque-measuring tribometer braking slip friction coefficient as a function of magnitude and direction of resistive force from a contaminant deposit in a calculation example



**Figure 20 - Difference between a force- and torque-measuring tribometer braking slip friction coefficient as a function of magnitude and direction of resistive force from a contaminant deposit in a calculation example**

If the static weight is used as the vertical force to calculate the friction coefficient, the corresponding surface plot of  $(F_M - F_B)/F_W$  is shown in Figure 20. It mainly differs from the true braking slip friction coefficients  $(F_M - F_B)/F_G$  difference by being smaller in value, but keeping the same shape.

#### 4.5.3.4 The Influence of Tire Radius and Position of Lift Force

The tire radius and the position of the vertical ground reaction force have large influence on the braking slip friction. A three-dimensional plot in Figure 21 shows how the distance,  $a$ , has a substantial influence on the braking slip friction coefficient  $F_B / F_G$  for a small tire radius.

The dynamic resistive force acts at an angle  $\alpha$  equal to 30 degrees in the calculation example for the plot. Snow deposit thickness and, therefore, the vertical position,  $c$ , of the point of application for the dynamic resistive force is kept the same as in all of the example calculations in sections 4.5.3.1 through 4.5.3.4. But the horizontal position,  $b$ , is made a function of the tire radius as shown in the small plot on the left in Figure 21. The  $b$  value follows a circular trajectory on the tire circumference less 1 cm for horizontal deflection.

For all values of tire radius shown, the braking slip friction increases with greater distance  $a$  (i.e., the distance of the ground reaction force is trailing the wheel axis). For a tire with a 40 cm radius, the friction coefficient value increases from 0.22 to 0.32 when  $a$  increases from zero to 4 cm. For a tire with a 10 cm radius, the friction theoretically increases from 0.20 to 0.36, as  $a$  may have a maximum of 2 cm for that tire.

With decreasing tire radius, the braking slip friction increases for all values of  $a$ . The increase is larger for larger  $a$  values.

When the braking slip friction coefficient is calculated as  $F_B / F_W$ , the variation with tire radius and distance  $a$  is a little smaller than for  $F_B / F_G$ . This can be observed in Figure 22.

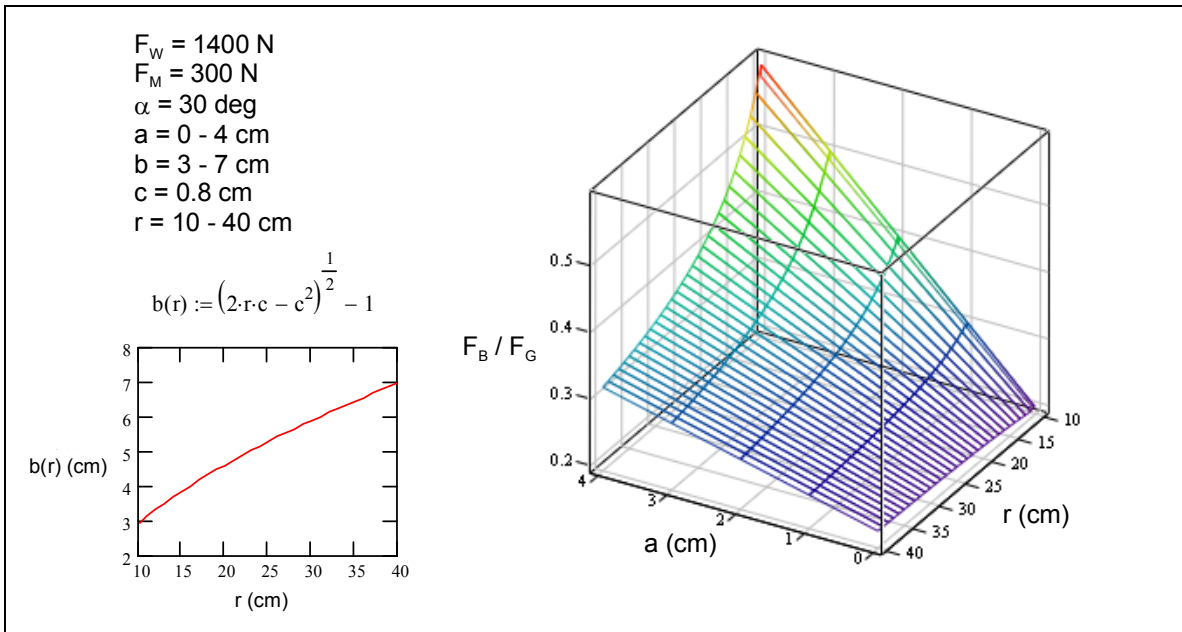


**Figure 21 - An example of the significance of tire radius and position of ground reaction force in loose snow for a braking slip friction coefficient calculated with the ground reaction force as the vertical force**

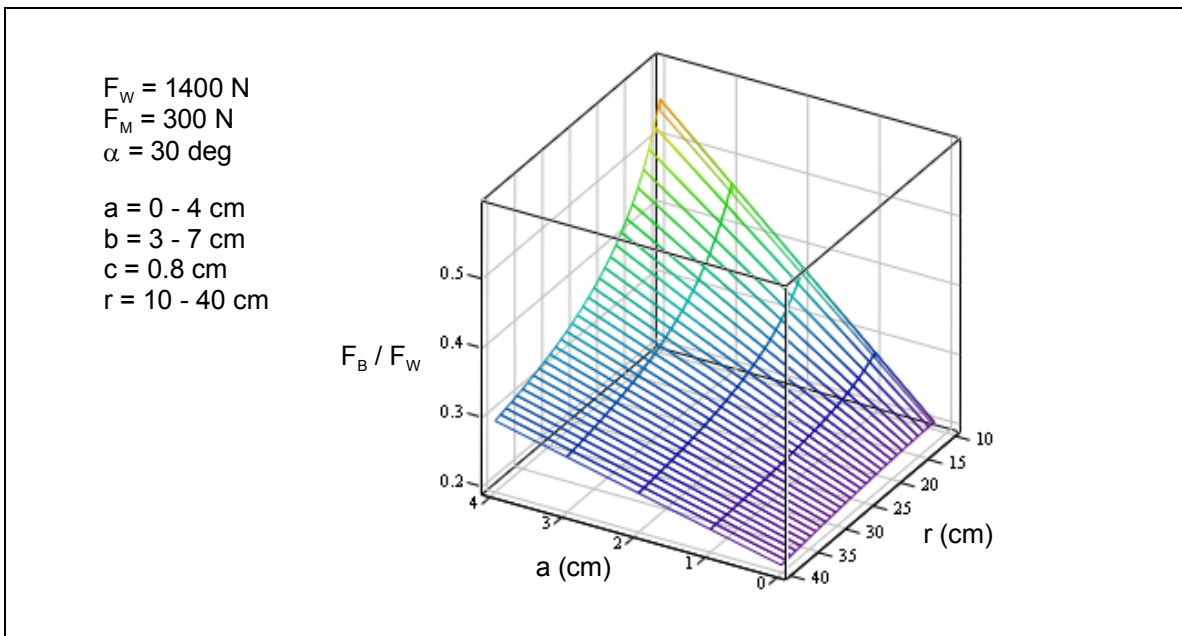


**Figure 22 - An example of the significance of tire radius and position of ground reaction force in loose snow for a braking slip friction coefficient calculated with static weight as the vertical force**

#### 4.5.3.5 An Actual Measurement Case in Fresh Natural Snow

Figure 23 shows data for a series of actual measurements by a combined force- and torque-measuring tribometer on virgin natural snow covering a runway. The snow had fallen during the night at  $-3^{\circ}\text{C}$ , and measurements were done in the late morning as the sun started to melt the snow. There was no wind, making the deposit depth of 2 cm very uniform. The friction values indicated by markers are averages from three runs at each of the three speeds 40, 65 and 90 km/h. The curved lines are fitted quadratic polynomials.

In Figure 23, the curve labelled F represents the force-measured friction value. The curve labelled T represents the torque-measured friction value. The curve labelled E represents the dynamic error expressed as friction coefficient.

On bare compacted snow, the friction-speed relationship has generally been found to have negligible speed dependency. Since the force- and torque-measured friction values decreased with increasing speed in this case, snow-planing may explain the speed dependency.

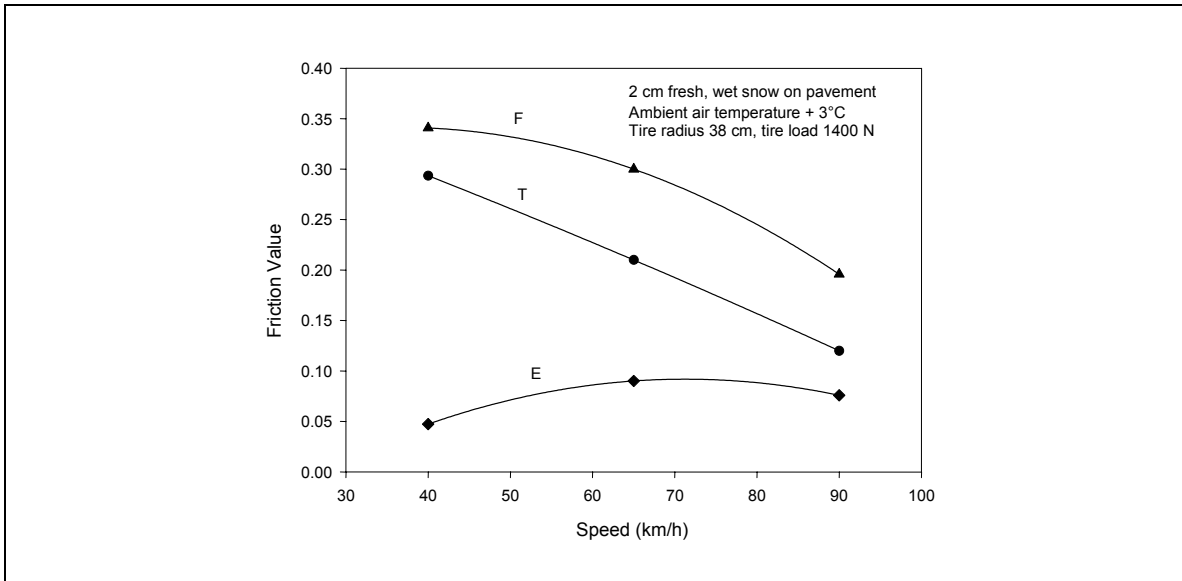


**Figure 23 - An actual case of reported friction values by a combined force- and torque-measuring tribometer for natural fresh snow**

#### 4.5.3.6 Ultimate Shear Force of Surface Material

From Figure 15, summation of horizontal forces in equilibrium yields the following relationship for the resultant resistive force in the tire-ground contact area.

$$F_S = F_M - F_E \cdot \cos\alpha \quad (98)$$

The value of  $F_S$  is always less than the measured force  $F_M$  and largest when  $\alpha$  is zero and  $F_E$  is zero (i.e., when  $F_S = F_M$ ).

The largest resultant force must be less than the ultimate resultant shear force of the surface material for the real contact area:

$$F_S = F_M = F_B + E \leq \tau_{ult} \cdot A_R \quad (99)$$

A measured horizontal force is the sum of a calculated braking slip force by a torque-measuring tribometer and a resultant resistive error force,  $E$ . When  $F_E$  is zero with a maximum value for  $F_M$ , the error term is equal to the tire-rolling resistance by definition.

## 5 CHARACTERISTICS OF DYNAMIC CONTAMINANT RESISTIVE FORCES

### 5.1 Resistance Force from the Compacting of Snow

A braked tire will compress, or sinter, loose snow caught under the tire tread to a higher density than it had before the wheel came into contact with it. Compacting has two force components: horizontal and vertical.

The vertical force can be treated as a rolling resistance due to lift. The horizontal force can be treated as a fluid shear force,  $F_C$ . If the shear force during compacting can be assumed to behave according to Newton's law of viscous flow, then the force is proportional to an equivalent dynamic viscosity and the rate of change of velocity across the layer thickness. If the rate of shear is a constant, then the shear stress is

$$\tau = \frac{F_C}{A} = \nu \cdot \frac{V}{t} \quad (100)$$

where  $\nu$  is the dynamic viscosity,  $t$  is the layer thickness and  $V$  the velocity. This equation can be rearranged as

$$F_C = \nu \cdot A \cdot \frac{1}{t} \cdot V \quad (101)$$

The dynamic viscosity is a characteristic of the contaminant material. The area for the acting shear force is an unknown part of the tire footprint.

For a given surface condition and device tire configuration,  $\nu$ ,  $A$  and  $t$  can be grouped into a compacting resistance factor,  $k_C = \nu \cdot A/t$ . The compacting force equation (101) may be simplified as

$$F_C = k_C \cdot V \quad (102)$$

### 5.2 The Compacting of Loose Snow with a Non-Braked Wheel

A theoretical method for predicting the compacting resistance of a free-rolling tire in dry, loose snow has been developed by van Es [5]. The model includes a resistive force due to snow volume compression energy,  $F_{compression}$ , and a resistive force due to the required vertical displacement or motion of the snow (kinetic energy),  $F_{verticaldisplacement}$ . In essence, the resistive compacting force is a sum of two forces:

$$F_{CV} = F_{compression} + F_{verticaldisplacement} \quad (103)$$

The compression force is a function of initial snow depth and initial snow density, as presented graphically in Figure 24.

The vertical displacement force is a function of speed squared and a non-linear factor,  $k_{VD}$ , representing a blend of parameters such as tire geometry, tire load, initial snow density and initial and final snow depth.

$$F_{verticaldisplacement} = k_{VD} \cdot v^2 \quad (104)$$

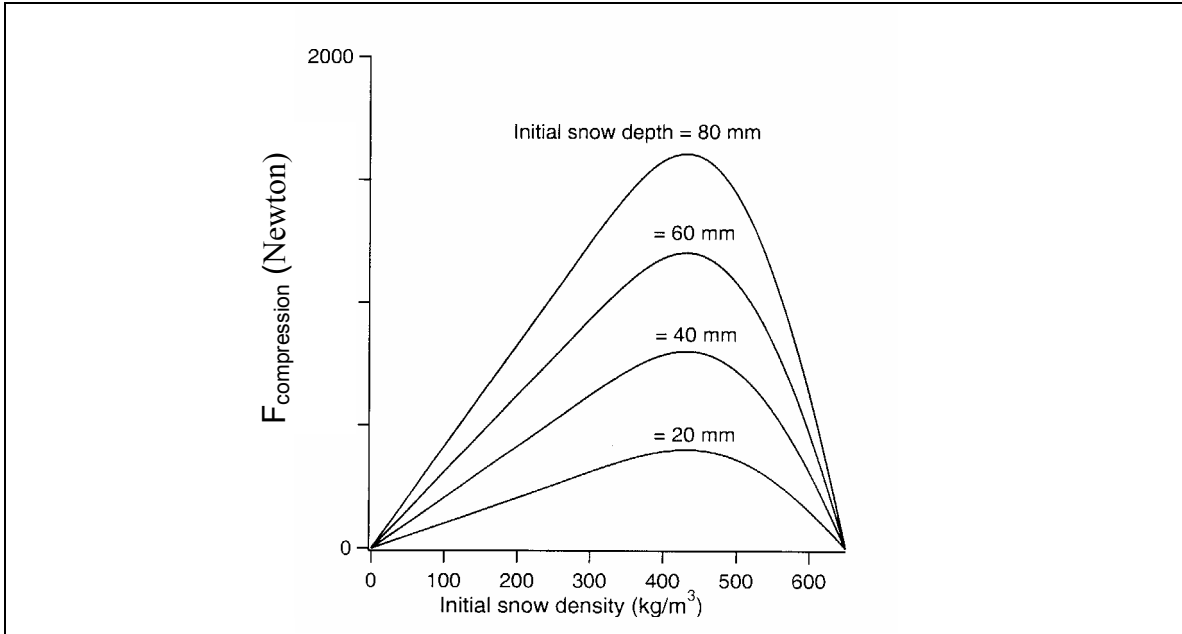


**Figure 24 - Resistive force due to compression of loose snow as influenced by initial snow depth and initial snow density [5]**

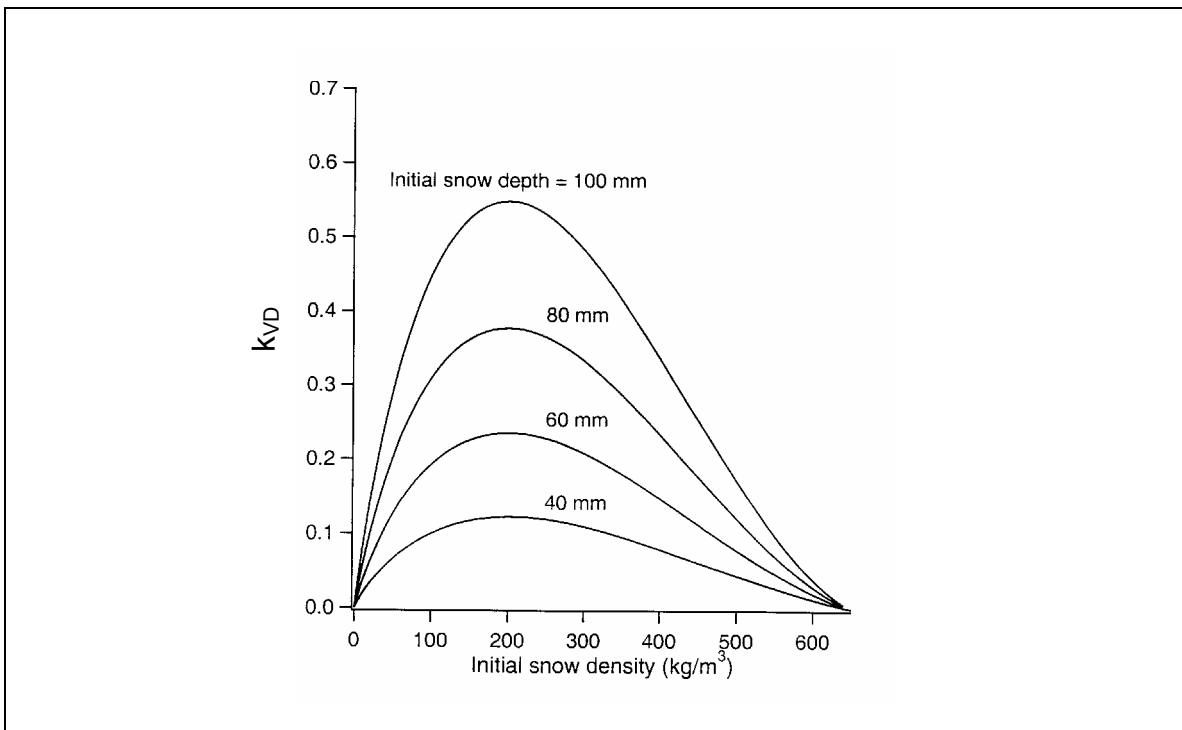


**Figure 25 - Vertical displacement factor,  $k_{VD}$ , for a type VII aircraft tire as a function of initial snow depth and initial snow density according to [5]**

The vertical displacement force factor for a type VII aircraft tire with a load of 4400 N and tire pressure 937 kPa is shown in Figure 25. The type VII aircraft tire has a nominal diameter of 37 cm.

The van Es model does not address the lateral displacement drag of some of the snow. Earlier models used by aviation engineers have applied the model of fluid displacement drag, converting the snow mass to its equivalent water depth.

### 5.3 Dynamic Contaminant Planing Propagation

The effect of dynamic contaminant planing is the loss of contact area for any braking slip friction to be generated. The tire configuration has a significant influence on the system of forces generated. To study this influence, two tire types will be selected that differ in the way they deform in the contact zone when planing. The position of the resultant fluid lift force will shift with travel speed and other parameters.

The tire is generally stronger along the sidewall than in the centre of the contact patch. The weaker centre area yields to the impingement forces of the fluid and allows it to penetrate under the centre of the tire contact area. The penetration of fluid lifts the tire from the leading edge and separates the tire from the ground with the interspersed fluid. The sidewalls carry normal load to press the area along the sidewall to the ground. Effectively, the fluid gets trapped in the centre where the tire is weaker. If it is present in sufficient amounts, it can escape to the sides in texture voids of the surface. Otherwise, it will push its way through the whole length of the centre portion of the contact area and leave the contact area at the centre of the trailing edge. The fluid has then lifted the centre portion of the tire contact area and reduced the net area of ground contact available for generating slip friction for braking. The same dry, powdery snow of the same moderate thickness may therefore affect the size of the net area of contact differently when present on good textured pavement versus smooth ice or a hard compacted snow base (negligible texture).

Research has shown that automotive-type tires remain longest in contact with the ground through the areas along the sidewalls, as the wedge of fluid penetrates the contact area at higher velocities. Aircraft-type tires, on the other hand, have a more uniform lift area across the width of the tire footprint because of another carcass design and the use of a higher inflation pressure. The trailing edge of the aircraft tire is the last part of the tire to detach from the ground.

Both automotive- and aircraft-type tires are models for many friction test tires. If the two categories of friction test tires have different force systems when planing, this must be accounted for when predicting forces for an actual aircraft tire configuration.

#### 5.3.1 Fluid Planing with Different Tire Designs

A fluid planing ratio can serve as a parameter to describe the intensity of fluid planing for a given device tire configuration and surface pair.

The fraction of contact patch area lifted versus the gross patch area is called a fluid planing ratio,  $k_p$ . A fluid planing ratio of 0.4 means that only 0.6 of the gross contact patch remains for slip friction braking. A fluid planing ratio of zero means that the whole gross contact patch is available for slip friction braking with the ground surface.

In Figure 26, a scenario with one automotive-type tire and one aircraft-type tire is depicted for different degrees of planing.



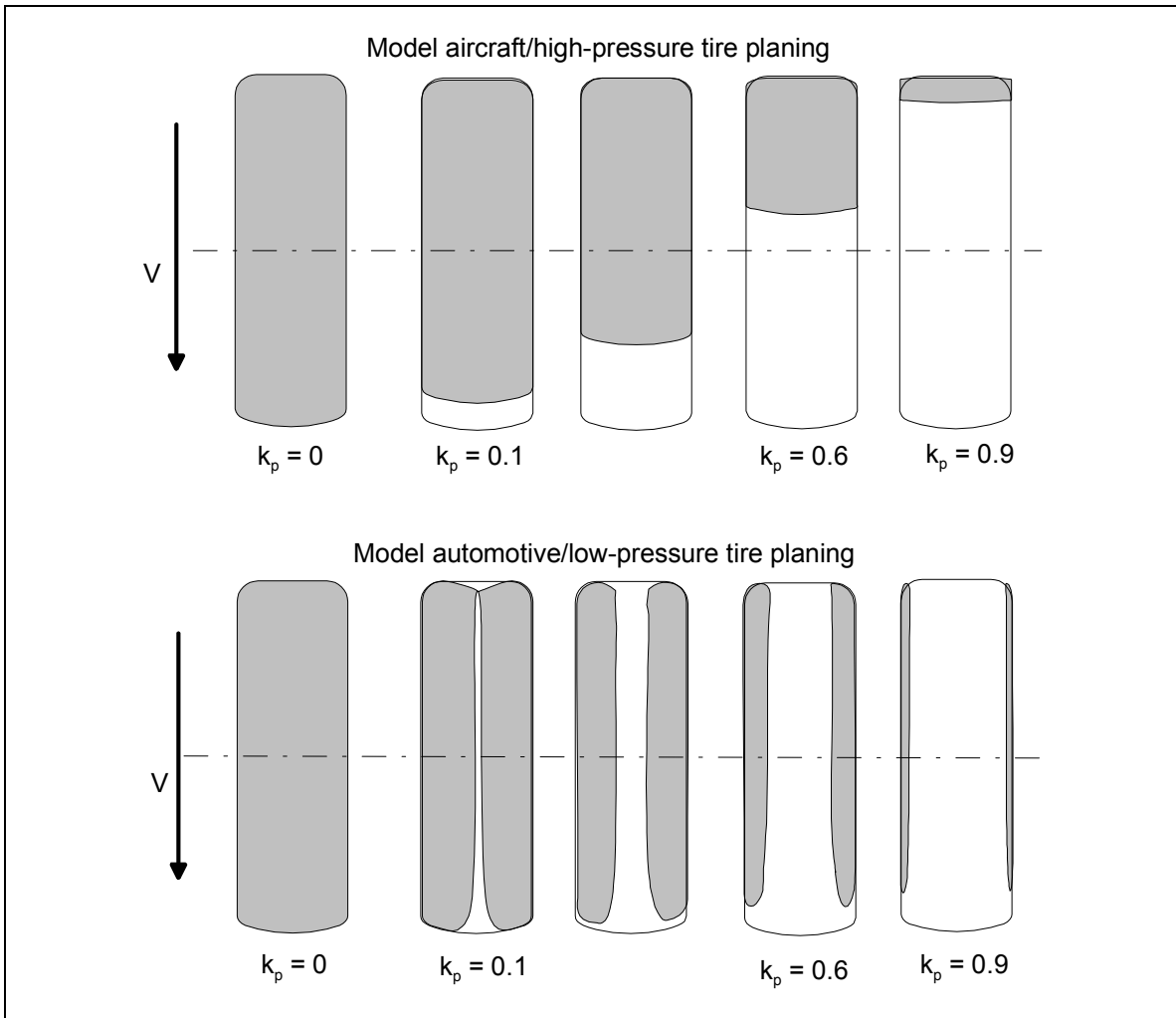


**Figure 26 - Two different fluid planing progress models used in study. Dark areas have base surface contact. Planing factors  $k_p$  indicated,  $k_p = 0$ , meaning no fluid planing**

The different planing mechanisms will create different lines of attack for the fluid planing lift force. It can be argued that an automotive tire will tend to keep the line of attack closer to a vertical plane than an aircraft tire because it detaches in the centre area of the footprint in almost the full length of the footprint before the sidewalls are lifted in the final stage.

For aircraft-type tires, the attack line of the fluid lift force may tend to have an angle with the vertical plane as the wedge progresses at full width of the footprint. It will create a horizontal force component acting against the direction of movement (i.e., an additional drag component to the fluid displacement drag force). It is a question, therefore, of whether an aircraft tire will measure more drag than an automotive tire of equal size under the same fluid contaminant conditions with free-rolling or moderate braking slip ratios.

Viscosity is a measure of the shear forces that a fluid can sustain when interspersed between opposing surfaces. Water has lower viscosity than slush or snow powder. The shear forces in the separation zone of the contact patch are therefore generally higher for snow powder than for water. The higher viscosity of snow powder also prevents it from escaping as quickly as water when there are escape voids or texture in the contact patch. Thus, the separation zone produced by the same thickness of water film and snow powder film will tend to yield a larger separation

zone for snow powder than for water. In conclusion, tires are apt to lift more on snow powder than on water. The lift phenomenon is called fluid planing.

### 5.3.2 Critical Planing Speed

The critical planing speed is a function of fluid mass density,  $\rho$ , and contact pressure,  $\sigma$ , such that

$$V_C = constant \cdot \sqrt{\frac{\sigma}{\rho}} \quad (105)$$

When  $V_C$  is determined for a tire configuration using water, the critical planing speed for a winter contaminant,  $V_{Ccontam}$ , can be estimated using

$$V_{Ccontam} = constant \cdot \sqrt{\frac{\sigma}{\frac{\rho_{contamination}}{\rho_{water}}}} = constant \cdot \sqrt{\frac{\sigma}{\gamma}} \quad (106)$$

where  $\gamma$  is the specific gravity of the contaminant.

## 5.4 Resistive Forces from Fluid Displacement Drag on Rigid Base Surfaces

The fluid displacement drag on the tire is given by the following equation:

$$F_D = \frac{1}{2} \cdot C_D \cdot \rho \cdot A_D \cdot V^2 \quad (107)$$

where  $C_D$  is the fluid drag coefficient,  $\rho$  is the fluid mass density,  $A_D$  is the tire-fluid contact area in the normal vertical plane and  $V$  is the travelling velocity. The drag force is not considered to have a significant vertical component. The fluid lift stems from the tire rolling over the fluid, which escapes under compression in texture voids or gives rise to planing.

The drag coefficient is the ratio of resistance over dynamic pressure multiplied by the maximum cross-sectional area of the body,  $A_D$ . There is a need to research drag coefficients for friction tester tires and aircraft tires for varying depths of contaminants.

For aircraft tire type planing, the area  $A_D$  is a constant:

$$A_D = w \cdot t \quad (108)$$

where  $w$  is the gross width of the tire footprint and  $t$  is the contaminant fluid layer thickness.

As shown in Figure 27 the frontal area for drag can be reduced as a result of the buckling of the tire. Some contaminant may then be trapped to flow under the tire rather than be displaced to the sides. The effective area,  $A_D$ , for the automotive tire type planing can be modelled as

$$A_D = w \cdot t \cdot \left(1 - \frac{1}{2} \cdot k_p\right) \quad (109)$$

where  $k_p$  is the planing factor.

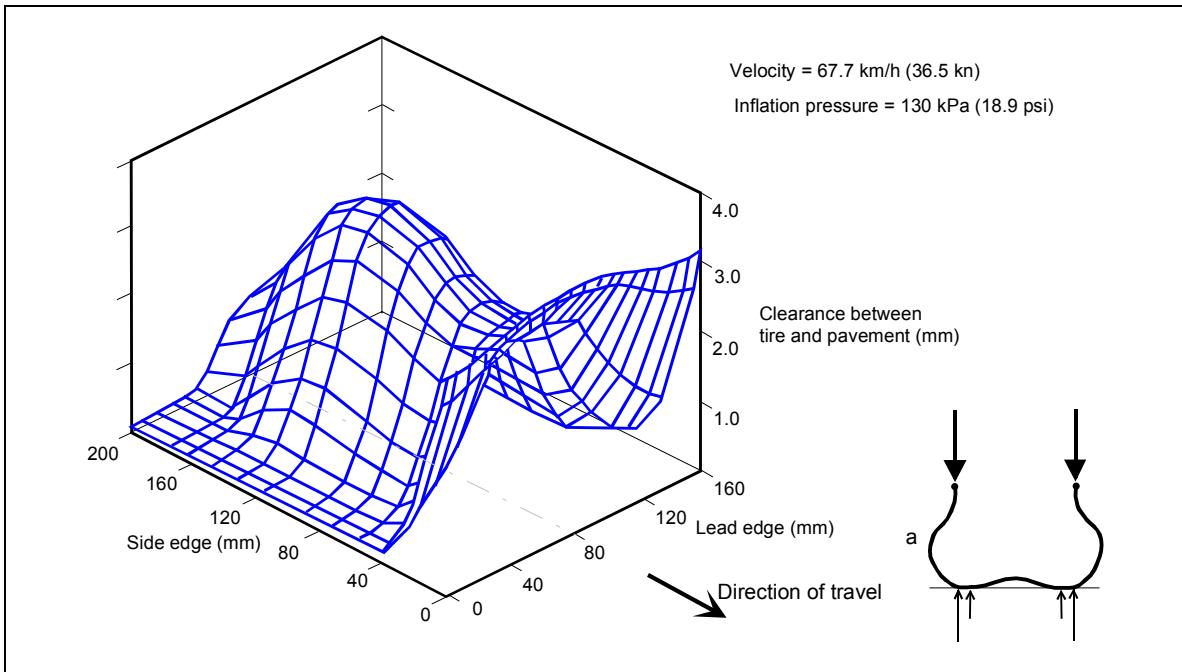


**Figure 27 - Fluid film distribution in automotive tire footprint**

Results of sample calculations for the drag force are shown in Figure 28. A value of  $C_D = 0.4$  has been assumed for the calculations.

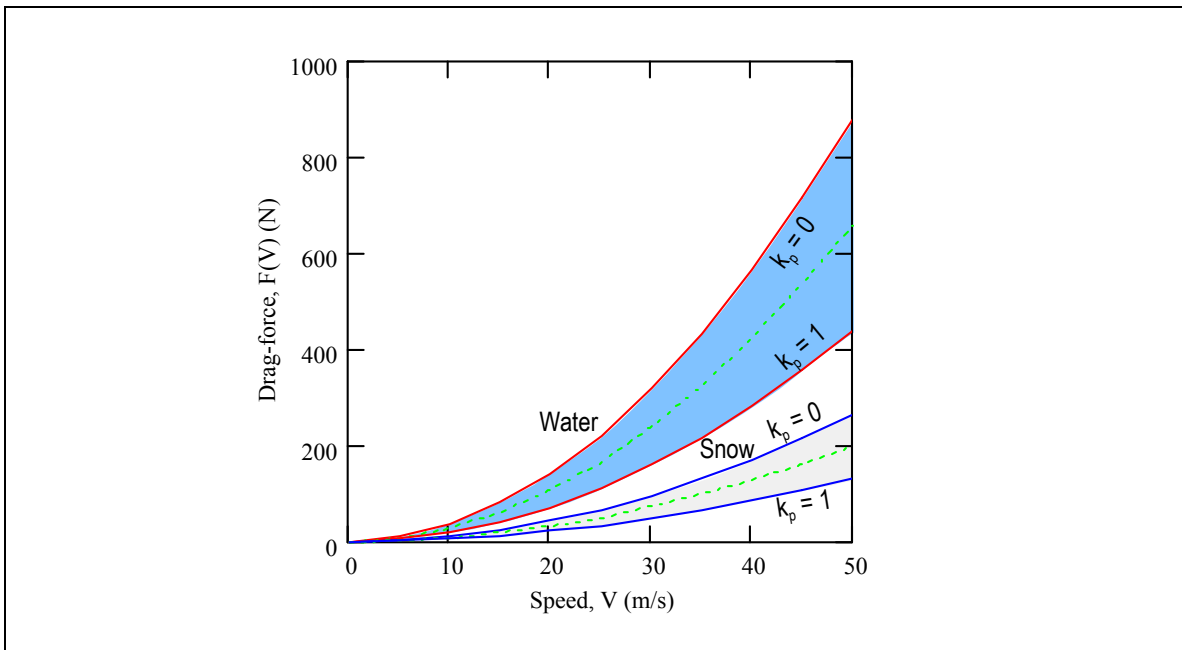


**Figure 28 - Theoretical fluid displacement drag force for a tire geometry equivalent to the ASTM E-1551 tire for a case with 3 mm water film and a case with 3 mm snow. The snow density is 30 percent of water.**

As can be expected, the forces are smaller for the lower density fluid and proportional to the densities. For full fluid planing, the forces are half the values of the non-planing values. This particular planing factor definition can be applied only to automotive tire types.

The aircraft tire type has the largest drag force in both cases. For the automotive tire type, the drag force can reach the same order of magnitude as the rolling resistance force from fluid lift at the highest velocity shown. For the aircraft tire type of our scenario, the maximum drag force shown is only a fraction (20 percent) of the maximum rolling resistance force.

## 5.5 Differences of Braking Slip Friction Between Rigid and Non-Rigid Surfaces

It has long been acknowledged that tire interaction with a bare, rigid pavement surface is different than interaction with a non-rigid surface, such as compacted snow. The observation is that friction values measured on a rigid surface include a large measure of mechanical tire properties, whereas on non-rigid surfaces the friction values include a large measure of surface mechanical properties. Interacting with a pavement, the tire is the sacrificial part. Interacting with a non-rigid surface, the surface is the sacrificial part. Between the extremes of rigid and non-rigid surfaces, the interaction is expected to be a blend of sacrifice from the tire and the surface.

## 5.6 Contact Pressure

The horizontal braking slip friction force of a braked wheel is the average tangential shear stresses acting in the contact area between the tire and the surface. It can be written as

$$F_X = \tau \cdot A_S = \mu \cdot F_G \quad (110)$$

where  $F_G$  is the ground reaction force. Note that the ground reaction force does not always equal the weight or the applied normal load. Acting on the same contact area is the average normal stress, also called the contact pressure:

$$\sigma = F_G / A_S \quad (111)$$

Substituting for  $F_G$  and rearranging, the friction coefficient can be expressed at the ratio of the normal stress to the shear stress in the contact area:

$$\mu = \tau / \sigma \quad (112)$$

The role of the shear stress may be illustrated with Figure 29 redrawn from [6]. In this figure, shear stresses at different braking levels are plotted along the length axis of a tire-surface contact area. It can be observed that the maximum shear stress occurs toward the end of the contact patch length.

If medium and hard braking exceeds the ultimate shear strength of the surface (compacted snow), the surface material will shear off (at, for example, 2.0 kp/cm<sup>2</sup>) and only light braking will not sacrifice the surface. In such a case, the shear stresses would be redistributed in another shape.

The friction coefficient of the form (112) is useful for discussion of the influence of the contact pressure on the pair of opposing materials, including a visco-elastic material such as tread rubber mounted on a flexible tire carcass. For opposing pairs of materials where rubber is one of the materials, the classic assumption that the friction coefficient is a constant of the material pair is, for the purposes of vehicle traction or braking and friction measurement, simply false. Rather, one may have

$$\mu(\sigma) = \tau / \sigma \quad (113)$$

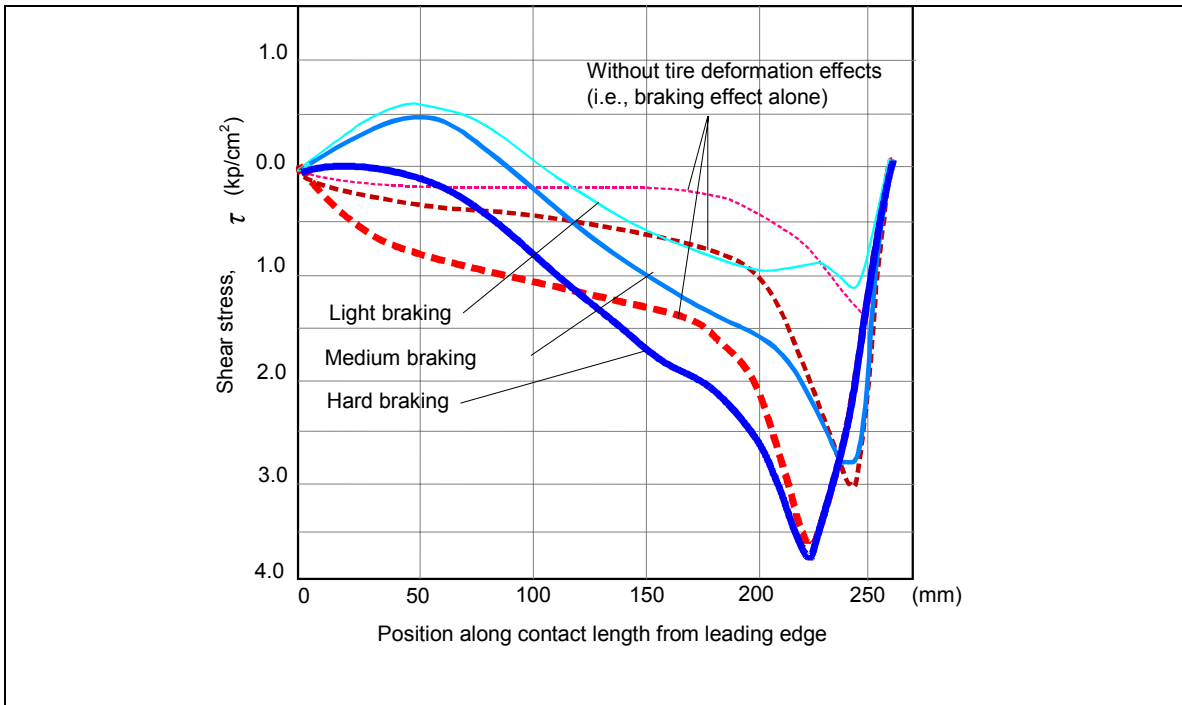


**Figure 29 - Shear stress distribution in the contact patch during braking on a rigid surface**

Contrary to popular expectations, the adhesion type of friction diminishes with increasing contact pressure on a dry, rigid surface. This is illustrated in Figure 30 and is taken from studies of a rubber slider subject to variable load on a dry surface [7]. A light-loaded tire may therefore exhibit higher shear stresses than a heavy-loaded tire of the same type when interacting with a dry, rigid surface. A friction measurement device with a light load on the measuring tire yields a higher reported friction value than a heavier load on the same tire on dry, rigid surfaces.

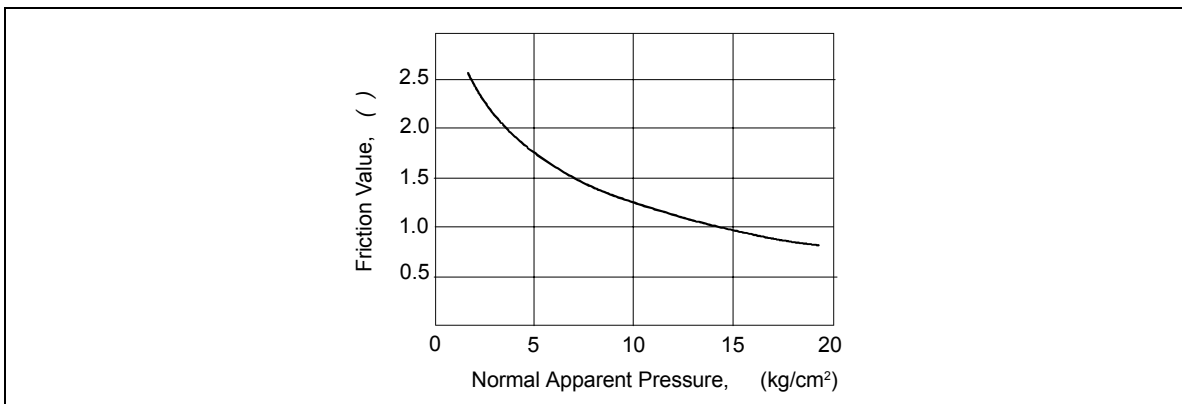


**Figure 30 - Friction due to adhesion by a rubber slider on a dry, rigid surface as a function of vertical contact pressure.**

On a non-rigid surface like compacted snow, the braking slip friction has been found to increase with increasing contact pressure. Truck operators with lift on one of two rear-drive axles have taken advantage of this fact ever since drive trains with such features were introduced. On winter contaminants they lift and disengage one of the drive axles to improve traction for the remaining working axle, thereby gaining more available friction from the surface than the two axles provided, as evidenced by spinning wheels.

Wambold [8] has found that as the normal load increases, the reported friction values of friction measurement devices increase asymptotically to a maximum level, which is believed to be close to the ultimate shear strength of the compacted snow material. If this is true, then any vehicle whose tires are loaded to the same high average normal stress will experience the same ultimate shear strength at maximum braking and show very good correlation of the respective braking forces. The limit of attainable friction will have been reached and is a mechanical property of the one material of the interacting pair.

When correlating the slope coefficient of a linear regression from the reported friction numbers of the participating friction devices in the JWRFMP, it was found by [9] that the slope coefficient correlated well ( $R^2 = 0.86$ ) with the net contact pressure of the corresponding devices. This indicates that the differences in reported friction values among different friction measurement devices are mainly due to differences in contact pressures, as seen in Figure 31.

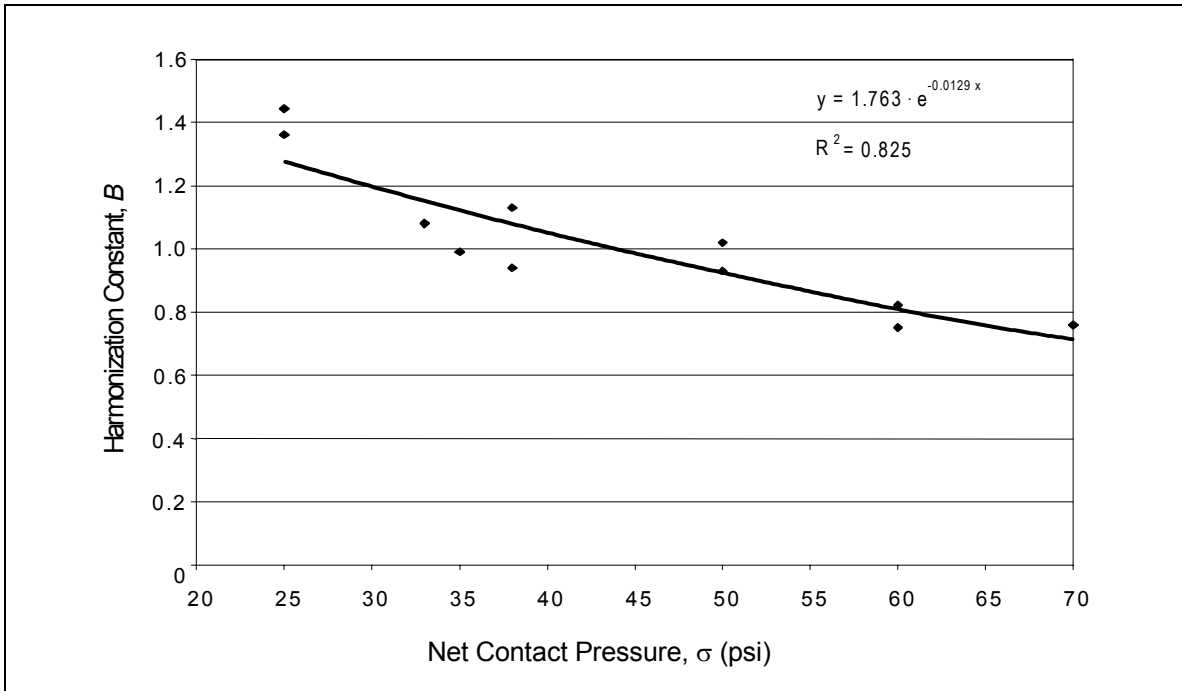


**Figure 31 - The slope correlation coefficient versus net contact pressure of friction measurement devices by [9]**

Research has confirmed that the melting of ice due to tire contact pressure is not an influential factor, such as it is for skates, because the contact pressure is not high enough. Contact pressure does, however, influence the braking slip friction in different ways on different surface types and conditions.

## 6 SUMMARY OF MECHANICS OF TIRE-SURFACE FRICTION

Given that the objective of tribometers is to report braking slip friction, the dynamic influences of winter contaminants in liquid, plastic or particle form introduce errors in the reported friction values. These adverse dynamic effects contribute differently to the reported friction values for various types of devices.

Generally, the adverse effects grow with increasing travel speed and the increasing deposit depth and density of the contaminate.

The braking slip friction force,  $F_B$ , depends on the slip speed and travel speed where adhesion and hysteresis constitute the principal mechanisms of friction.

When planing occurs, the effective contact area for generating braking slip friction forces is gradually reduced with increasing travel speed.

The displacement drag force,  $F_D$ , depends on the squared velocity and increases rapidly with accelerating travel speed. The drag term grows and the braking slip friction term diminishes in relative and absolute terms.

The rolling resistance force due to fluid lift effects,  $F_L$ , will increase on surfaces with loose contaminants, as it combines with vertical components of compacting resistance forces.

The fluid forces are closely related to tire geometry, tire carcass design, inflation pressure, and weight carried by the wheel. Different tire types exhibit different behaviour with planing.

The speed dependency of the error terms indicates that a measuring speed limit may exist in order to report below acceptable errors for a given surface material, contaminant type and deposit depth. In general, the error of the reported friction increases with increasing measuring speed for both a force- and torque-measuring tribometer. To minimize the error, measuring should be done at low speeds if there is a possibility for significant contaminant deposit depths.

When there is no significant deposit depth of a fluid or loose winter contaminant on the base surface, the difference between reported friction values from a force- and torque-measuring tribometer using the same tire configuration will be the tire-rolling resistance value.

## 7 VARIABILITY OF FRICTION MEASURES

### 7.1 Descriptive Statistics

Friction measures are well-known for large variability and therefore must frequently be reported with appropriate descriptive statistics. The most common statistics are mean or average friction value, sample size, standard deviation, standard error, coefficient of variation, and confidence. In sections 7.1.1 through 7.1.5, some practical properties of the statistics are discussed,<sup>5</sup> as they may apply to friction measurement.

#### 7.1.1 Average (Mean)

Averages can be propagated to higher aggregated levels provided the friction measures are linear in nature and represent the equal or weighted sample sizes.

For friction devices operating at a constant speed and producing a fixed number of samples per distance unit, the sample size is a function of the distance measured. A friction measurement must therefore be associated with a defined distance to reflect a consistent sample size. The weighted average friction value may therefore be calculated for several different distances,  $l_i$ , that constitute a total length,  $L$ , according to (114):

$$\mu_{avg} = \frac{1}{L} \sum (l_i \cdot \mu_i) \quad (114)$$

When the distances,  $l$ , are of equal length, the average of  $n$  friction measurement can be calculated with (114) to give a correct average friction value. This is the arithmetic mean often referred to as simple averaging.

$$\mu_{avg} = \frac{1}{n} \sum (\mu_i) \quad (115)$$

#### 7.1.2 Standard Deviation

The standard deviation of any series of friction measurements is the most widely used measure of dispersion. The difference of each measured friction value relative to the arithmetic mean friction value is squared, summed and divided by the number of measurements less one.

$$StdDev = \sqrt{\frac{\sum_{i=1}^n (\mu_i - \mu_{avg})^2}{n-1}} \quad (116)$$

The standard deviation according to equation (116) is only valid for arithmetic means of the friction values.

The standard deviation is not dimensionless. Since different friction devices report different friction values for the same surface, a standard deviation is valid only for the friction device that produced the values.

---

<sup>5</sup> The reader should consult a statistics textbook for definitions and more in-depth discussion.



When comparing friction devices based on standard deviation, similar, or harmonized, friction values should be used.

### 7.1.3 Coefficient of Variation

The coefficient of variation,  $CV$ , is an adaptation of the standard deviation used to express the variability of a set of numbers on a relative scale rather than on an absolute scale. It is therefore a dimensionless number. As a dimensionless number, it is often more suited for comparing variability of different tribometers when measuring the same surface. The average friction value should always be stated along with the  $CV$  number.

The coefficient of variation is frequently expressed as a percentage:

$$CV = \frac{StdDev}{\mu_{avg}} \cdot 100\% \quad (117)$$

### 7.1.4 Standard Error

The standard error is the standard deviation of the arithmetic averages, which can be shown to be the same as the sample standard deviation divided by the square root of the number of samples.

$$StdErr = \frac{StdDev}{\sqrt{n}} \quad (118)$$

Like the standard deviation, the  $StdErr$  is also expressed in units of the actual friction measurement device producing the friction values.

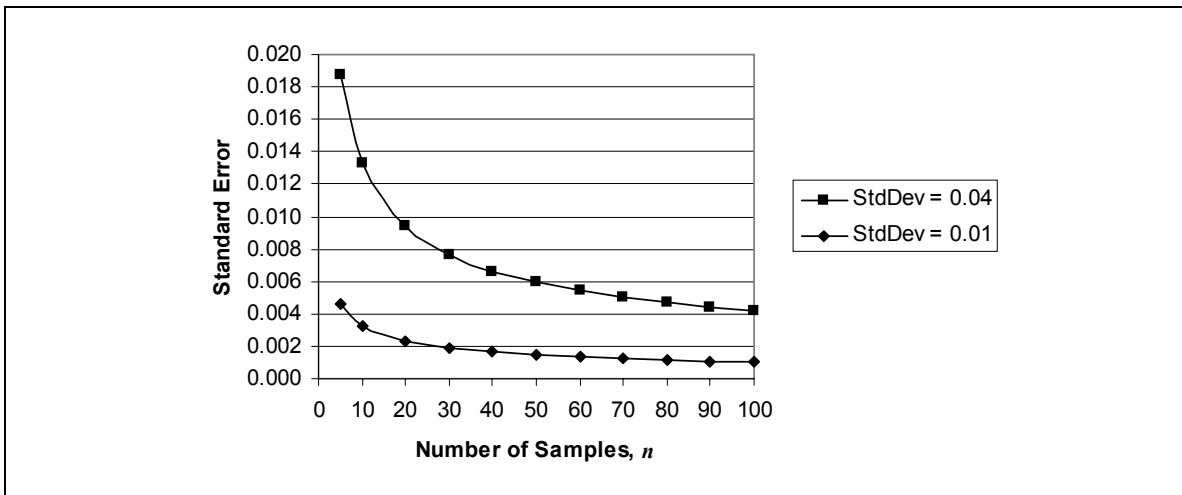


**Figure 32 - Sample data from wet pavement friction measurements showing  $StdErr$  as a function of number of samples. The average friction value was 0.66 and 0.68 for the surfaces with a high and low  $StdDev$  respectively.**

An important property of the  $StdErr$  is that it diminishes with increasing sample size. Two cases of  $StdErr$  versus number of samples for the same friction device are shown in Figure 32. The one case is a coarse textured surface with  $StdDev$  equal to 0.04. The other case is a medium textured surface with  $StdDev$  equal to 0.01.

### 7.1.5 Confidence Level

The confidence level expresses a probability that the average friction values fall within a lower and an upper value. It is probable that the average value is within

$$\mu_{avg} \pm \frac{1}{2} \cdot \text{confidence range} \quad (119)$$

The confidence range is the value of the extent between the two limits of a confidence interval. The confidence interval limits are functions of the observed average friction value ( $\mu_{avg}$ ), the critical t value from the Student t Distribution ( $t$ ), the standard deviation ( $StdDev$ ) and the number of samples ( $n$ ):

$$\mu_{avg} \pm \frac{1}{2} \cdot t\left(\frac{\alpha}{2}; n-1\right) \cdot \frac{StdDev}{\sqrt{n}} \quad (120)$$

where  $\alpha$  is equal to  $(1 - \text{confidence level})$

The limits of this interval are commonly set to a probability (confidence level) of 0.90, 0.95 or 0.99, corresponding to a 90 percent, 95 percent or 99 percent chance. Equation 120 can be written in terms of  $StdErr$  rather than  $StdDev$ :

$$\mu_{avg} \pm \frac{1}{2} \cdot t\left(\frac{\alpha}{2}; n-1\right) \cdot StdErr \quad (121)$$

In Figure 33 the expected deviation about the mean for a 95 percent confidence level is plotted for two cases of wet pavement friction measurements where the standard deviations were 0.01 and 0.04.

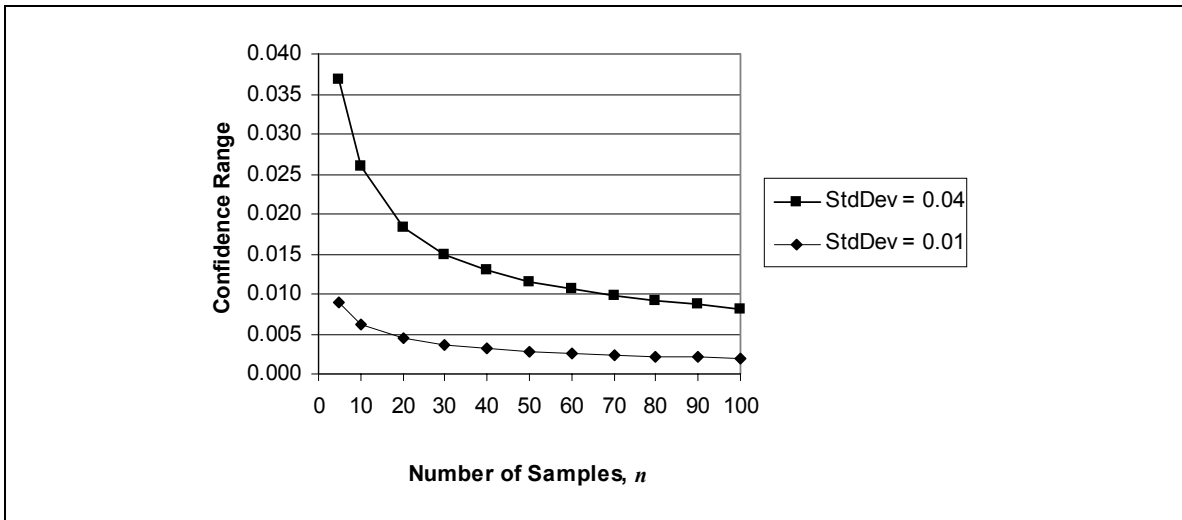


**Figure 33 - Sample data from wet pavement friction showing how the confidence range for a 95 percent confidence level may vary in two cases of  $StdDev$  as a function of number of samples. The average friction value was 0.66 and 0.68 for the surfaces with a high and low  $StdDev$  respectively.**

The longer the distance measured on the same surface (higher samples,  $n$ ), the better the confidence of the average friction value.

## 7.2 Normalized Friction Measurements

Since descriptive statistics are so important for the evaluation of friction measurements, essential information may be lost if a full set of descriptive statistics is not produced. The mandatory minimum set of descriptive statistics includes the average friction value, the sample size and the standard deviation. With these statistics, the standard error, coefficient of variation and confidence may be calculated for a set of friction measurements.

For continuous fixed-slip measurements, the sample size is a function of the distance measured. Different devices work with different sample rates and thereby produce different sample sizes for the same distance measured. Even if measured for the same distance, the descriptive statistics for two or more different friction devices with different sample rates are not comparable, except for the average friction value.

Especially for the comparison of friction devices, there is a need to normalize friction measurements where the reported friction values represent one or more standardized fixed distances with a fixed sample size. A basic unit of distance should be one metre. Other derived distances should be tenfold increments of that.

As many legacy friction devices are unable to report a friction value for such a short distance, the mandatory smallest standard distance should be 10 m. However, the standard normalized friction measurement should be for a 100 m distance. This normalized friction measurement would then be based on a sample size of 10 measurements of 10 m length, a fixed sample size. The standard deviation of the normalized friction measurement is, as a result of the normalization, the only mandatory supplemental information to the average friction value in order to have a full set of descriptive statistics. A set of friction measurements related to each other in such a matrix may be called a determinant.

Figure 34 depicts the concept of normalized friction measurements. To be able to include all legacy and current friction devices and give vendors freedom of design, the lower, or detailed determinant, is free or proprietary. The upper determinant is mandatory and standardized.

A normalized friction measurement, will not only facilitate comparisons of different devices, but also become a reference, enabling statements to be made about accuracy of friction measurements.

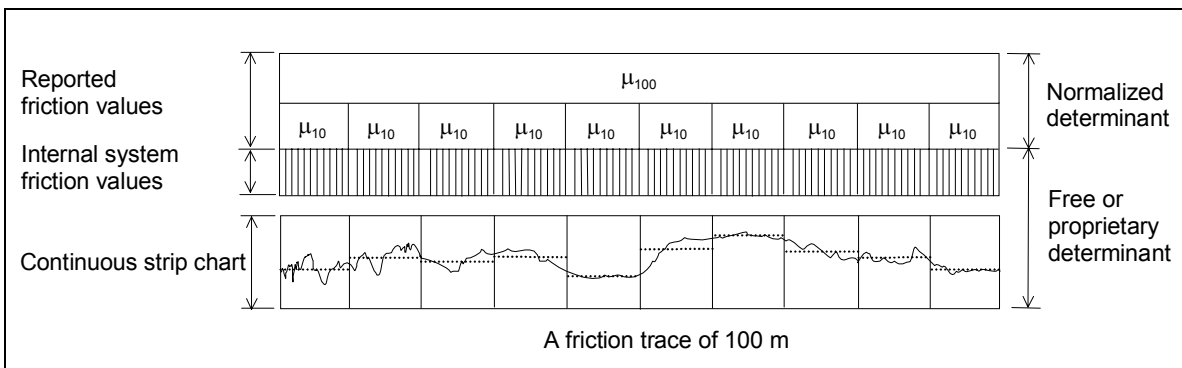


Figure 34 - Proposed system of normalized friction measurements

## 7.3 Device Variability

Friction measurement devices are subject to careful calibration of critical instrumentation components as part of the set-up procedures before measurements are done or daily maintenance is carried out. This set-up is static in the sense that the device does not move or

perform a typical measurement of a surface when the set-up is carried out. Experience has shown that the dynamic performance of a friction device may be quite different from the static performance.

Figure 35, produced from the database of [10], shows the range of average reported friction values for 12 friction devices of the same type in self-wetting mode at 65 km/h. The average was calculated from six repeat runs on the same 800 m test track. The test track had eight different 100 m asphalt surfaces laid out in a series.

The average difference in friction value between the lowest and highest reporting device was 0.1 friction units. The average standard deviation of the reported friction values of each of the 12 devices for each surface was 0.03. Similar reproducibility values have been obtained for other device types at the same test track.

The findings of [10] suggest that friction devices of the same type perform within a reproducibility range of  $\pm 0.05$  friction coefficient units.

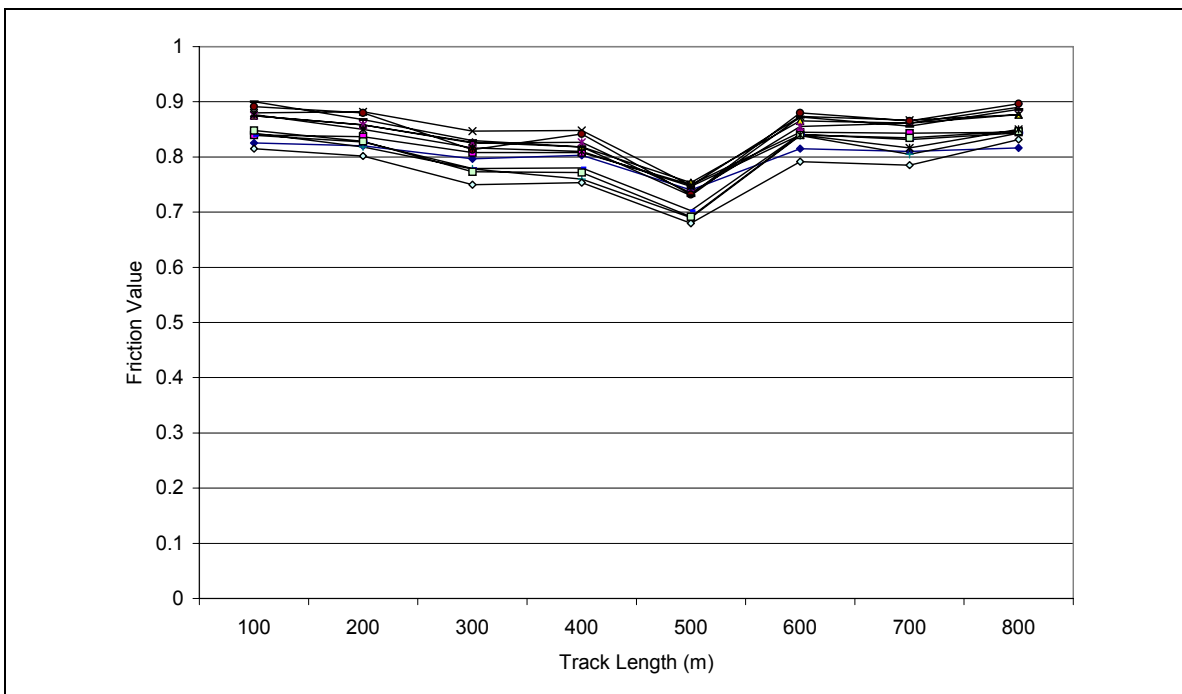


**Figure 35 - Average of 6 reported friction values for 12 tribometers of the same type at 65 km/h in self-wetting mode on a continuous track of 8 asphalt pavements each 100 m in length and of different asphalt recipe.**

## 7.4 Surface Variability

An established practice has been to measure several hundred metres of a surface before reporting the average friction value.

Surface variability for wet pavement is significantly influenced by macrotexture, as shown in Figure 36. The standard deviation of the friction values for a device was computed for three parallel sections of the same asphalt recipe. These standard deviations were then averaged for all 12 tribometers that participated in the test of Figure 35. The average standard deviations are shown in a scatter plot versus average macrotexture measurements of the same asphalt recipe.

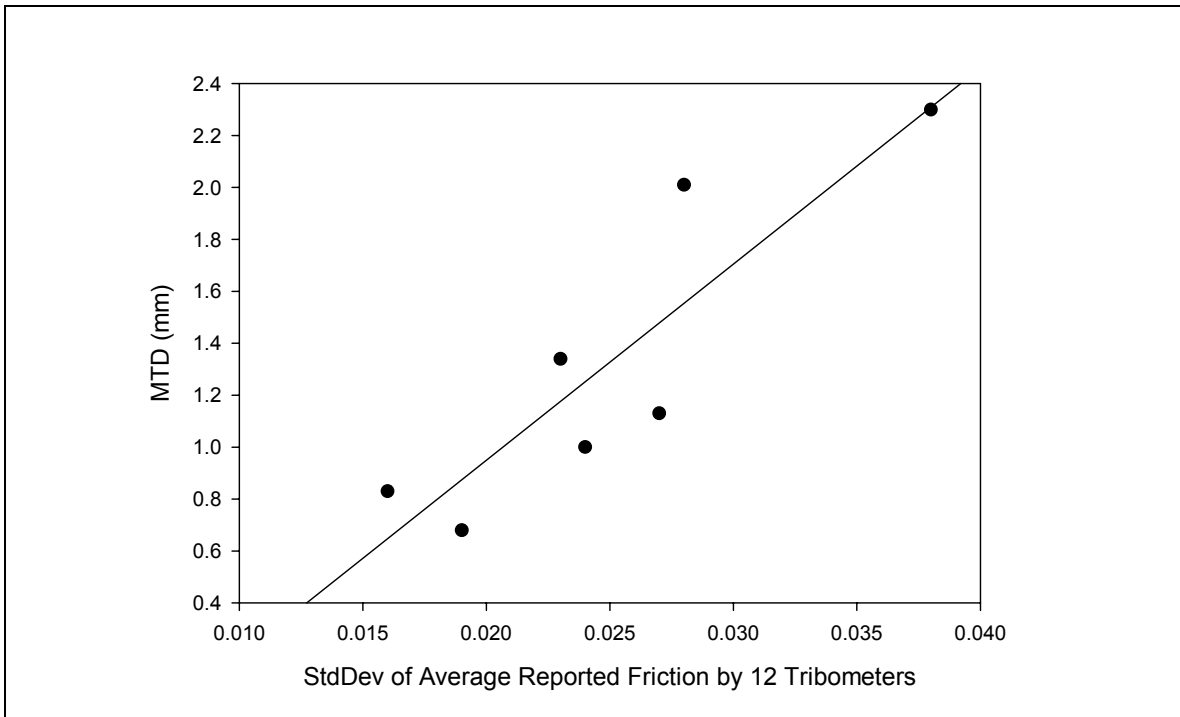


**Figure 36 - Surface variability expressed as average standard deviation versus macrotexture based on the test data of Figure 35**

One should not be led to believe that a tribometer has constant properties such that any variance of the reported friction value can be interpreted as surface variability.

Because the force and/or torque that a friction measurement device senses is a result of the interaction of a tire-surface materials pair, it is not possible to extract that part of the variability that is due to either one of the interacting parts from a friction measurement.

It is important to distinguish variability of one continuous measurement of a surface from variability of repeated measurement runs of the same surface. The latter form of variability is called repeatability. Since it is practically impossible to measure exactly the same surface track repeatedly, the repeatability measurement will also contain variance from surface non-homogeneities.

## 7.5 Variance in Friction Device Comparisons

The device and surface variability propagates to variance in device comparisons. To give the reader an appreciation of the magnitude and nature of variance, three examples will be discussed.

When comparing two tribometers, analysis is usually based on a scatter plot of the paired measurement values. Figures 37 and 38 show scatter plots of pairs of devices on ice and snow. Figure 39 shows a scatter plot for wetted asphalt pavement. The sample data populations include three to six repeated runs over the same surfaces of 100 m in length.

The average friction transformation line, also called the fitted regression line, is shown together with a 95 percent confidence interval as the pair of dotted lines.

In Figure 37 each device had a sample size of 241 measurements. The correlation coefficient was 0.85. The fitted regression line was

$$\mu_{Device1} = 0.047 + 0.8063 \cdot \mu_{Device2} \quad (122)$$

The standard error of estimate of the averages of the friction transformation line was 0.032 friction units.

The prediction interval lines cover a range of 0.13 friction units. If a single 0.25 friction value was measured with Device 2, there is a 95 percent chance that Device 1 would have measured a single value between 0.18 and 0.31. If the 0.25 value of Device 2 was an average of several measurements, the transformation equation can be used, which predicts the Device 1 value to be 0.25 with a standard error of 0.032.

It is not common practice to measure several times (i.e., perform repeated runs) to obtain an average for parts of a runway for so-called operational friction measurements. The confidence of a single measurement of a part of a runway is poorer than an average of several measurements from repeated runs.

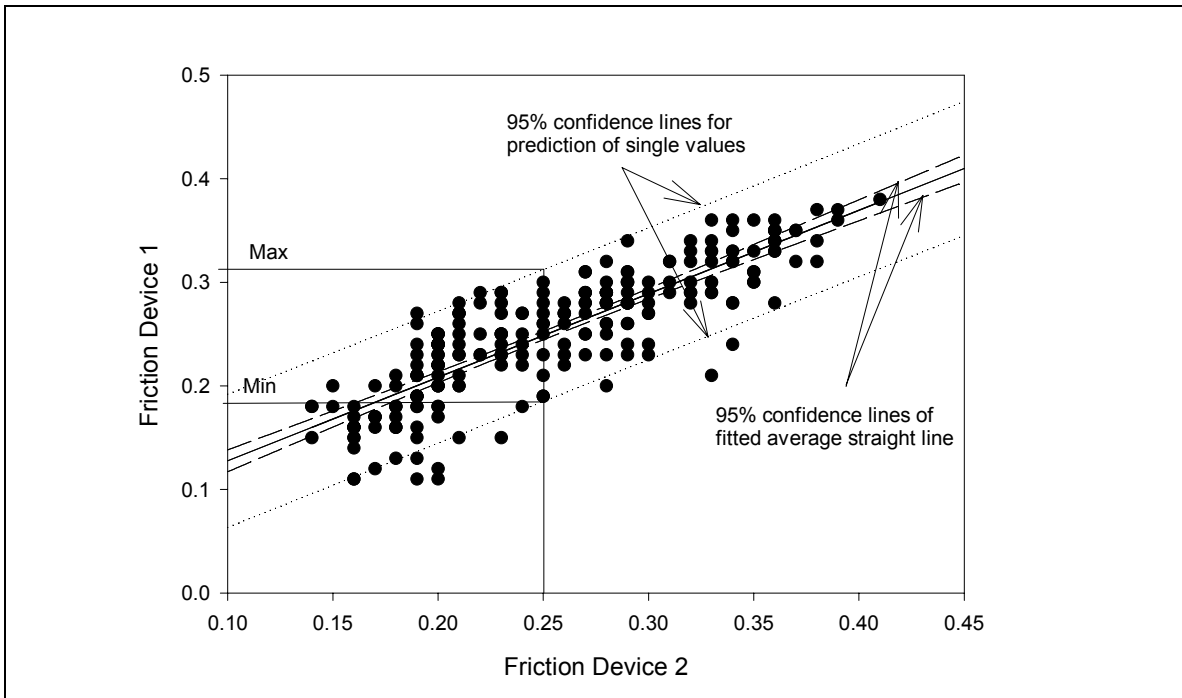


**Figure 37 - A scatter chart of two friction devices that have measured on the same variety of ice and snow surfaces at speeds ranging from 40 to 90 km/h**

In Figure 38, each device had a sample size of 96 measurements. The correlation coefficient was 0.62. The fitted regression line was

$$\mu_{Device3} = -0.039 + 0.8983 \cdot \mu_{Device1} \quad (123)$$

The standard error of estimate of the averages of the friction transformation line was 0.055 friction units.

The prediction interval lines cover a range of 0.22 friction units. If a 0.25 friction value was measured with Device 1, there is a 95 percent chance that Device 3 would have measured

between 0.07 and 0.29. If the 0.25 value was an average of several measurements the transformation equation can be used, which predicts the Device 3 value to be 0.19 with a standard error of 0.055.

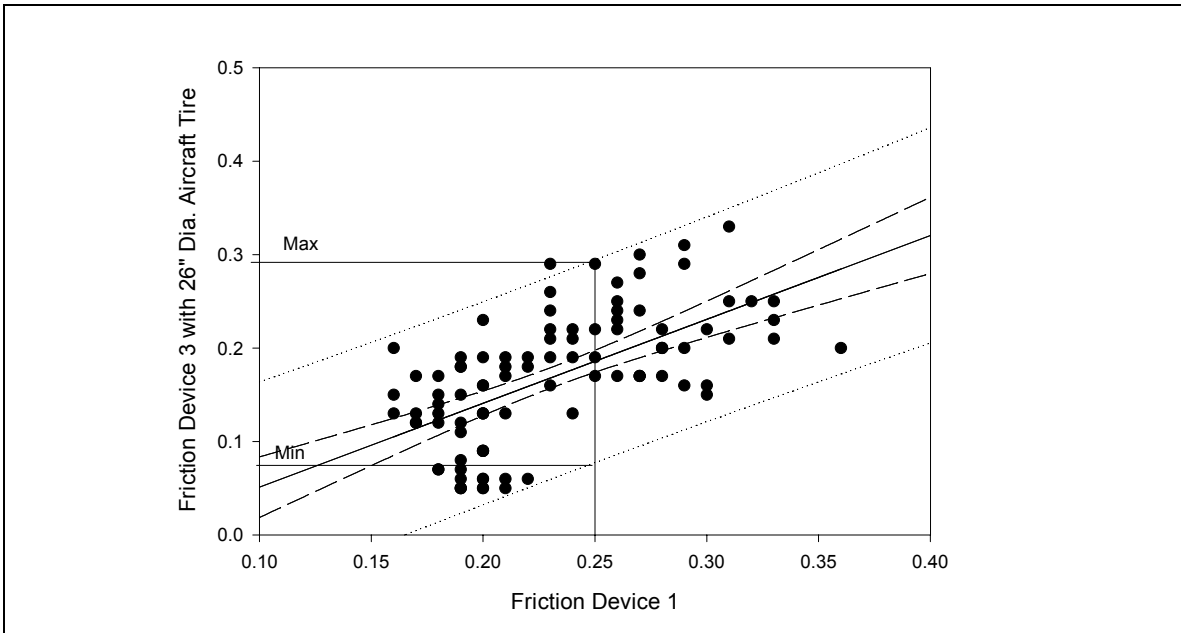


**Figure 38 - A scatter chart of two friction devices that have measured on the same variety of ice and snow surfaces at speeds ranging from 40 to 90 km/h**

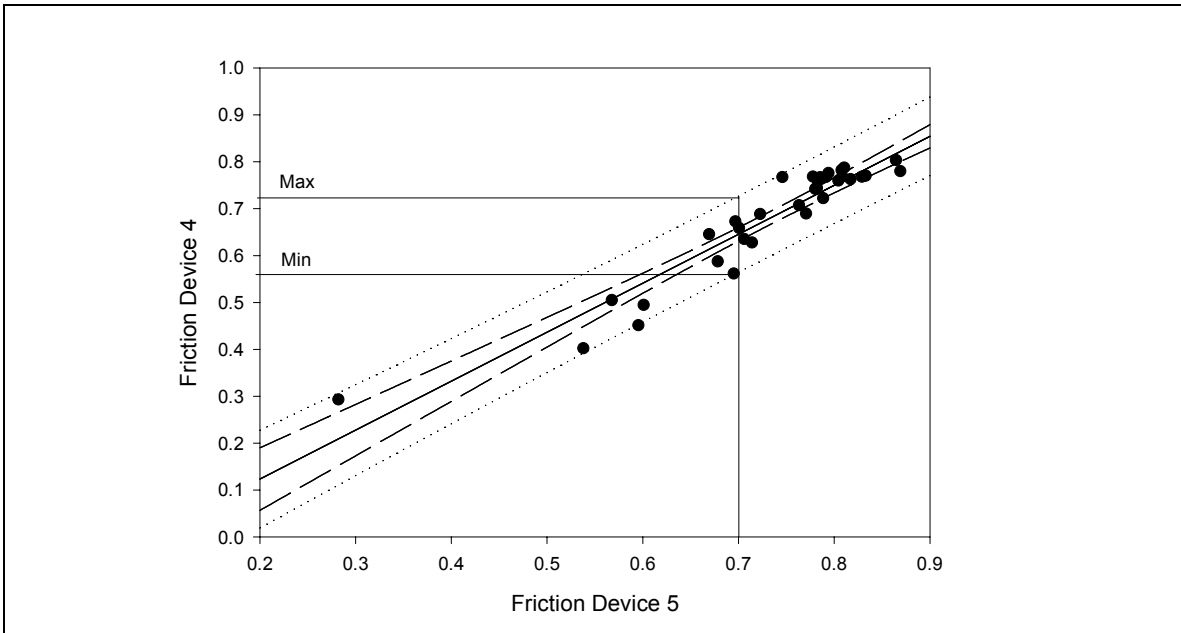


**Figure 39 - A scatter chart of two friction devices that have measured on the same wet asphalt surfaces at 65 km/h**

In Figure 39 each device had a sample size of 32 measurements. In this case, Device 4 was set up for 0.25 mm theoretical water film thickness and Device 5 was set up for 0.50 mm. The target measuring speed was 65 km/h.

The correlation coefficient was 0.95. The fitted regression line was

$$\mu_{Device4} = -0.086 + 1.044 \cdot \mu_{Device5} \quad (124)$$

The standard error of estimate of the averages of the friction transformation line was 0.040 friction units.

The prediction interval lines cover a range of 0.16 friction units. If a 0.70 friction value was measured with Device 5, there is a 95 percent chance that Device 4 would have measured between 0.56 and 0.72. If the 0.70 value was an average of several measurements, the transformation equation can be used, which predicts the value of Device 4 to be 0.65 with a standard error of 0.040.

In summary, the preceding examples show that the 95 percent confidence can be improved up to four times, approximately, by performing several repeat runs.

### 7.5.1 Assumptions when Evaluating Friction Values

When evaluating friction measurements, a common assumption is that the surface will have the same general frictional characteristic for the length averaged and reported. If this assumption is true, the friction values of a series of sequentially segmented parts of the surface length may be treated as repeated measurements of the same surface material, and the segment averages for prediction may be used.

What constitutes a general frictional characteristic needs to be defined. The parameters may include a kind of surface material (adhesion properties), the speed influence it has on the friction values (macrotecture), and whether the material exhibits contact pressure influence on the friction value (the tire or surface being the sacrificial part). If ranges of these parameter values can be grouped, such ranges may be used to construct groups of the same general of frictional characteristics.

In operational friction measurements that are typically performed during weather changes, the full runway length frequently cannot be regarded as having the same general frictional characteristic. A segmented approach is required. A sample of a segmented approach in use today is the spot measuring of parts of a runway having the same general frictional characteristic such as ice or snow patches. The ice or snow parts are evaluated apart from the bare or wet parts of the runway.



## 8 SURFACE CLASSIFICATIONS

Travelled surfaces may consist of many combinations of pavement material, deposits of weather precipitation and maintenance actions. When precipitation deposits are present on the pavement, the tire may be partially or completely out of contact with the pavement. The tire may also be in contact with ice or compacted snow that yields markedly different braking slip characteristics than pavement.

Several general surface classification systems are available. By general it is meant that the classification schemes are not specifically developed to relate to frictional properties. Deposits on a travelled surface give rise to other resistive forces acting on free-rolling wheels such as aircraft landing gear during take-off manoeuvres. The magnitude of such resistive forces may impair the ability of an aircraft to take off on the available runway. This information is therefore equally as important as the friction information. A sample surface classification scheme serving multiple purposes are the deposit codes by the International Civil Aviation Organization (ICAO).

### 8.1 ICAO Deposit Codes

The international deposit codes of ICAO used in the Snow Warning to Airmen (SNOWTAM) runway condition reports are shown in Table 1.

Table 1 – ICAO Deposit Codes

Code	Runway Deposit Description
NIL	Clear and dry
1	Damp
2	Wet or water patches
3	Rime or frost cover
4	Dry snow
5	Wet snow
6	Slush
7	Ice
8	Compacted or rolled snow
9	Frozen ruts or ridges

The codes are applied to each third of a runway length. Several codes may be applied to describe occurrence of several deposits or aggregated deposits starting from the top deposit down toward the pavement.

Mean depths of deposits are reported for each third of the runway in units of 2 mm for slush, 10 mm for wet snow and 20 mm for dry snow. Any maintenance action such as application of sand or de-icer is reported in free text as remarks in a SNOWTAM report. Friction values are measured and reported for each third of the runway.

### 8.2 Frictional Characteristics of Surfaces

To identify and describe a tire-surface interaction process, the inclusion of the surface part is crucial. It is common knowledge that the reported friction values from any braking slip friction measurement device are highly dependent on the surface. Moreover, the ranges of friction values

are commonly observed to fall into groups indicative of the surface. When no friction device is available, a chart of deposit types like the one in Figure 40 can be provided as a guide to friction values on the James Brake Index (JBI) friction scale.<sup>6</sup> The chart shown is taken from [11], Appendix C, Table D.

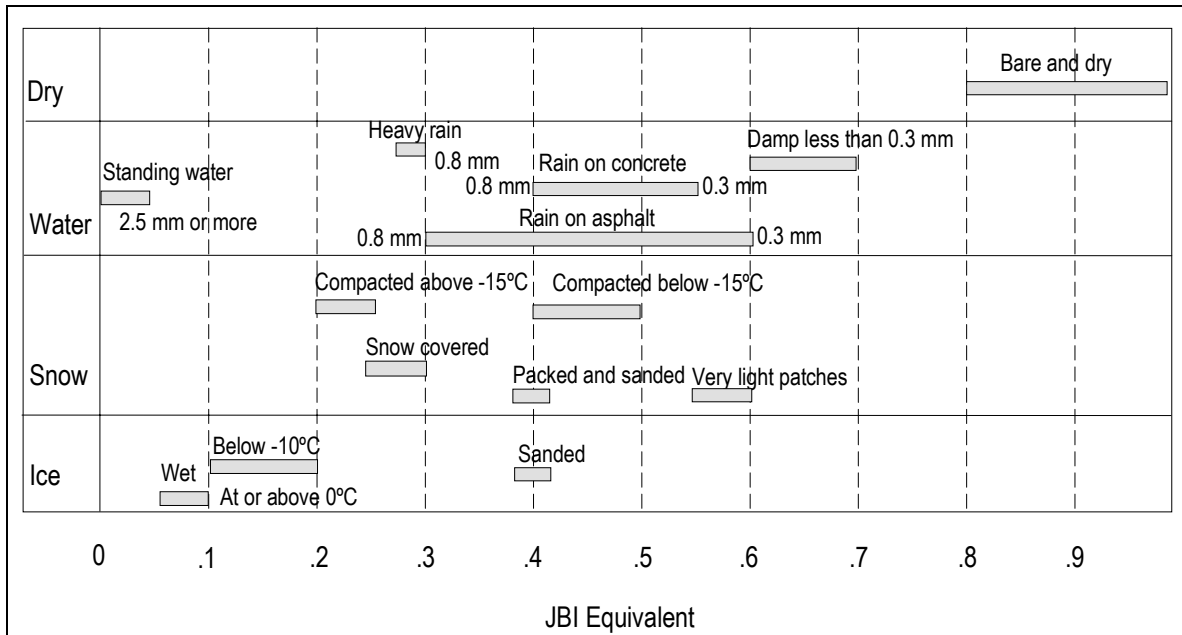


**Figure 40 - Friction values for runway surface conditions**

Within each principal deposit type it can be observed that friction values vary over a wide range. For ice and snow deposits, the temperature influences the friction level. There is an overlapping of ranges of friction values across the deposit types.

The ranges of friction numbers may be taken as indications of different types of friction processes taking place. For standing water on asphalt or concrete, there may be hydroplaning, which is acknowledged as a unique friction process entailing viscous shear, dynamic fluid lift and displacement drag forces arising from the presence of water. Before full planing, there are stages of partial planing. On the other hand, there may just be wet friction where there is insufficient water or speed to cause hydroplaning.

For snow, similar processes have not been as clearly identified, but it is obvious that wheel braking on a snow base will eventually sacrifice the snow when the degree of braking is increased sufficiently. The friction attainable is strongly dependent on the shear strength of the snow material. The friction processes with a snow base involve a non-rigid surface base, unlike bare pavement, which is considered rigid. Research institutions have used friction testers as the chosen device for measuring the shear strength of compacted snow on roadways.

Ice may be considered a rigid surface at well below subfreezing temperatures; however, as the freezing point is reached and water, wet snow or de-icers are present, ice has to be regarded as non-rigid.

Obviously, when the base surface of the runway changes from rigid to non-rigid and the presence of precipitation contaminants has additional effects (drag, lift, lubrication) on the friction process, the characteristics of different tire-surface friction processes must be studied. The engineering

<sup>6</sup> The JBI was replaced by the similar Canadian Runway Friction Index (CRFI) in 1997.

formulas for pavement braking slip friction are not valid for non-rigid surfaces. The equations for hydroplaning (i.e., liquid water) are not demonstrated to be valid for snow planing (i.e., “solid” water as crystals and often mixed with free water droplets).

The snow will undergo sintering processes when compacted by mechanical means (e.g., by rolling tires). Ageing, temperature and humidity changes affect the shear strength as the deposit is left on the pavement over time.

### 8.2.1 Base Surface and Surface Conditions

In the study of friction, it is essential to know the type of material with which the braking slip is interacting. Under winter conditions, the three basic surface types observed are pavement, ice and compacted snow. Weather changes and maintenance actions influence these to become dry, damp, wet, sanded or sprayed with de-icer. Precipitation deposits, including rain or new snow on compacted snow or ice, occur on all surface types. To identify the surface type and condition more clearly, the basic surface type deserves its own label. Base surface is suggested.

A base surface can be defined as a surface on which the braked vehicle wheel generates most of its useful braking slip deceleration force.

In a surface friction classification scheme, the base surface should have the highest rank. It gives the opportunity to classify the weather precipitation effects as complementary descriptions called surface conditions. Figure 41 illustrates the suggested visual classification scheme.

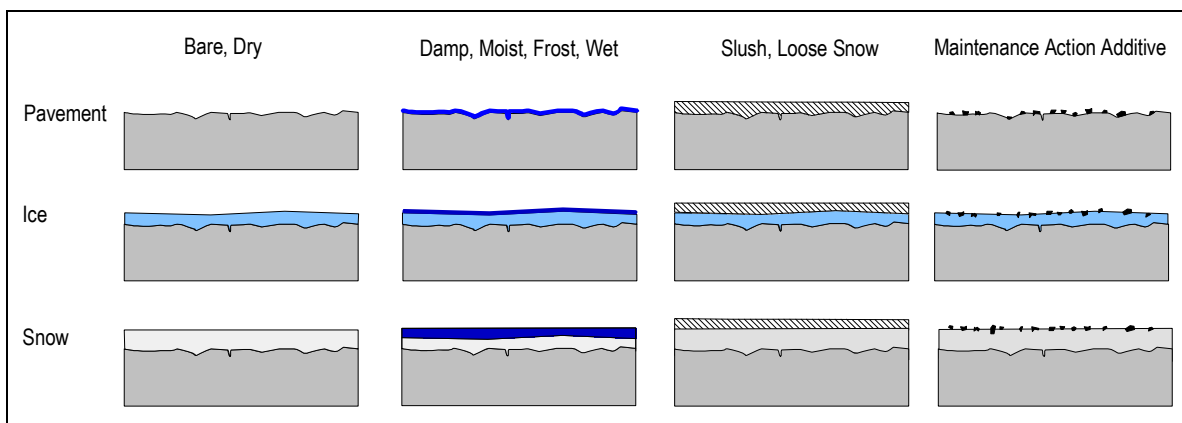


**Figure 41 - Cross sections of travelled surfaces illustrating a suggested visual surface classification**

In the left column of cross sections, the base surfaces are bare and dry. In the columns to the right, precipitation deposits and effects of maintenance actions are indicated.

The precipitation deposit can have two gradations: shallow and deep. The degree of depth is targeted at assessment of deposit displacement drag.

### 8.2.2 Grouping Friction Processes from Friction-Slip Speed Curves

The friction processes can to some extent be classified according to the shape of braking friction-slip speed curves. A general grouping of processes are illustrated in Figure 42. Two modes of measuring are shown: variable slip, representing new technology; and fixed slip, representing traditional technology. With the variable-slip mode, a characteristic curve is reported that represents a signature of the friction process.

Mathematical friction models have been introduced on the market in recent years as extensions of the measurement output of the variable-slip measuring mode. Characteristic parameters such as maximum friction values, slip speed of the maximum friction value and parameters describing the shape of the friction model are reported. Indications are that characteristic sets of these parameters can be used to identify the surface types involved in the braking friction process. These parameters can be a supplement to the visual observations in surface classification.

From Figure 42 it can be observed that measured friction values of fixed-slip measuring mode may differ significantly from the maximum friction values attainable for different surface types. The figure depicts a measuring speed of 65 km/h. The fixed-slip mode operated at 15 percent slip will yield a slip speed of 9.75 km/h at this measuring speed. Following the vertical line at 9.75 km/h in the variable-slip method set of curves, the corresponding fixed-slip mode values are transposed horizontally to the fixed-slip method graph. For wet pavement, compacted snow and loose snow, the differences between maximum and measured fixed-slip friction values stand out.

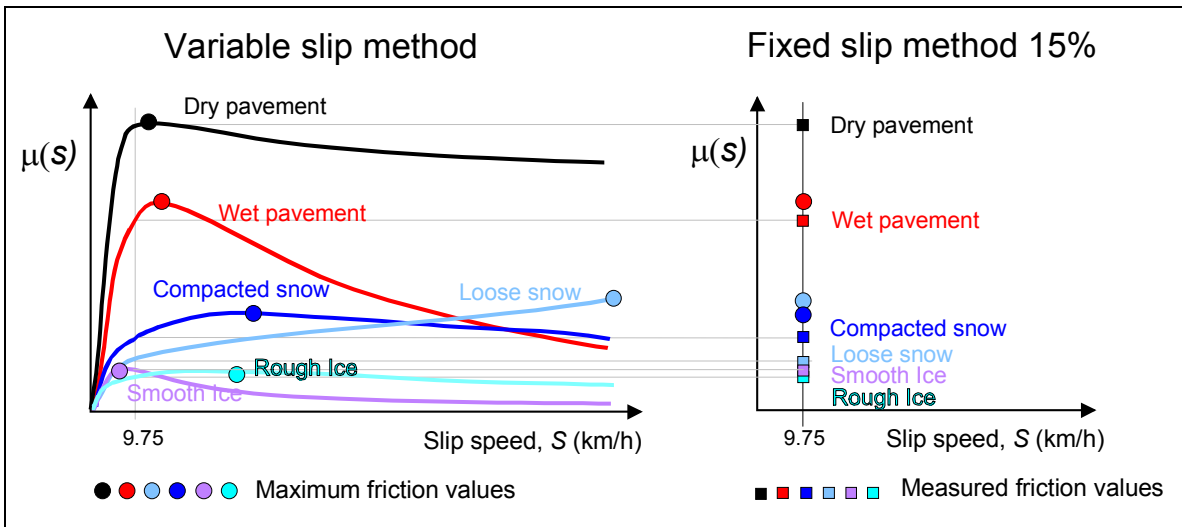


Figure 42 - Characteristic friction values for variable- and fixed-slip measuring modes on different surfaces

### 8.2.3 Measuring Speed as a Variable

Continuous fixed-slip friction measurement devices report different friction values at different measuring speeds for the same surface segment, when the base surfaces have certain conditions that support partial planing, compacting or displacement drag. Figure 43 illustrates typical friction-speed ranges for common base surfaces and conditions occurring on a runway segment during weather changes.

The type of surface and condition that exhibits the most change with variation in measuring speed is the wet pavement group. Dry pavement and base surfaces of winter contaminants exhibit little change with varying speed.

The general grouping of speed relationships in Figure 43 may be useful when applied to segments of a runway to capture surface variability more accurately.

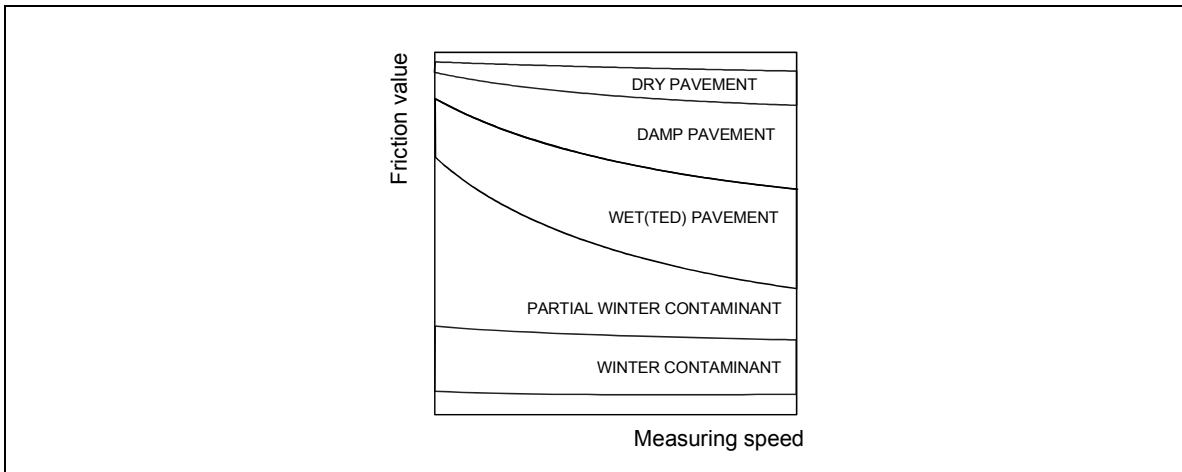


**Figure 43 - Simplified general relationships of friction with speed as variable for different conditions of a runway surface segment**

#### 8.2.4 Measuring Speed and Slip Speed as Variables

Most continuous fixed-slip friction measurement devices at airports are operated within a measuring speed range of 50 to 100 km/h and a 12 to 20 percent slip setting. The slip speeds obtained are in the range of 6 to 20 km/h. Spot measuring friction devices that operate at airports typically measure at a 50 km/h slip speed when the vehicle wheels are locked for measurement.

For spot measuring devices mounted in trucks, the tires are treaded and thus allow for higher stress concentrations and rubber protrusions that can break up the winter contaminant material to a larger degree than fixed-slip devices can with a bald measuring tire.

## 9 RUNWAY FRICTION MAPPING

### 9.1.1 Average Friction Values

The primary purpose for measuring runway friction is to use the information to predict the braking performance of an aircraft for accelerate-stop or landing manoeuvres. When including friction properties of the runway in their performance calculations, flight operations planners or pilots request a simple aggregated number expressing the runway friction status. Aggregated friction averages for each third of the runway are the current practice in most countries that report runway friction in the winter.

In section 7.2, a standardized friction determinant with a 100-m runway distance was suggested (see Figure 34). Friction averages for longer distances may be calculated for larger parts of the runway to the nearest 100-m unit length. For a short runway, a calculation of descriptive statistics for a third of a runway would then have a sample size of 3  $\mu_{100}$  values. For a long runway, the sample size would be 12  $\mu_{100}$  values.

Using the  $\mu_{10}$  values for computing the runway third averages may be an option with sample sizes of 30 to 120  $\mu_{10}$  values. The average friction value for a third will be the same as when using the  $\mu_{100}$ , but the standard deviation, the standard error, the coefficient of variation and the confidence will differ.

For users who include only the average friction value in their estimations, the other descriptive statistics that have different values for  $\mu_{10}$  and  $\mu_{100}$  populations are of little or no interest. For advanced interpretation of the friction characteristics of a runway, the descriptive statistics may have some merit. A larger population of friction values, such as the  $\mu_{10}$  population, is then preferred as it yields more reliable descriptive statistics.

A main criterion for justifying the use of  $\mu_{10}$  instead of  $\mu_{100}$  would be surface homogeneity. The  $\mu_{100}$  population would fail to report non-homogeneity if all 100-m lengths within the third of the runway did not represent the same surface type and surface condition.

### 9.1.2 The Runway Grid as an Extended Measurement Tool

When 100 m becomes the standard determinant runway distance for reported friction values, frictional characteristics may be mapped to a physically segmented runway. The mapping of a segment includes storing an average friction value, descriptive statistics for the average and any other friction parameters that can be linked to the physically unique segment.

Segmented runway mapping requires computerization for ease of implementation and consistency of operation. With the advent of inexpensive digital information systems, it seems that continuous mapping of a runway should no longer be overlooked as a measurement tool that can greatly enhance the quality and manageability of runway friction monitoring with improved support in decision-making for the airport maintenance staff.

The storing and retrieval of data from such a runway grid repository may form the back plane for new processing of measured data that greatly enhances the friction measurement services. Some of these new data processes are discussed in sections 9.1.2.1 through 9.1.2.5.

#### 9.1.2.1 Harmonization

To achieve harmonization of two tribometers, a reference tribometer and the local tribometer must produce a number of paired friction measurements of the same surface types and conditions. The harmonization procedure ends up with a transformation relationship that contains specific parameter values for the particular harmonized pair of tribometers. These relationships

and parameters can be stored as long-term constants in the runway grid repository and be retrieved for the automated calculation of harmonized friction values at the segment level with every measurement run.

#### *9.1.2.2 Equipment Performance Monitoring*

With measurement data stored in the runway grid repository for a number of operational runway friction runs, the data can be processed in the form of trend analysis or checks against discrete limit values to give warnings about possible errors with a friction device that may need corrective service. This is a monitoring of dynamic performance of tribometers to complement the static calibration and set-up routines by the operator.

#### *9.1.2.3 Local Verification of Harmonizing Relationships*

For devices that undergo unscheduled major service with parts replacements that may have an impact on the harmonization relationship, a temporary local harmonizing process may be run based on the previous history of local designated reference segments, so that the device can continue operation as a tertiary harmonized unit.

#### *9.1.2.4 Runway Surface Trend Analysis*

Rubber buildup or other intermediate or long-term polishing effects may be captured on an ongoing basis from regular operational measurements as well as from scheduled runway maintenance runs.

#### *9.1.2.5 Common Repository Format for Distribution of Data*

To facilitate various requirements of research within the local organization or in co-operation with others, a repository should have a common data format. Making the data available for analysis by other agencies can facilitate checks and enhancements with subsequent updates of the harmonizing relationships for the local friction measurement devices.

### 9.1.3 Runway Grid Geometry

A segment should be a minimum of 3 m wide, reflecting the width covered by the drive wheels and measuring wheel of a friction measurement device. The grid should have a minimum of four parallel measurement courses or measuring lanes.

Segmented runway mapping requires the friction device and operator to assign the values to a predefined layout of the runway. For instance, the measurements should always start and stop at the same defined start and end lines across the runway.

### 9.1.4 Data Content of a Runway Grid Repository

The typical wet and dry segment friction characteristics should be stored as reference values. These references may be valuable in evaluating the nature and impact of a winter contaminant, aggregate wear and polishing, buildup of rubber deposits, etc.

The wet friction characteristic in particular is strongly influenced by measuring speed and slip speed. This speed influence is mainly a result of the macrotexture of the pavement. Storing values for macrotexture in the runway grid repository is therefore useful.

The friction characteristics of the interaction of the local friction device and the runway segments may be stored in terms of parameters describing the typical or average friction-speed relationships. For dry, wet and contaminated surfaces, the friction-speed relationships are

different; different models may be exploited to more accurately assess the nature of runway slipperiness and improve prediction of friction values for other device configurations or vehicles.

### 9.1.5 Friction-Speed Relationships for Different Surfaces

Braking slip friction may have slip speed and driving speed as two principal variables when other variables such as surface type and conditions, device configuration and ambient conditions are kept the same. By measuring the same surface repeatedly at several measuring speeds, the friction-speed characteristic can be mapped. A variable-slip measuring tribometer can map friction-slip speed relationships and the same device operated in fixed-slip mode can map the friction-speed relationships.

In Figure 44, friction-slip speed curves and friction-speed curves for different surface types are drawn at the same scale to illustrate how the measured friction values from each mode of friction measurement relate to each other. In the variable-slip method, there is one curve for each measuring speed (65, 95 and 130 km/h) for each surface type. The friction values for 15 percent slip on each curve are identified and the friction values are plotted at the corresponding measuring speed in the friction-speed diagram.

When the typical dry and wet pavement friction speed characteristics are known for a runway segment, interpretations can be made as to whether a contaminant is present on the segment.

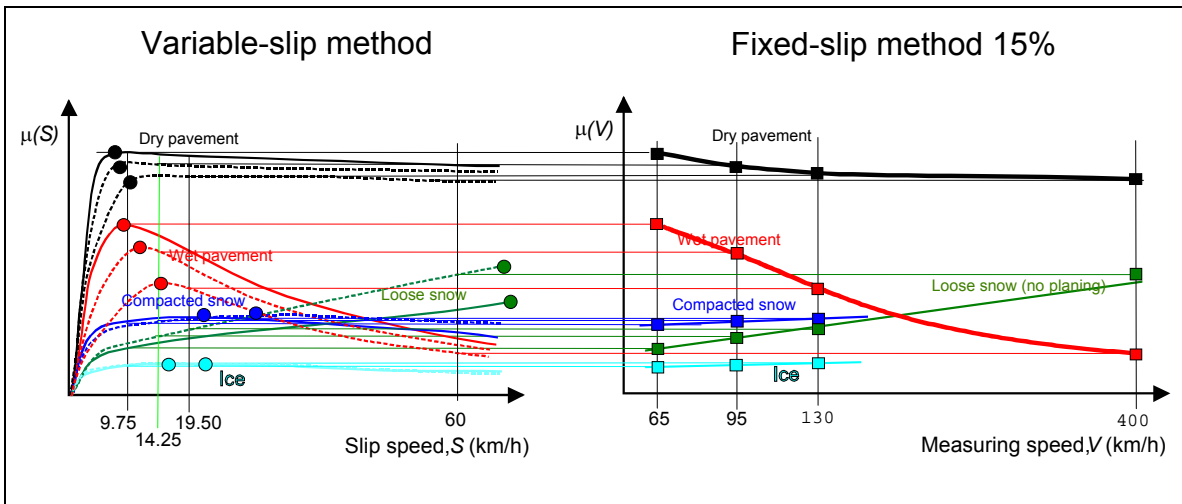


**Figure 44 - Empirical translation between variable-slip speed and fixed-slip friction relationships**

Illustrations of friction-speed signatures for different surface types that may occur on a runway are shown in Figure 45. Both slip and measuring speed signatures are depicted in separate rows, with slip speed in the upper row.

Rarely will so many types of surfaces occur at the same time, as most major airports expend considerable effort to keep their runways free from contaminants. De-icer chemicals and the application of sand add more signatures. Since the use of de-icers is common, whether to prevent frost and ice layers or to melt small amounts of fresh snow and remnant snow from snow removal, the runway stays wet for long periods during weather changes. Combinations of wet pavement and slush are common at temperatures close to 0°C. At low temperatures, combinations of dry pavement and ice patches or compacted snow can frequently be observed. In periods between runway snow removals, a continuous snow precipitation may cause aircraft landing gears to build hard compacted snow or ice tracks during ground manoeuvres. Thus, a variety of surface types and conditions can be found at any airport with winter operations.



The deviations from dry and wet signatures can be useful when comparing tribometers.

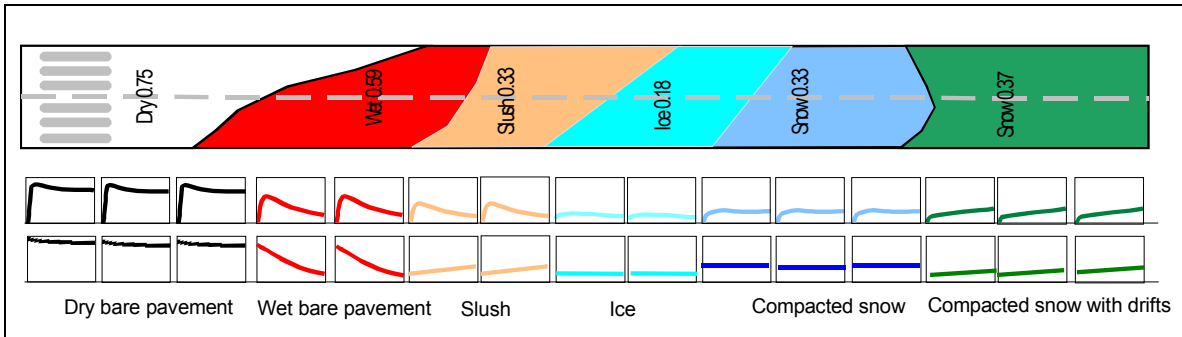


**Figure 45 - Sample distribution of friction-speed relationships for different surface types and conditions on a runway**

An actual sample of a runway with mixed conditions is shown in Figure 46. The sample is from the departing traffic runway of an airport with separate runways for take-off and landing. The friction values are high in the first half of the runway as aircraft engine blasts contribute to contaminant removal and dry up the surface. It is also believed that some aircraft de-icer liquid was dropped from the aircraft fuselages to the ground in the start area. With steady traffic for take-off, the continuous supply of aircraft wing de-icer chemicals compounded the effects of the ground staff spraying de-icer liquid to keep the runway damp.

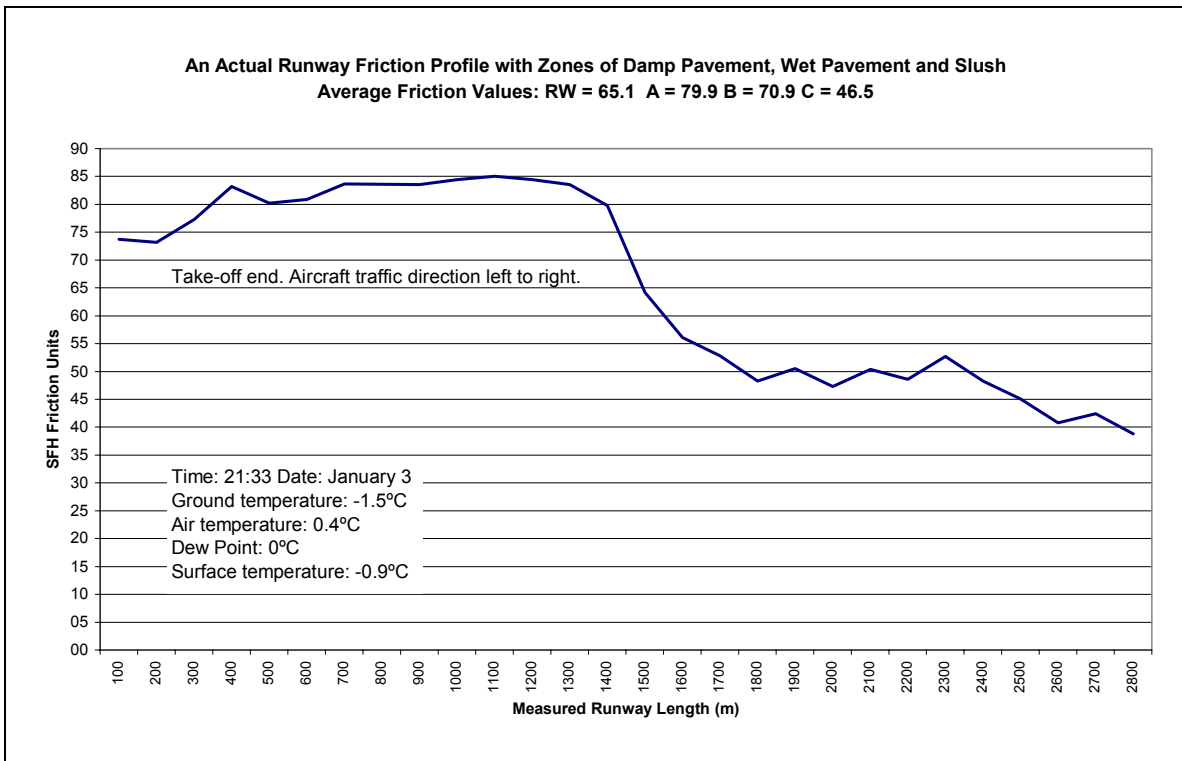


**Figure 46 - A sample actual runway friction profile of mixed conditions during a weather change with light precipitation, 2 hours after application of de-icer liquid**

## 10 MODERN TIRE-PAVEMENT FRICTION MODELS

### 10.1 Penn State, PIARC and Rado Models

The World Road Association (PIARC) conducted an exemplary field investigation in 1992 [12]. In a large international measurement experiment, wet pavement was studied across a wide variety of pavement materials for highways, including some runways. The objective was to harmonize friction and texture measurement devices. Several important outcomes have been reported from that experiment. One is that macrotexture is the principal reason for the speed dependency of friction. Harmonization of the tribometers participating in the experiment was achieved with the support of texture information. The harmonized friction measure was therefore proposed as a two-parametric International Friction Index (IFI): a friction number associated with a reference slip-speed value and a speed number associated with the slip-speed gradient of friction.

The participating tribometers measured friction at different slip values. The successful harmonization resulted when the measured friction values were adjusted to a common slip-speed value of 60 km/h. These adjustments were calculated with an exponential equation derived from what is known as the Pennsylvania State University model. It is widely used to predict friction at speeds other than the measured speed for a surface. The model is of the following form:

$$\mu(V) = \mu_0 \cdot e^{\left(\frac{-V}{V_0}\right)} \quad (125)$$

where  $\mu_0$  is the zero intercept and  $V_0$  is an exponential constant.<sup>7</sup> Both parameters are valid for a surface only and can be determined by measuring friction at several speeds.

In the derived PIARC model, the zero intercept of (125) is replaced by a constant friction value at an arbitrarily chosen reference slip speed of 60 km/h and another exponential term.

$$\mu(S) = \mu(60) \cdot e^{\frac{60-S}{S_p}} \quad (126)$$

The slip speed of 60 km/h was chosen as a representative median value for road vehicles during emergency braking. The value of friction at that speed is  $\mu(60)$ .<sup>8</sup> The slip-speed value is a parameter of the exponential term. A second parameter of the exponential term is the so-called Speed Constant,  $S_p$ , which is closely related to measurements of macrotexture for the same surface. A sample graph produced with equation (126) is shown in Figure 47.

---

<sup>7</sup> The original Penn State Model uses so-called skid numbers for friction coefficient and the term  $100/PNG$  instead of  $V_0$  as used here.  $PNG$  is a percent normalized gradient.

<sup>8</sup> The original model uses the notation  $F$  for friction coefficient instead of  $\mu$  as used here to differentiate between force and coefficient.

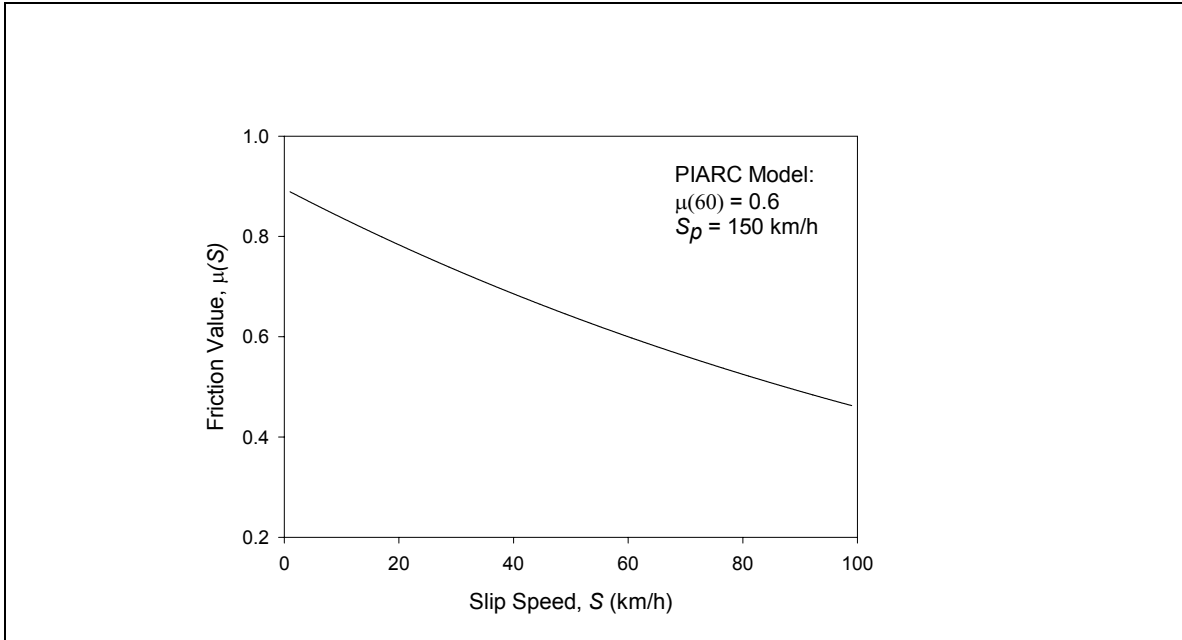


**Figure 47 - A sample plot of friction model for the International Friction Index (IFI)**

When the IFI parameters for a surface are known, the friction value can be calculated for all slip speeds for the surface.

For braking slip friction, the basic friction model of Amontons can be replaced with the following friction model:

$$F(S) = \mu(60) \cdot e^{\frac{60-S}{S_p}} \cdot N \quad (127)$$

Mathematical model (127) is valid for wet pavement only. It has successfully captured the commonly observed influences of texture and slip speed for a device tire configuration-surface pair. For the same surface, another device would have another set of parameters,  $\mu(60)$  and  $S_p$ .

Inspired by PIARC's success, we should continue our quest for more precise friction models for other tire-surface pairs. Indications are that one mathematical model may not be able to describe all the different tire-surface pairs found on the runway during winter.

A potential problem of extending the PIARC model to another hard surface, such as rough ice, is the lack of texture measurement devices that can be used on ice. The gradient of the friction curve cannot be determined from texture devices. Additionally, the surface rather than the tire becomes the sacrificial part of the tire-surface pair. The texture effect of a sacrificial surface is usually regarded as insignificant or nil.

Another outcome of the PIARC experiment seems to have the potential to rectify this problem: combining the logarithmic friction model with variable-slip measuring techniques. One of the researchers at Pennsylvania State University, Dr. Zoltan Rado, who analysed the experiment results, came up with a good fit for a new friction model he invented. The model is an implementation of a three-parameter lognormal equation, often referred to as the Rado model.

This model captures the influence of the tire design and material in addition to texture, slip speed and measuring speed. The model is valid for wet pavement as it was derived from such a database. It has the following form:

$$\mu(S) = \mu_{peak} \cdot e^{-\left(\frac{\ln \frac{S}{S_c}}{\hat{C}^2}\right)^2} \quad (128)$$

where  $\mu_{peak}$  is the maximum or peak friction coefficient value measured during a controlled, linearly ramped braking from free rolling to locked wheel at a constant measuring speed.  $S_c$  is the slip speed at which the maximum friction occurred and  $\hat{C}^2$  is a shape factor related to texture measurements in a slightly different manner than the speed constant,  $S_p$ , of the IFI. All three model parameters are determined by measurements of the ground friction measurement device using variable-slip technique. The friction value at other slip speeds can therefore also be calculated with this model.

A graphical presentation of the model is shown in Figure 48. The maximum friction value is 0.75, the slip speed at which it occurred is 20 km/h and the shape factor is 1.05.

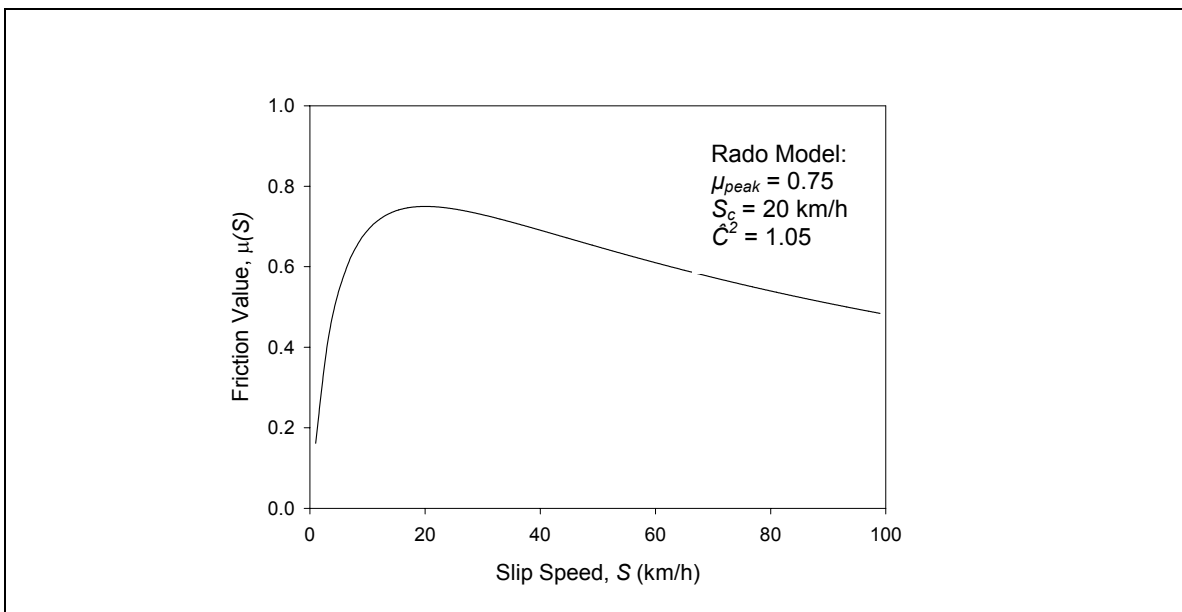


**Figure 48 - A sample Rado model plot**

A notable difference between the PIARC and Rado models is found at low slip speeds. Figure 49 shows the two graphs superimposed: the Rado model is the transient phase when the brakes are first applied up to some slip, then the PIARC model follows as the speed of the vehicle slows. The PIARC model is the steady-state value of friction. In a stopping situation, the transient part happens so quickly that only the steady-state, the PIARC Model, needs to be used. However, when antilock braking systems (ABS) are used, both models must be used to evaluate stopping and stopping distance.

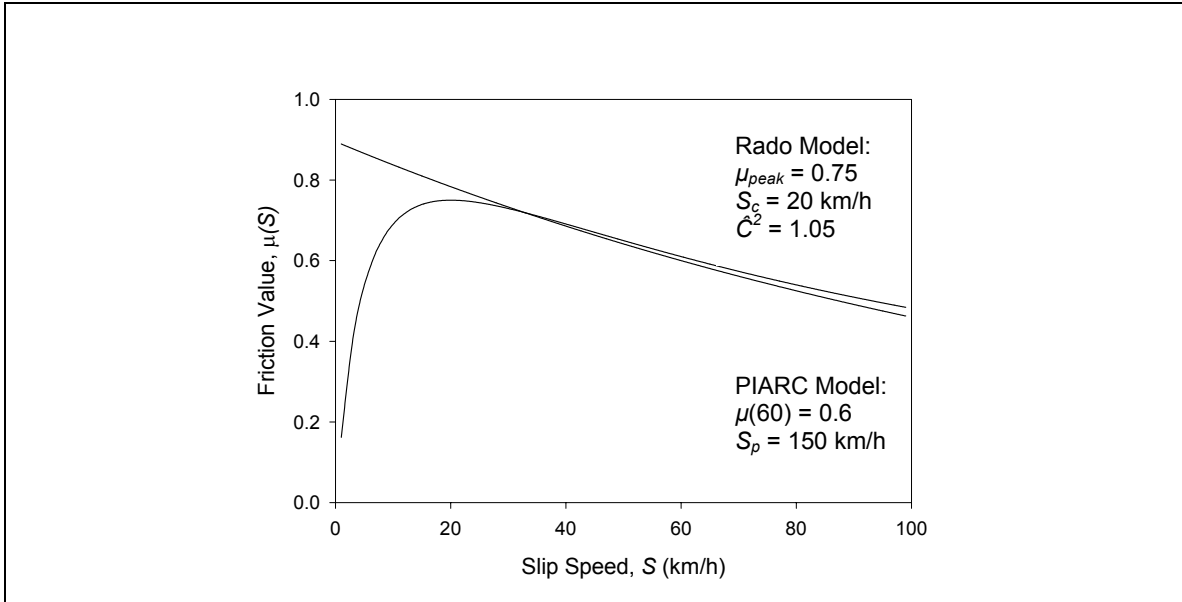


**Figure 49 - A sample comparison between PIARC and Rado friction models**

The PIARC model and its IFI are primarily intended for long-term monitoring of the pavement for budgeting renewal of the surface when polished or worn to unacceptable levels. The Rado model is intended for the prediction of braking performance. Both automotive ABS brakes and aircraft anti-skid systems operate on the initial rising part of the friction-slip speed curve of the Rado model. This part of the curve is often called the tire influence segment. Beyond the maximum friction value, the curve has a surface influence segment.

ABS and other automatically modulated brakes are not designed to operate beyond the maximum friction point. The braking systems operate on the tire influence segment of the Rado model friction curve.

Now we have a model that can predict the braking force,  $F$ , of a single wheel at a constant travel speed:

$$F(S) = \mu_{peak} \cdot e^{-\frac{\left(\ln \frac{S}{S_c}\right)^2}{C^2}} \cdot F_W \quad (129)$$

Preliminary findings of the Joint Winter Runway Friction Measurement Program suggest that the Rado model parameters -- maximum friction, slip speed at maximum friction and shape factor -- are unique for a tire-surface pair. Thus, surfaces may be classified with this technique.

In summary, the PIARC Model is best for use with fixed-slip devices and varying measuring speeds. The Rado Model is for use with fixed measuring speed and varying slip speed. When the two models are combined, three-dimensional models are obtained as described in section 10.2.

## 10.2 Three-Dimensional Modelling of Tire-Surface Friction

Since travel speed and slip speed have been treated separately by different friction models as two independent variables, it would be desirable to have a combined three-dimensional friction model including travel and slip speeds as variables.

Bachmann [13] has found that repeated runs with variable-slip devices can provide data for deriving three-dimensional friction models with travel and slip speeds as variables. As can be seen from Figure 50, the series of measurements almost constitute a surface plot of friction. The curves are measured with a treaded automotive tire on dry, concrete pavement.

It is more practical to use slip ratio rather than slip speed as an independent variable to view the surface plot as a full area cover. Since the upper limit slip speed at any travel speed equals the travel speed of the device, plotting with slip speed on one axis would generate a triangular shape plot projected in the speed plane.

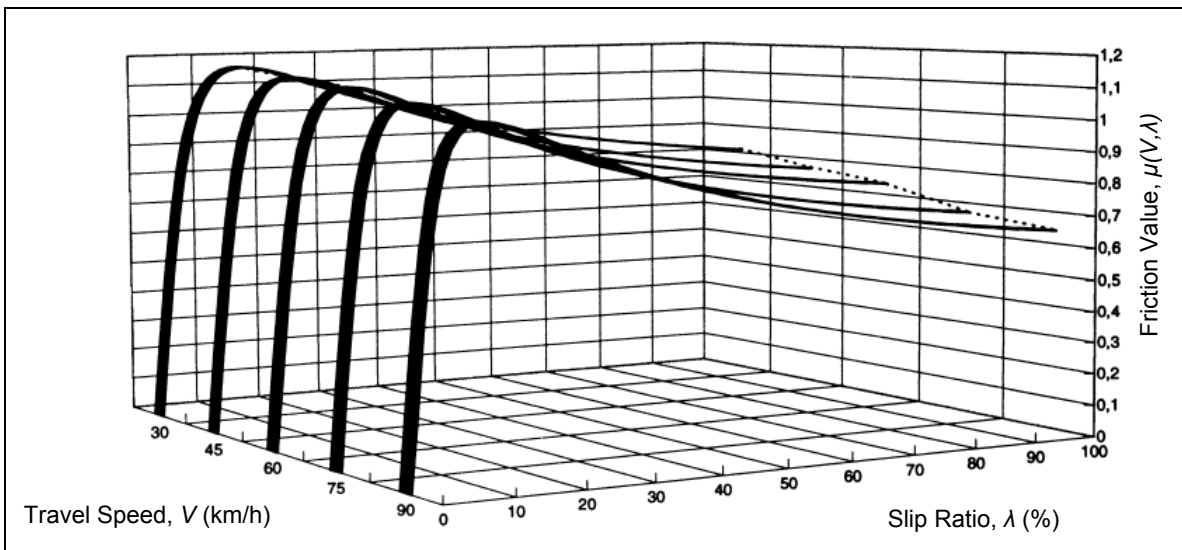


**Figure 50 - Series of variable-slip measurements with an automotive tire at different measuring speeds on dry concrete pavement [13]**

For bald measuring tires, Wambold [8] derived transient friction versus slip ratio curves for a number of different surface types shown in Figure 51. On sacrificial surface interactions (ice and snow), there are no distinctly defined peak friction values like the ones that may be observed for sacrificial tire interactions (bare and dry, bare and wet pavement).

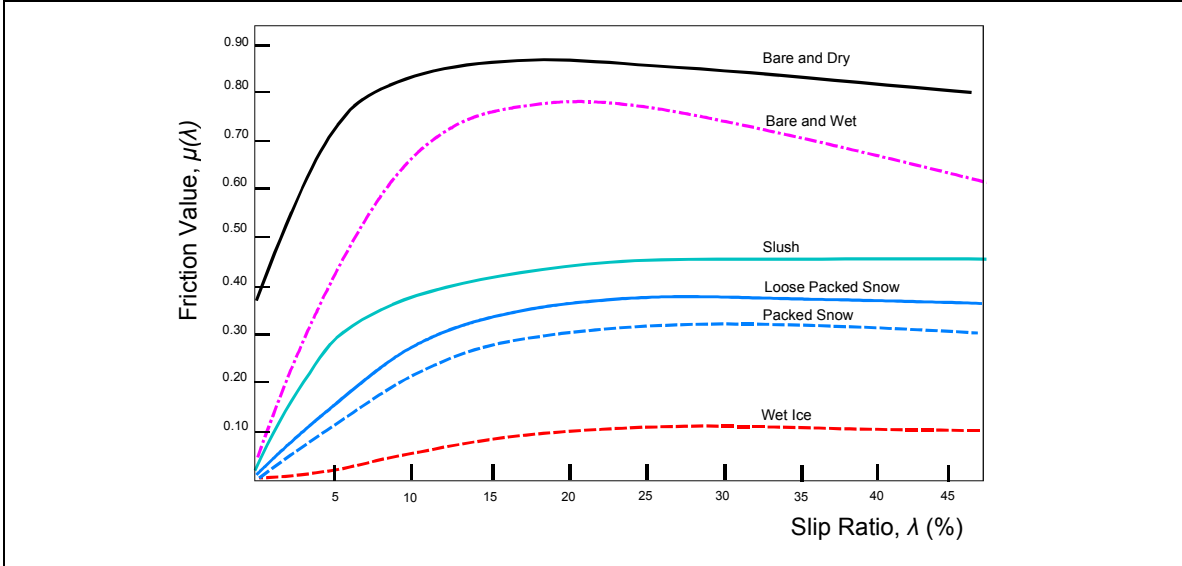


**Figure 51 - Friction as a function of slip ratio for different surfaces and conditions as measured by a variable-slip device at the same measuring speed 65 km/h**

Based on the characteristic shapes of the curves in Figures 50 and 51, it is conceivable that three-dimensional plots of standard types of measuring tires may be produced. This can be used as documentation of the typical friction speed characteristics of a tire as an instrument sensor for different surface types and conditions. Figures 51, 53 and 54 are empirical illustrations of three-dimensional friction plots for a tire on three different types of surfaces.

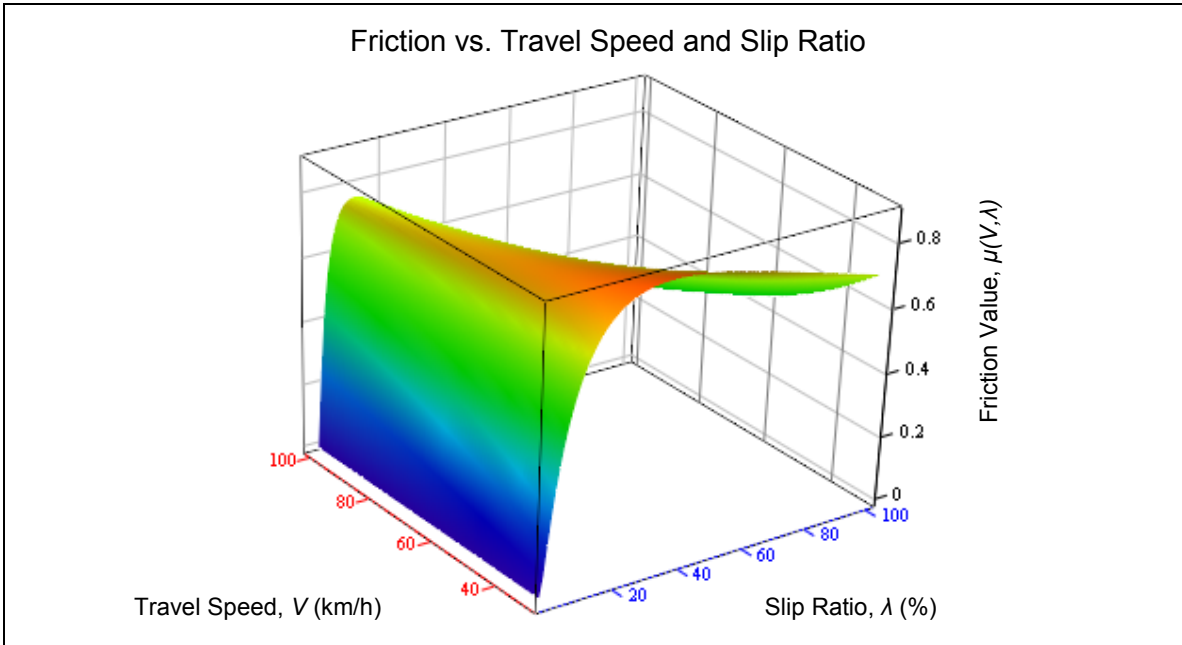


**Figure 52 - Three-dimensional plot of friction versus travel speed and slip ratio for a sacrificial tire scenario**

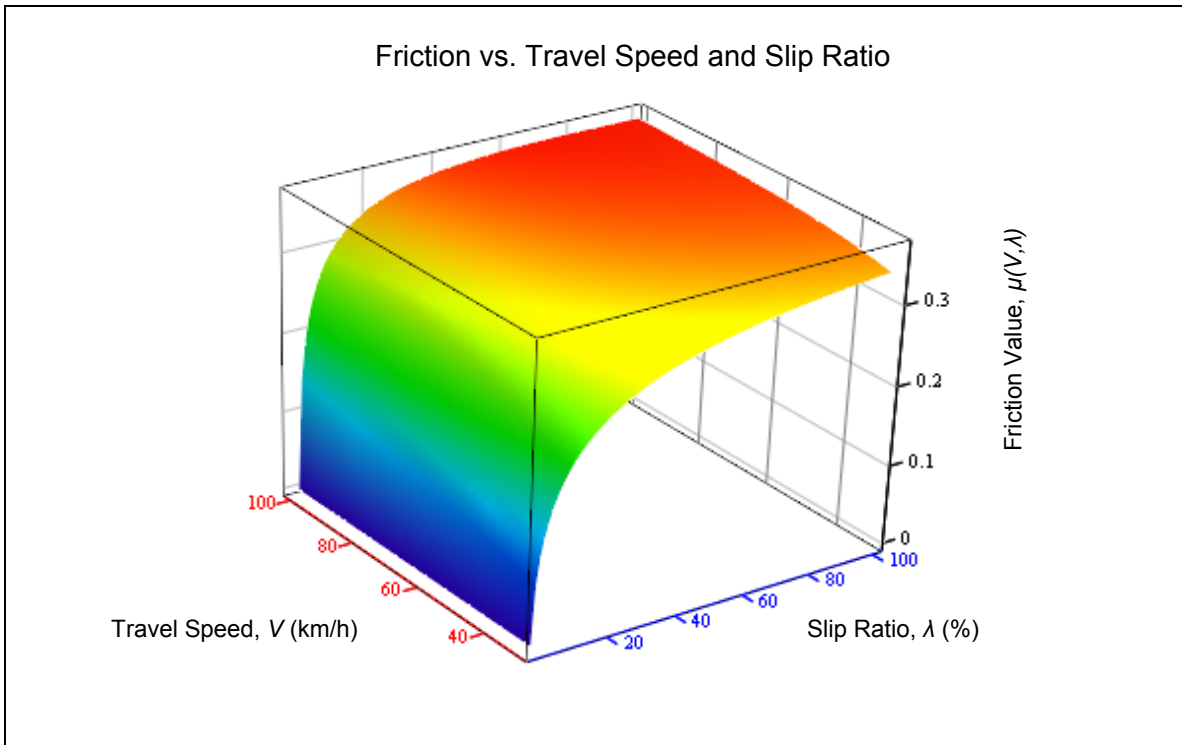


**Figure 53 - Three-dimensional plot of friction versus travel speed and slip ratio for a sacrificial surface scenario**

Figure 52 depicts tire-braking interaction with a wet pavement. The friction has a region of maximum friction values at intermediate slip ratio values. This peak region is explained as the transition region where the tire yields to the surface and becomes the sacrificial part of the interaction. In Figure 53, the scenario is tire-braking interaction with snow. In this scenario the region of maximum friction values is at the highest travel speeds and slip ratios. It means that the hardest braking generates the highest friction values up to a maximum level that the surface material can sustain. The surface is sacrificial. It should be pointed out, however, that at high slip and higher speed, vehicle steering control is lost.

Not all winter contaminants will yield friction processes with sacrificial surfaces. Figure 54 shows a sample of a smooth and dry ice surface interacting with a smooth treaded tire. The plot is modelled after data from a test in the JWRFMP. The friction values drop versus slip ratio, but stay constant versus travel speed. This scenario has commonality with the interaction between a braked tire and low texture rigid surfaces.



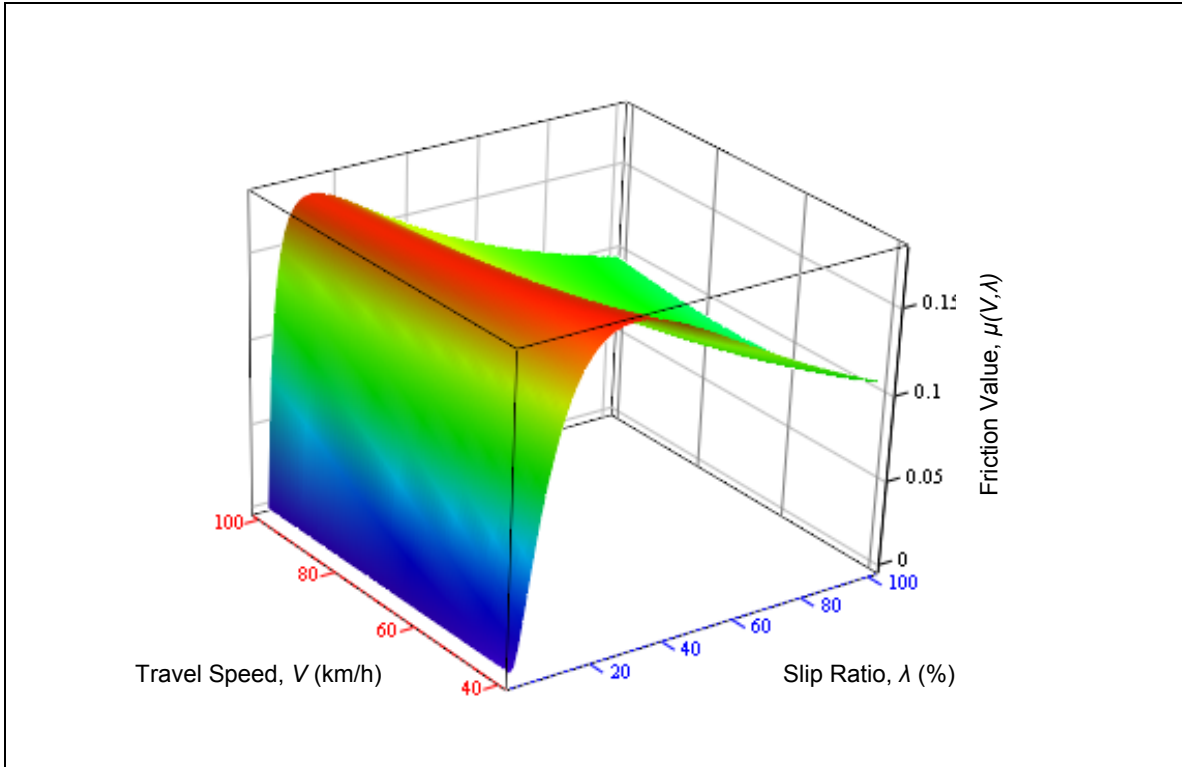


**Figure 54 - Three-dimensional plot of friction versus travel speed and slip ratio for a smooth ice surface**

Although research strongly indicates that braking slip friction can be presented in a three-dimensional manner as shown, researched and documented universal three-dimensional mathematical models are not yet available unless the Rado and PIARC models are combined.

The surface plots of Figures 52, 53 and 54 are generated from such a combined model by manipulating the parameters to yield results that agree with observations from numerous field tests. The combined friction model is the Rado Model (128) with the peak friction parameter replaced by the Penn State Model (125):

$$\mu(S, V) = \mu_0 \cdot e^{-\left(\frac{V}{V_0}\right)} \cdot e^{-\frac{\left(\ln \frac{S}{S_c}\right)^2}{c^2}} \quad (130)$$

The three-dimensional plots are useful illustrations in comparing friction measurement devices on different types of surfaces. When the wheel brake system is a form of anti-skid or other automatically controlled brake system, three-dimensional models like (130) are required for friction analysis.

It has been observed in the JWRFMP that tribometers operating in hard braking mode have demonstrated the best correlation with aircraft braking on snow. This may indicate that the ultimate shear strength of the surface material is the upper limit for friction values and that both the friction tester and the aircraft operate in a region of maximum friction values. The strong common influence of the same ultimate material strength facilitates a strong correlation. The remaining difference in nominal friction values can be explained, to a large extent, by differences in contact pressure and, to a lesser extent, by differences in speeds or slip ratios.

For the sacrificial tire scenario, the strongest correlation between friction measurement devices and aircraft braking is at slip ratios between 8 and 15 percent. To avoid excessive wear on the sacrificed tire, aircraft brake controls do not allow higher slip ratios. Continuous operating friction measurement devices are therefore set up with slip ratios in this range when measuring on pavement.

This rationale shows the dilemma of measuring runway friction during weather changes. Those parts of the runway that are covered with ice or snow have the best potential for a strong correlation between aircraft and hard-braking friction measurement devices. The bare wet or dry parts of the runway have the best potential for strong correlation at low slip ratio settings. Available friction measurement devices currently operate with either of the two slip ratio ranges, not both.

### **10.3 Comparison of Exponentially Modelled Friction Measurement Devices**

When tribometers operate in fixed-slip mode, friction versus speed curves can be established for the same strip of pavement. Curve fitting the measured data to exponential equations, the curves for a reference device and a local tribometer may look like the pair in Figure 55.

It can be shown that the transform equation between friction values of one of the devices to the other is a power equation that is conveniently determined with common spreadsheet regression tools. In Figure 56, the resulting transform equation for the pair of exponential friction versus speed curves is shown.

Note that speed is eliminated in the transform, which is a value-to-value relationship. To predict what friction value the reference device measured on the pavement strip in the scenario of Figure 55, the measured friction value is raised to the power of 0.3431 and the result is multiplied by 0.5395 as given in Figure 56.

The power transform is accurate in the sense that there is no statistical uncertainty or confidence associated with the transform. The uncertainty is associated with changes in the pavement strip and ambient environment, such as amount and nature of precipitation deposits during weather changes and temperature. The quality of the exponential friction versus speed curve fit lies in determining the uncertainty of prediction.

When applying the power transform technique, average values of several friction measurements should be used.

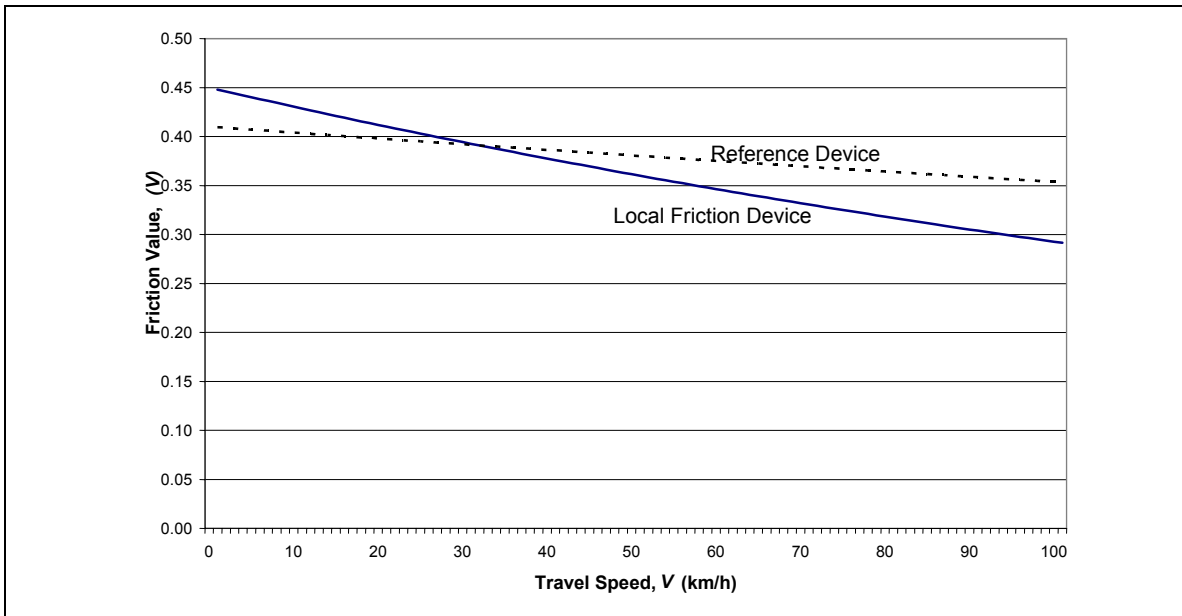


Figure 55 - Fitted exponential friction-speed curves for two devices

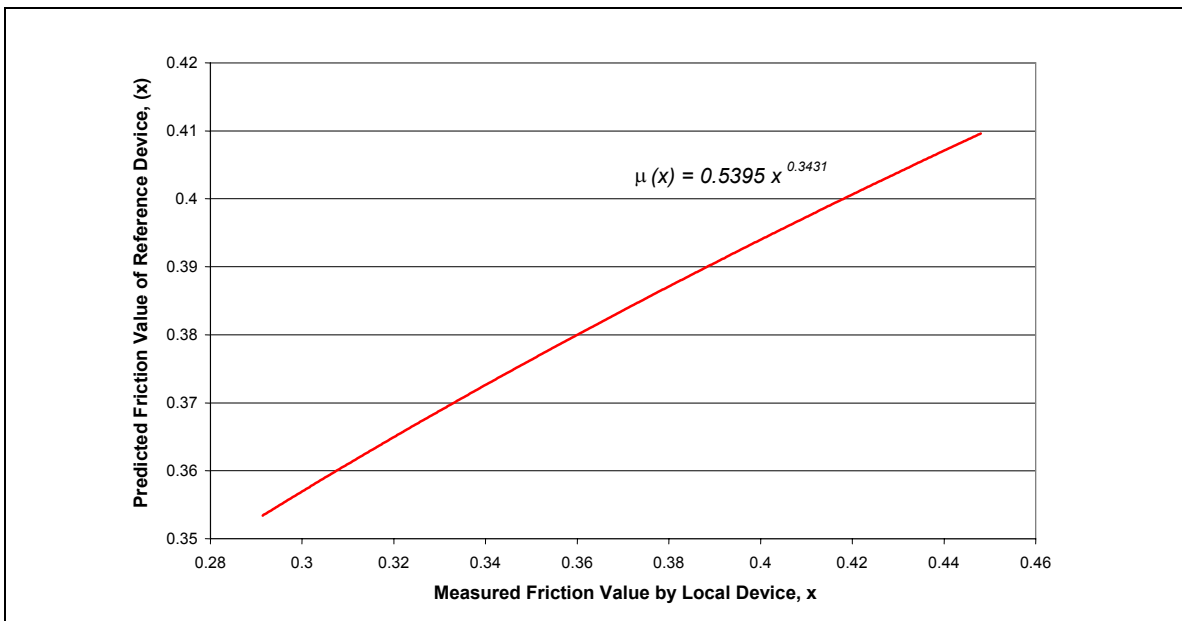


Figure 56 - The power transform equation for the pair of exponential equations plotted in Figure 55

# 11 STANDARD TIRE-SURFACE FRICTION MEASUREMENT

## 11.1 The International Friction Index (IFI)

The World Road Association (PIARC) conducted the *International PIARC Experiment to Compare and Harmonize Texture and Skid Resistance Measurements* [12], in September and October 1992. Forty-seven different measuring systems surveyed 54 sites, encompassing a wide variety of pavement types on roads and airfields in Belgium and Spain. The systems measured 67 different parameters (33 texture parameters and 34 friction parameters). The results of the experiment were presented in Montreal in 1995.

The World Road Association had recognized that methods and systems used throughout the world for measuring texture and skid resistance vary significantly, causing barriers for much-needed international information exchange and comparisons. It was necessary to convert results produced by different devices to a common scale. The PIARC Technical Committee C1 on Surface Characteristics decided to conduct an experiment to see whether harmonization could be achieved. The data collected and analysed enabled an international scale of friction values called IFI to be defined. The IFI is now an ASTM standard [14] and an ISO standard [15].

Several of the devices that participated in the experiment are also commonly used for airport friction and texture surveys. The focus of the experiment was on pavement management (i.e., pavement surface monitoring) to plan actions for improvement of texture and friction characteristics. Wet pavement was the only basic type of surface surveyed; winter contaminated surfaces were not included in the experiment.

The concept and techniques of the PIARC friction and texture model are applicable for runway maintenance. Procedures are also given that permit the method to be extended to equipment that did not participate in the experiment.

Since wet pavement friction is speed-dependent, the PIARC model incorporates macrotexture measurements to enable the side-force, fixed-slip, and locked-wheel types of friction measurements to be related. The IFI can be calculated from the results of any friction measurement combined with a macrotexture measurement that predicts the speed gradient of the friction.

The IFI consists of two parameters:  $F_{60}$  and  $S_p$ .  $F_{60}$  is the harmonized estimate of the friction at 60 km/h and  $S_p$  is the speed constant. Friction values can be calculated for any slip speed.

The PIARC model and IFI therefore represent universal engineering tools that are valid for braked tires interacting with wet pavement types such as those encountered on highways and runways.

It was found that friction devices could be harmonized. The reference of harmonization was the average performance of all participating devices. The average performance is represented by a mathematical equation; a decaying exponential called the Golden Curve. Each device has a calibration factor to this Golden Curve at the speed of harmonization (60 km/h slip speed).

Calibration constants were worked out for all of the participating devices and are published in the report of the experiment [12]. The calibration constants used with the corresponding friction devices enable the Golden Curve to be recreated for surfaces, thus allowing secondary calibrations of new equipment to be performed or friction values obtained with one device to be translated to the measuring units of another calibrated device.

## 11.2 The Harmonization Procedure

The PIARC harmonization procedure is as follows.

1. The speed constant is calculated using a texture measurement of the surface. The equation used is

$$S_p = a + b \cdot Tx \quad (131)$$

where  $Tx$  is a texture measurement and  $a$  and  $b$  are harmonization constants for the texture measuring device determined in the international experiment and published in [12].

2. The friction measurement is adjusted to the harmonization slip speed of 60 km/h using the following equation:

$$\mu(60)_{device} = \mu(S)_{device} \cdot e^{\frac{S-60}{S_p}} \quad (132)$$

where  $S$  is the slip speed of the measurement and  $\mu(S)_{device}$  is the measured friction value by the device. For a fixed-slip tribometer, the slip speed is the measuring speed multiplied by the slip ratio.

3. The harmonized friction value at 60 km/h slip speed is then calculated using the equation

$$\mu(60)_{harmonized} = A + B \cdot \mu(60)_{device} \quad (133)$$

when the measuring tire has a blank tread, or

$$\mu(60)_{harmonized} = A + B \cdot \mu(60)_{device} + C \cdot Tx \quad (134)$$

when the measuring tire tread is ribbed or has a pattern.  $A$ ,  $B$  and  $C$  are calibration constants for the friction device determined in the international experiment and published in [12]. The calibration constants are regression constants.

4. The International Friction Index is then reported as  $IFI_{60}(\mu(60)_{harmonized}, S_p)$ . The PIARC Model can also adjust the IFI to another slip reference value using the following equation:

$$\mu(S)_{harmonized} = \mu(60)_{harmonized} \cdot e^{\frac{60-S}{S_p}} \quad (135)$$

where  $S$  is the slip speed for which a friction value is desired. For instance, the IFI friction value at 90 km/h, which is a high value for a braked aircraft wheel at 30 percent slip ratio, the friction value would be

$$\mu(90)_{harmonized} = \mu(60)_{harmonized} \cdot e^{\frac{60-90}{S_p}} = \mu(60)_{harmonized} \cdot e^{\frac{-30}{S_p}} \quad (136)$$

The IFI is then reported as  $IFI_{90}(\mu(90)_{harmonized}, S_p)$ .

The management beauty of the IFI is that regulations can be made stipulating IFI parameters, which are universal (i.e., no tie to a particular friction device). But a friction device must have calibration constants determined, as demonstrated by Figure 57. It is natural that they initially

come with the device as part of the documentation from the manufacturer, as is the common industry practice by other instrument manufacturers.

The published calibration constants for one tester that participated in the PIARC experiment with a blank tire were  $A = 0.08$ ,  $B = 0.91$  and  $C = 0$ . For another device participating in the experiment with a treaded tire, the published calibration constants were  $A = 0.04$ ,  $B = 0.86$  and  $C = -0.02$ . These constants were valid for a wide range of textures for self-wetted pavements, including runway pavements.

As for texture devices used at airports, the sand patch method according to ASTM E-965 has the published texture calibration constants  $a = -11.6$  and  $b = 113.6$ .

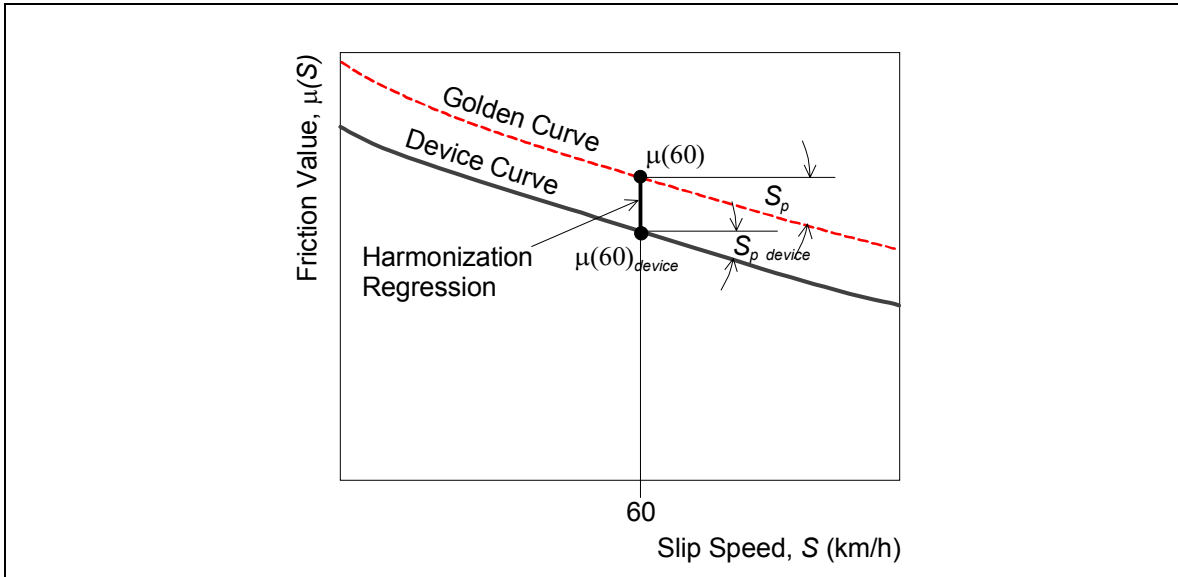


**Figure 57 - Calibration constants for IFI are taken at a harmonizing slip speed of 60 km/h. The reference curve is named the Golden Curve. It is an average of all participating devices in the 1992 experiment.**

In effect, the PIARC experiment was a mapping of ground friction device performance on wet pavement. It is therefore a continuance of these efforts to think that a mapping of devices on other surfaces would be equally useful in finding and defining a way to translate measured values from one device to another, or to a common index of friction valid for other surfaces. The basic ingredients are field experiments, a harmonization reference and tables of calibration constants. Correlations and regressions are key techniques.

### 11.3 The International Runway Friction Index (IRFI)

The World Road Association has shown that friction devices can be harmonized for the purpose of monitoring pavement friction characteristics for maintenance use. Inspired by PIARC's success and recognizing the need for harmonization of friction device measurement results for operational use in aviation, the JWRFMP and ASTM have developed an International Runway Friction Index (IRFI).

ASTM published the first IRFI standard E-2100-00 in year 2000 [16] and the phased standards development process is continuing. The IRFI differs from the IFI in that the IRFI covers any travelled surface type and condition and the IFI covers wetted pavement only.

Friction measurement services are operated together with runway condition reporting at airports in the winter. Complementary data is therefore available to interpret the friction values and to support decision-making both for airport maintenance staff and flight operations related to the current runway characteristics.

### 11.3.1 Some Design Requirements for the IRFI

The principal objective of the IRFI is to provide one common scale of reporting runway friction regardless of the friction measurement device used.

The methodology to achieve this is harmonization, which means correlation of measurement results of all device types and models used at airports worldwide where winter conditions occur. The correlation must be with a reference device or an aggregated result from a number of devices. Each device type may already be standardized according to manufacturer, industry, national or international standards.

A harmonized scale of friction values must meet a number of requirements:

- All present and future friction measurement devices for airport use must be provided for.
- A harmonization reference must cover all surface types and conditions found at airports.
- A range of friction values from a low of 0.05 to a high of 1.2 may represent data from several different tire-surface friction processes. Tire configuration and surface type, surface condition and surface treatment are key descriptors of these processes.
- The complexity of handling several different tire-surface pairs, each with different friction characteristics, warrants the use of digital computing and databases to be able to deliver a harmonized value as quickly as the airport service must respond to operator requests.
- A new method must provide better quality predictions than previous methods.
- A new method must lend itself to integration with runway surface condition reporting and flight operations planning methods, both in manual and different degrees of digitally automated modes.

### 11.3.2 Inhibiting Progress

The absence of harmonization of friction measurement devices inhibited progress in the area of operational applications of friction measurements. The small industry of making friction measurement devices has not had the resources and organized initiative to deal with this problem. It has taken the determination of customers of this small industry, primarily Transport Canada, to initiate the necessary co-operative processes to investigate the possibilities for and development of harmonization methods and techniques.

Harmonizing entails a common unit of measurement for devices that have proprietary or manufacturer's standard units of measure. The proliferation of friction measurement device types and updated models, and introduction of new tire types and new friction measurement products on a continual basis represents a managerial and technical challenge to ensure that the use of any of these devices will have the same effect when used to report runway friction values. Friction

values published in regulations and guidance material are in proprietary units of friction. Any changes in the device models quoted in these publications require an updated value of friction reference for publication. Internationally, this challenge has so far not been met.

The challenge as it pertains to operational use of friction values can be visualized with the illustration in Figure 58. A traditional method has been to correlate measured friction values with measured stopping distance or deceleration of aircraft. The friction tester and the aircraft perform tests on the same surfaces and a correlation equation is determined for each pair of vehicles. Each line between boxes in Figure 58 represents a correlation.

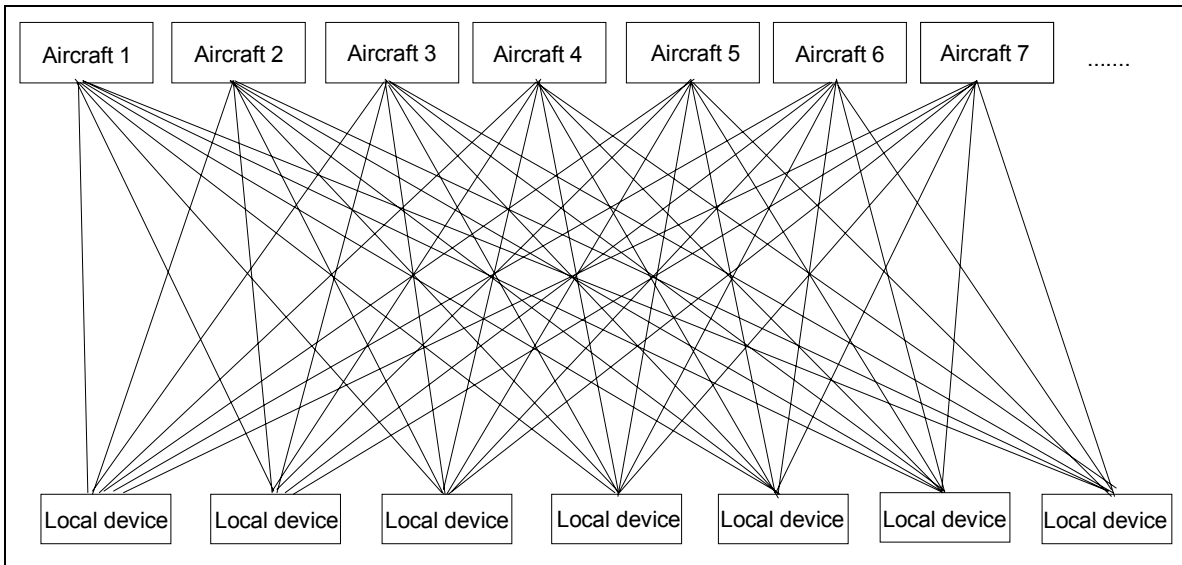


**Figure 58 - Many-to-many correlation of friction devices to aircraft. A small number of arbitrarily chosen aircraft types and friction devices are shown.**

To remove the inhibitor to progress, it was proposed on October 22, 1996, at an International Meeting on Aircraft Performance on Winter Contaminated Runways held in Montreal, Quebec, to harmonize the friction testers in the industry. The proposal was supported by the rationale of Figures 58 and 59.

The common unit of friction measurement should be designed for the operational needs of aircraft operators. The World Road Association had already introduced a harmonized unit of measure (IFI) for pavement monitoring in 1995. For use with air vehicles on ground, the name of the new unit was proposed to be the International Runway Friction Index (IRFI).



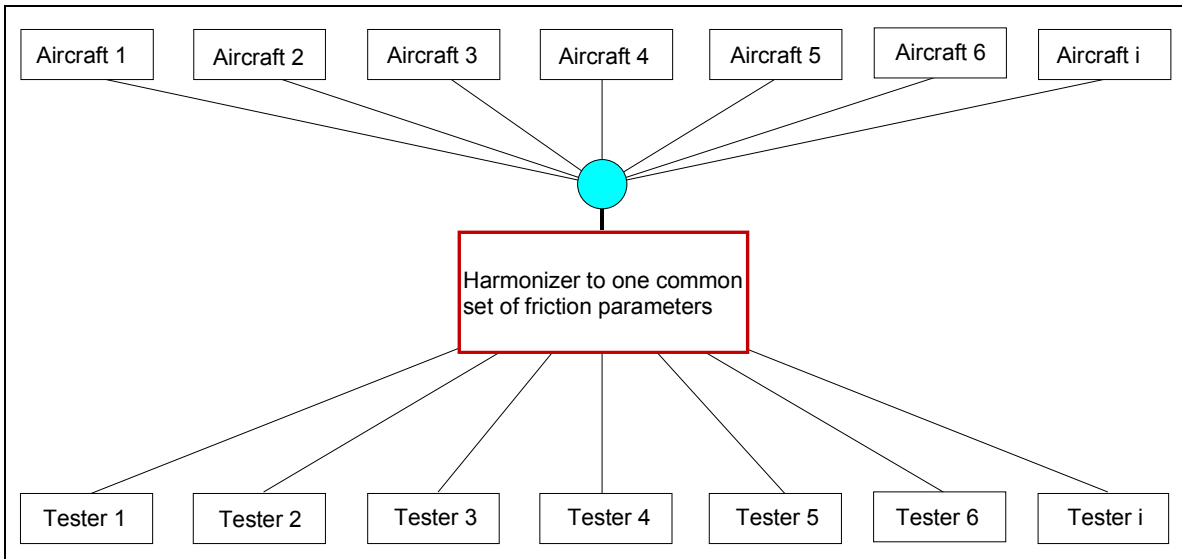


**Figure 59 - Harmonizing to a common set of friction parameters for friction testers**

This report was a response to the quest for engineering to support a common unit of measure. The implementation of methods and techniques to achieve a common unit of measure was called a harmonizer. Given the international scene for aircraft operations, it was a given prerogative to develop the harmonizer as an international standard.

### 11.4 An Architecture for the IRFI and the AFI

The first milestone was to establish the IRFI as a common unit of measurement for all types of friction measurement devices operated at airports. A dedicated device was chosen as a common reference device.

The methodology for establishing harmonizing relationships between the reference device and a local friction device is based on linear regression of paired data from a variety of surfaces for the two devices.

The next milestone was to establish relationships between the IRFI and different aircraft types and sizes. A computed friction index from one of these relationships is called an Aircraft Friction Index (AFI). The AFI is specific for a class of aircraft as grouped by type and size for the current runway friction. It includes the influence of parameters such as braking efficiency (system type, torque limiter settings, etc.), landing wheel geometry and tire load, which are parameters for transforming an IRFI to an actual wheel-braking performance prediction of an aircraft type. Two principal differences of the AFI relative to the IRFI are: the AFI relates to braking slip friction for a decreasing, variable ground speed, while the IRFI relates to a fixed, standardized speed; and the IRFI is a common value for all friction measurement devices for surface type and condition, while the AFI are different values for different types of aircraft.

Figure 60 is a schematic presentation of the architecture of the two friction indexes. Two boxed frames associate each friction index to standards development. Contrary to this figure, the JWRFMP has found that a single AFI harmonizer has worked for all aircraft tested to date.

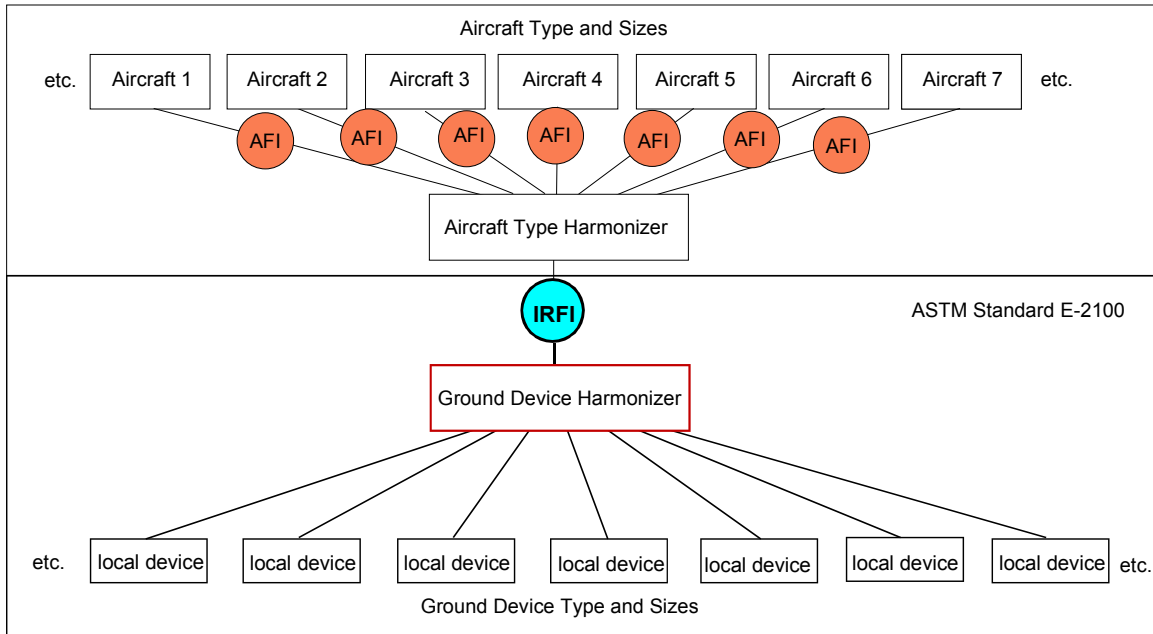


**Figure 60 - Schematic of IRFI and AFI architecture and association with ASTM standards development**

### 11.5 The ASTM E-2100-00 Ground Device Harmonizer

The principal objective of the IRFI is to provide one common scale of reporting runway friction regardless of friction measurement device used.

The principal method is the traditional linear regression correlation of one device output to another device output. More precisely, one device configuration working on one surface class will be correlated with another device configuration on the same surface under the same conditions. The correlation equation coefficients will be valid only for the surfaces and conditions that were measured, but include a wide variety and a large number of surfaces and conditions results in a generalized regression line. Great care must be exercised in doing this to ensure the pairs are run on the same surface. The two devices being correlated need to be run in pairs within a few minutes of each other for each run made.

Figure 61 depicts the first ASTM E-2100-00 harmonizer. One dedicated reference device is the IRFI device. To accommodate harmonization of the large number of local friction devices at airports around the world, a number of dedicated master devices are required. The master devices can be owned and operated regionally to facilitate harmonization trial runs with local friction measurement devices. The master devices should be harmonized with the IRFI reference device periodically.

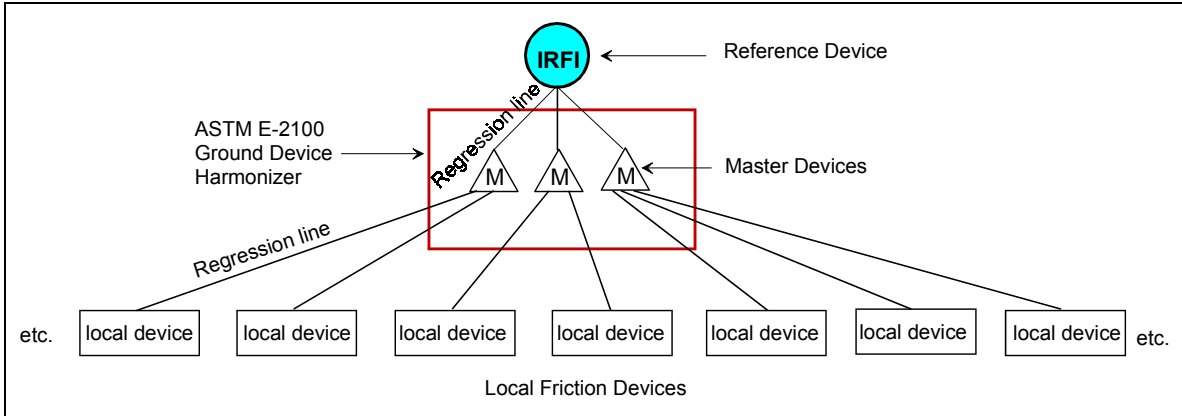


**Figure 61 - A schematic of the ASTM E-2100-00 Harmonizer**

Each line in Figure 61 represents one harmonization relationship as defined by the following linear equations:

$$\mu_{IRFIref} = A + B \cdot \mu_{master} \quad (137)$$

$$\mu_{master} = a + b \cdot \mu_{local} \quad (138)$$

The equation coefficients  $A$ ,  $B$ ,  $a$  and  $b$  are master and local device harmonization constants. Since  $A$  and  $B$  are regarded as constant between periodic IRFI reference harmonization trials, the equations may be combined to produce

$$\mu_{IRFIref} = A + B \cdot (a + b \cdot \mu_{local}) \quad (139)$$

The ASTM E-2100 harmonizer is valid for bare dry pavement, bare wet pavement, bare compacted snow and bare ice surfaces. Up to 5 mm of loose snow particles are tolerated on these bare surfaces.

### 11.5.1 The Quality of the ASTM E-2100-00 Harmonizer

To evaluate the quality of the ASTM E-2100-00 harmonizer, one must keep in mind the prime purpose of the harmonization. Pilots land aircraft on many different airport runways. The airports may have different types of friction measurement devices that report different friction values for the same experienced braking action for that aircraft. Hence, the main issue is how close the harmonization has brought the different friction devices into agreement of the unified IRFI values.

Without harmonization, the range of reported friction values for the same surface type and condition has frequently been observed to differ by as much as 0.25 in average nominal or proprietary friction coefficient units. The standard errors of estimates of IRFI harmonization have been found to be in the 0.03 to 0.05 IRFI range in 19 of 20 cases. Since the IRFI harmonization relationships as fitted linear equations represent the average of several friction values of a surface, the uncertainty of a single measured friction value for a 100 m surface length is greater than 0.05 IRFI.

In harmonization trials for the development of the IRFI, the surface length for averaging a friction value was 100 m. The variability at the 100-m level of detail may be nominally different from the variability of averages for one third of a runway that is the level of detail reported to airmen. Because single device measurements are averaged to higher aggregate levels, or include

different parts of a runway, the variance value of the aggregated averages may change significantly.

When dividing a runway into smaller parts, each part has its own unique standard deviation, since the parts constitute different surfaces from a statistical point of view. For example, the standard deviation for each third of the runway in Figure 46 was 0.042, 0.154 and 0.046. The standard deviation for the whole runway, all 28 segment averages, was 0.172.

Variability of friction average values for 100-m segments taken from operational runway conditions has been observed to range from 0.005 to 0.25. It is more common to observe low standard deviation values obtained for ice and snow base surfaces than for wet or dry pavements.

If a runway has mixed surface conditions, the standard deviation figures will tend to be larger than a standard deviation for a single and constant condition.

An approach to have the least variance when harmonizing friction values is therefore to divide a runway into shorter lengths representing an approximated constant condition and carry out the harmonization for each part. This intent is embodied in the first version of the ASTM E-2100 harmonizer; however, harmonization constants have not yet been developed for different unique surface types and conditions to make use of this approach.

The underlying causes of variability of friction measurements naturally affect the quality of the IRFI. Many of these causes must be addressed as problems of friction measurement and not harmonization. That is not to say that harmonization methods cannot also be improved. The present IRFI has been shown to reduce the standard error to a fraction (as much as one fifth) of current measurements not using the IRFI.

## 11.6 Other Ground Device Harmonizers

Since friction measurements have a large variability, the linear regression approach forces the inclusion of a large range of friction levels in order to be able to perform a linear curve fit with a high confidence. To reach this confidence, dry and wet pavement surface types and conditions are included with the ice and snow surfaces in the regression data population. From statistical and tribological points of view, this mix is not homogeneous and a sizeable variance should be expected.

It is conceivable that other approaches may improve harmonization results by including additional data and modelling techniques or by grouping the tribological systems into separate harmonizations per group.

### 11.6.1 A Simple Modelling Harmonizer

A pure modelling harmonizer using exponential friction-speed functions for different surface classifications has been investigated [9]. The friction models were of the following form:

$$\mu(V) = a \cdot e^{bV} \quad (140)$$

From analysis of the function intercept,  $a$ , and speed coefficient parameters,  $b$ , a grouping of surfaces into “slippery” and “dragging” types was identified. A slippery surface has decreasing friction values with increasing speed and a dragging surface has increasing friction with increasing speed.

The friction values of the intercept parameter could be grouped into 11 friction ranges, including ice and snow surfaces in 4 groups arbitrarily divided at a 0.2 friction coefficient value of the reference device. Another 7 groups for dry and wet pavement were defined. Figure 62 is a schematic of a surface classification based on these parameters. The boxed value ranges cover the parameter values as found for a reference device in the JWRFMP/NASA work database.

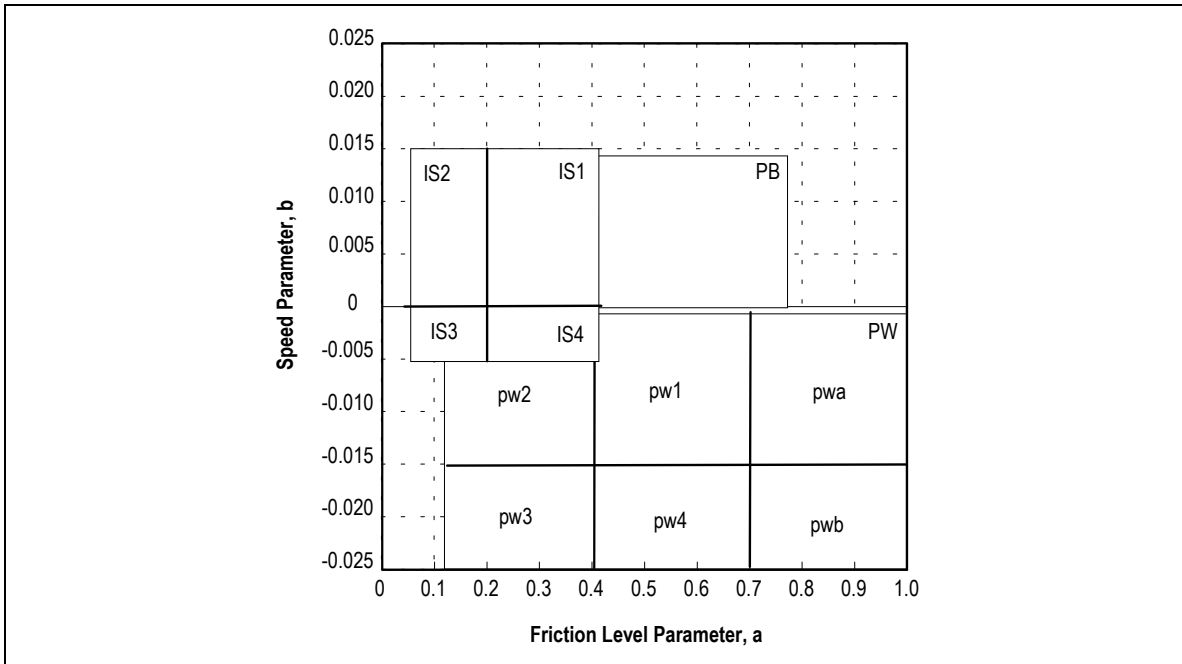


**Figure 62 - A surface classification scheme based on exponential friction model parameters**

Within each surface class, a typical or average exponential friction-speed function -- called a master friction model -- was determined for each tribometer on surfaces of this class. Master models for all surface classes for a pair of tribometers having been mapped, the harmonization can be modelled and computed per surface classification.

For simple exponential friction-speed functions, the transform of friction values of one master model to another is a simple power equation, as was shown in section 10.3. This transform is computationally exact with no uncertainty. With this master-to-master model transform as a guide, the variability of friction measurements can be processed as master model variances within known or assumed surface classes.

The application of the harmonizer on the data of the JWRFMP yielded equal or slightly better predictions than a statistical approach similar to the one described for the IRFI reference and master devices in section 11.5.

### 11.6.2 A Hybrid Statistical and Modelling Harmonizer

It is the policy of most airports to have runways clean of winter contaminants. To fulfil this policy, de-icer chemicals are sprayed on the surfaces that melt any ice or snow. This tactic successfully works down to -6 to -9°C or lower, depending on the chemical used, leaving runways wet and damp over long periods in the winter. The wet pavement condition is therefore a good base for a design of a hybrid harmonizer.

With a computerized approach, a harmonizer can work with dissimilar techniques or algorithms guided by additional data or references.

A runway grid data repository may be used as a back plane to control computerized processing of measured friction data (see section 9.1.4).

Previously stored friction parameters may be retrieved for harmonization purposes. For harmonization needs, the IRFI reference device or a master harmonization device must map the friction characteristics per runway segment by measuring the runway periodically. Among the mapped friction characteristics should be the exponential friction-speed parameters of (140) for a wet pavement condition as a reference master model for each segment.

The wet pavement master model is chosen because it has the most pronounced speed and slip speed dependencies. The slip speed dependency is strongly related to the macrotexture properties of the pavement. It can be assumed that the macrotexture properties of a pavement change less over time than microtexture or other frictional properties. The speed dependency of friction measurements from a fixed-slip device may therefore be more constant than the friction level.

This assumption can be applied to adjust the harmonization relationship for wet pavement friction measurement to the actual conditions per segment at any time after the harmonization mapping has been completed. As shown in Figures 41 and 43, a surface segment may exhibit a number of surface conditions and these conditions produce different speed characteristics of the interaction between a braked tire and the opposing surface. The friction measurements can be tested against calculated average friction values using the average wet pavement friction-speed formula for the segment.

When measured friction values are outside set limits for the wet pavement master model values computed for the measuring speed and segment, another technique may be employed by the computer program for the harmonization. For instance, the statistical technique may be applied for higher friction values assuming dry pavement conditions are reached. Or, the statistical technique may be applied for low friction values assuming an ice or snow base is formed on the segment analysed. Since net contact pressure is the principal influence of measured differences between different types of tribometers, a contact pressure ratio between the local device and the IRFI reference device may be applied in the adjustment.

In essence, the logic of the computerized harmonizer would model what friction value the IRFI reference would have measured at the instant of a local friction measurement based on the stored data history and other characteristics of the reference in the repository.

## **11.7 Harmonization Reference**

Harmonization is a comparison of a measurement device to a designated physical or virtual reference. A virtual reference can be the averages of several designated reference devices, as the case is for the IFI.

For practical technical, management and cost reasons, one device is preferred. Since the purpose of the IRFI is to predict the braking slip of aircraft tire configurations, a reference device that can operate aircraft tires as the measuring tire can be expected to have the best potential for producing good predictions of aircraft friction indexes.

The operation of a reference device must be limited to the correlation runs with regional master friction testers and correlation runs with aircraft. To preserve the device, it should not be used for other friction measurement services at airports.

## 11.8 Information Flow of Harmonized Friction Values to Principal Users

One principal use of the IRFI is to estimate flight ground operation constraints.

The friction information is but one of several pieces of information needed to estimate the ground operations constraints such as required runway length, permissible load, etc.

The major preparations to be able to produce harmonized friction values can be shown in an information flow diagram as in Figure 63.

A major preparatory step is to compare the IRFI reference device with regional master friction devices or local friction devices and with different types of aircraft. These comparisons need to be done as field tests on a range of surface types and conditions during a variety of ambient conditions. The results of the comparisons are stored in databases. Subset copies of the field test database can be distributed for local use. The subset databases include data pertaining to the local devices and local aircraft types.

Computational tools may be used to analyse the comparisons and feed the results to the databases. These preparatory tools or processes may be called reference device harmonizers.

To make use of the reference data in calculations of IRFI values for each measurement run of a runway, a computational tool may be called for to post-process the measurement data and integrate the friction measures with the runway condition report. The subroutine doing the IRFI calculations may be called a run harmonizer.

The friction information is provided by the airport measurement service for general use by the airlines or other aircraft operators. The information delivered is the IRFI, which is not tailored to any specific aircraft or flight scenario. For the aircraft operator to use the IRFI, a further adaptation of the friction information to a particular aircraft is foreseen. This is the reverse harmonization of the reference device with aircraft wheel-braking performance of selected aircraft types. The aircraft-specific and reverse harmonized friction information is called the AFI. A computation tool called an AFI estimator may perform the calculations.

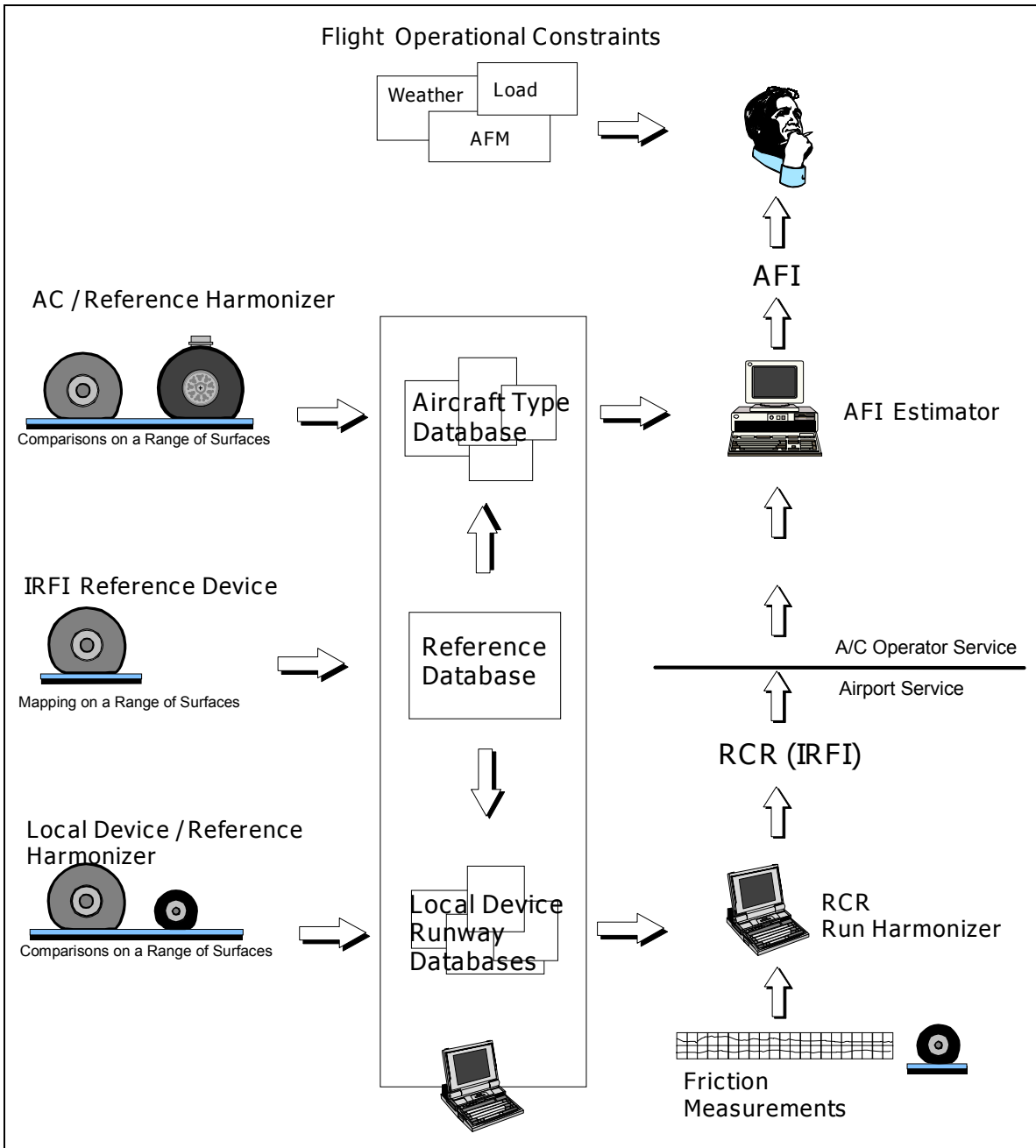


**Figure 63 - Information flow of harmonized friction values**

As the information flow diagram in Figure 63 implies, the reference device comparisons are a continuous field-test process in order to include new friction measurement devices and aircraft types as they come into operation. An appointed service institution must therefore regularly maintain the databases and the computational processes must be standardized to avoid subjective influence of the reference relationships.



## REFERENCES

1. Horne, W.B. and Dreher, R.C., "Phenomena of Pneumatic Tire Hydroplaning", NASA TN D-2056, 1963.
2. Bhushan, B., "Principles and Applications of Tribology", John Wiley & Sons, Inc., 1999.
3. Clark, S.K., ed., "Mechanics of Pneumatic Tires", U.S. Department of Transportation, National Highway Traffic Safety Administration, 1981.
4. Goodenow, G., Kolhoff, T. and Smithson, F., "Tire-Road Friction Measuring System - A Second Generation", SAE Paper No. 680137, Society of Automotive Engineers, 1968.
5. van Es, G.W.H., "A Method for Predicting the Rolling Resistance of Aircraft Tires in Dry Snow", Technical Paper TP-99240, National Aerospace Laboratory, The Netherlands, 1999.
6. Bode, G., "Kräfte und Bewegungen unter rollenden Lastwagenreifen", A.T.Z. 64 (10), 1962: 300-306.
7. Yeager, R.W. and Tuttle, J.L., "Testing and Analysis of Tire Hydroplaning", SAE Paper No. 720471, Society of Automotive Engineers, 1972.
8. CDRM Inc., "Evaluation of Ground Test Friction Measuring Equipment on Runways and Taxiways under Winter Conditions", Transportation Development Centre of Transport Canada, TP 12866E, September 1996.
9. Wambold, J.C., Henry, J.J. and Andresen, A., "Fourth Year – Joint Winter Runway Friction Measurement Program", NASA Contractor report, March 2000.
10. Andresen, A., "OKK Friction Profiles of NATAM Operated Friction Measuring Devices 1998-2000", Norwegian Air Traffic and Airport Management, report No. OKK 2000-1, 2000.
11. Transport Canada, "Runway Condition Monitoring" (draft report), Vol. 3, Appendix C, Table D, Transport Canada Training Institute, TP 11827, November 1993.
12. Wambold, J.C., Antle, C.E., Henry, J.J. and Rado, Z. "International PIARC Experiment to Compare and Harmonize Texture and Skid Resistance Measurements", AIPCR-01.04.T, 1995.
13. Bachmann, T., "Wechselwirkungen im Prozess der Reibung zwischen Reifen und Farbahn", VDI Reihe 12 Nr. 360, 1998.
14. ASTM, "Standard Practice for Calculating International Friction Index of a Pavement Surface", Standard No. E-1960-98.
15. ISO, "Acoustics-Characterization of Pavement Texture using Surface Profiles-Part 1: Determination of Mean Profile Depth", Standard No. ISO 13473-1.
16. ASTM, "Standard Practice for Calculating International Runway Friction Index", Standard No. E-2100-01.

## BIBLIOGRAPHY

ASTM, "Standard Practice for Calculating Pavement Macrottexture Mean Profile Depth", Standard No. E-1845-96.

ASTM Committee E-11 on Quality and Statistics, "Manual on Presentation of Data and Control Chart Analysis", ASTM Manual Series, MNL 7, 1990.

Balkwill, K.J. and Mitchell, D.J. "Statistically-Based Methods for Relating Aircraft and Ground-Test Machine Friction Data", ESDU International, 1997.

Croll, J.B., Martin, J.C.T. and Bastian, M., "Falcon 20 Aircraft Performance Testing On Contaminated Runway Surfaces During the Winter of 1996/1997", National Research Council Canada, report LTR-FR-137, August 1997.

Doogan, M., Herrmann, E. and Lamont, P., "Braking Friction Coefficient and Contamination Drag for the Dash 8 on Winter Contaminated Runways", de Havilland Inc., report DHC-D4547-97-09, September 1997.

Fleet Technology Limited, "Aircraft Tire Braking Friction under Winter Conditions: Laboratory Testing", Transportation Development Centre of Transport Canada, TP 12584E, June 1996.

Fristedt, K. and Norrbom, B., "Studies of Contaminated Runways", The Aeronautical Research Institute of Sweden, 1980.

Gillespie, T.D., "Fundamentals of Vehicle Dynamics", Society of Automotive Engineers, 1992.

Henry, J.J. and Wambold, J.C., eds, "Vehicle, Tire, Pavement Interface", ASTM Special Technical Publication 1164, 1992.

ICAO, "Airport Services Manual", ICAO Doc 9137-AN/898, Part 2 Pavement Surface Conditions, 1984.

Joint Aviation Authority, "Joint Airworthiness Requirements", AMJ 25X1591, 1999.

Kovac, F.J., "Tire Technology", Goodyear Tire and Rubber Co., 1973.

Kulakowski, B.T., "Vehicle-Road Interaction", ASTM Special Technical Publication 1225, 1994.

Milliken, W.F., "Race Car Vehicle Dynamics", Society of Automotive Engineers, 1995.

SAE, "Vehicle Dynamics Related to Braking and Steering", SP-801, Society of Automotive Engineers, 1989.

Sypher-Muller International Inc., "Aircraft Take-Off Performance and Risks for Wet and Contaminated Runways Validation and Implementation Program", Transportation Development Centre of Transport Canada, TP 11966E, March 1994.

Transportation Development Centre, "Proceedings of the International Meeting on Aircraft Performance on Contaminated Runways", Transport Canada, TP 12943, October 1996.

Wong, J.Y., "Theory of Ground Vehicles, 2<sup>nd</sup> edition", John Wiley & Sons, Inc., 1993.